Lawrence Berkeley National Laboratory
Recent Work

Title
THERMAL ION-MOLECULE REACTIONS IN GASEOUS METHANE-OXYGEN MIXTURES

Permalink
https://escholarship.org/uc/item/0sz2w0dk

Author
Horton, Robert Louis.

Publication Date
1971-08-01

eScholarship.org Powered by the California Digital Library
University of California

LBL-114 c.1

RECEIVED
LAWRENCE
RADIATION LABORATORY

OCT 22 1971

LIBRARY AND
DOCUMENTS SECTION

THERMAL ION-MOLECULE REACTIONS IN GASEOUS METHANE-OXYGEN MIXTURES

Robert Louis Horton
(Ph. D. Thesis)

August 1971

AEC Contract No. W-7405-eng-48

For Reference

Not to be taken from this room

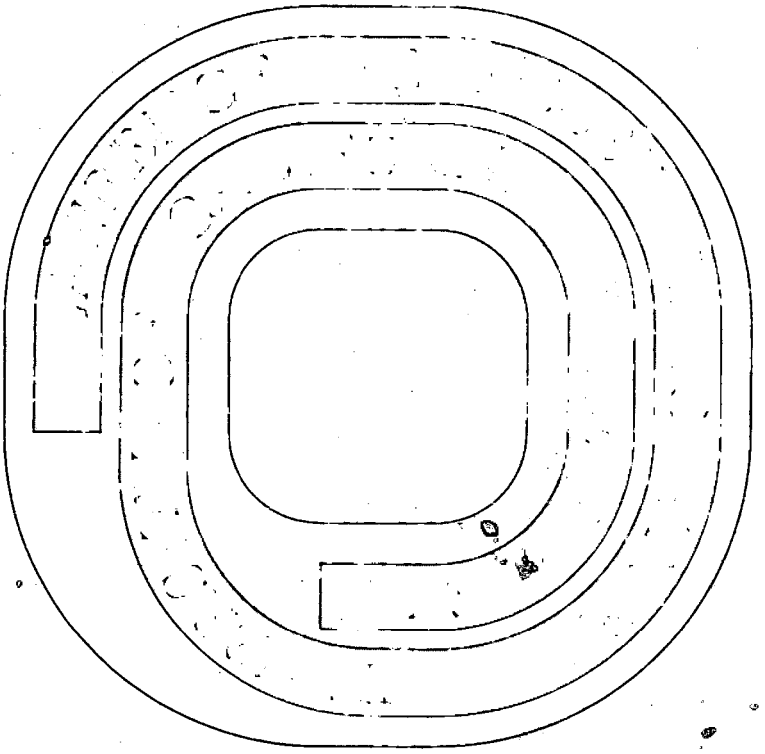

LBL-114

DISCLAIMER

This document was prepared as an account of work sponsored by the United States Government. While this document is believed to contain correct information, neither the United States Government nor any agency thereof, nor the Regents of the University of California, nor any of their employees, makes any warranty, express or implied, or assumes any legal responsibility for the accuracy, completeness, or usefulness of any information, apparatus, product, or process disclosed, or represents that its use would not infringe privately owned rights. Reference herein to any specific commercial product, process, or service by its trade name, trademark, manufacturer, or otherwise, does not necessarily constitute or imply its endorsement, recommendation, or favoring by the United States Government or any agency thereof, or the Regents of the University of California. The views and opinions of authors expressed herein do not necessarily state or reflect those of the United States Government or any agency thereof or the Regents of the University of California.

0 0 0 0 3 6 0 . 7 8 3

CONTENTS

Abstract v

I. Introduction and Background 1

Summary 8

References for Chapter I 10

II. Ion Cyclotron Resonance Mass Spectometry 11

A. General Basis of the Technique 11

1. The Cyclotron Frequency 11

2. Cyclotron Resonance 12

B. The Development of Cyclotron Resonance Instrumentation 12

C. Ion Cyclotron Double Resonance 16

D. Description of the Apparatus 19

1. Gas Inlet and Flow 19

2. The ICR Cell 21

3. Techniques of Modulation 29

a. Magnetic Field Modulation 31

b. Drift Potential Modulation 32

c. Electron Energy Modulation 32

d. Pulsed Ion Cyclotron Double Resonance . . 33

e. Pulsed Ion Ejection 35

E. Quantitative Measurement of Thermal Ion-molecule Reaction Rates 35

1. Theory of Ion Cyclotron Resonance Lineshape . . 35

2. Chemical Kinetics 37

3. How Ion Drift Time is Determined 40

4. How the Neutral Density is Determined 46

F. Summary 50

References for Chapter II 54

III. Results for the Methane System 57

A. The Reactions of C^+ with Methane 62

B. The Reactions of CH^+ with Methane 68

C. The Reactions of CH_2^+ with Methane 69

D. The Reactions of CH_3^+ with Methane 73

E. The Reactions of CH_4^+ with Methane 74

Summary 76

IV. The Fast Reactions of Impurity and Contaminant Species . . . 78

A. Hydrogen Species 79

B. Water Species 85

C. Carbon Monoxide Species 87

D. Carbon Dioxide Species 89

Summary 90

References for Chapter IV 94

V. The Oxygen System 96

Summary 110

References for Chapter V 111

VI. The Cross Reactions in Methane-Oxygen Mixtures 114

Summary 159

References for Chapter VI 160

VII. Conclusion 161

References for Chapter VII 175

VIII. Acknowledgements 176

IX. Appendix 177

0 0 0 0 3 6 0 3 7 8 4

Thermal Ion-Molecule Reactions in Gaseous Methane-Oxygen Mixtures

Robert Louis Horton

Inorganic Materials Research Division, Lawrence Berkeley Laboratory,
and Department of Chemistry; University of California
Berkeley, California 94720

ABSTRACT

Ion cyclotron resonance mass spectrometry was applied to the study of the thermal ion-molecule reactions occurring in methane-oxygen mixtures. The reactant ion-product ion relationships were more firmly established by using ion cyclotron and ion ejection double resonance and by examining some of the ion-molecule reactions occurring in mixtures of oxygen and chloromethanes. The ion-molecule reactions which take place in pure methane were re-examined and found to account for most of the product ions found in methane-oxygen mixtures. The remainder is due to the reactions which occur in pure oxygen, to the fast reactions involving contaminant species, and to the cross ion-molecule reactions of methane species with oxygen species. The contaminants were largely produced by chemical activity at the hot filament in the electron impact ion source. Additional experiments augment the earlier measurements of the rates of the relevant reactions of the contaminant species. Literature data and the results of a re-examination of the pure oxygen system were critically discussed in an attempt to assess the rates of collision-induced and spontaneous relaxation of electronically excited O_2^+. The reaction of oxygen

ions, both ground state and electronically excited, with methane was found to be very slow not because of an energy barrier to reaction but because only a few percent of the collisions bring the reactants into proper position to permit a concerted bond-breaking, bond-forming step. This preliminary indication is that a potentially long-lived intermediate of structure $(H_2{=}C{=}(OH)_2^+)^*$ is formed in the reaction of O_2^+ with methane. The reaction of CH_4^+ with oxygen proceeds with much higher rate but by way of charge and H-atom transfer rather than by way of the stable but difficult to reach intermediate. Much more study of this system of reactions is needed in order to establish and explain the mechanisms and dynamics of the ion-molecule reactions.

0 0 0 0 3 6 0 . 7 8 5

I. Introduction and Background

The past decade has witnessed a mushrooming of the ion-molecule reactions realm of chemical kinetics. The interest in ion-molecule reactions stems from the ease with which ions can be made to serve the experimenters' purposes. Ions can be mass selected, formed into beams, accelerated, deflected, and so forth. The rapid growth of the field correlates in large part with technological advancements. Physicists, for example, have been using the cyclotron principle for most of this century; their applications have ranged from high energy particle accelerators to the study of the electrons in solids by means of electron cyclotron resonance. Some research proposals involving the use of ion cyclotron resonance as a basis of mass spectrometry date back twenty years or more;[1] however, full exploitation of the technique has awaited technological developments in high vacuum and the advent of relatively inexpensive, highly uniform, and high field strength magnets, an out-growth of the development of NMR in the 1950's. Ion cyclotron resonance mass spectrometry is now accepted as an honest technique for establishing the precursors for each product species and for measuring the rate coefficients for the reactions even in complex systems of many simultaneous ion-molecule reactions. The details of the technique and its operation will be discussed in Chapter II.

Then we will examine the application of this technique to study a system having unique chemistry - the ion-molecule reactions occurring in gaseous mixtures of methane and oxygen. In 1965 Franklin and Munson[2] pointed out some of this uniqueness in a study using a conventional high pressure mass spectrometer (HPMS). They found "comparatively few and relatively slow [ion-molecule] reactions between the hydrocarbons and

oxygen."[2] While the exothermic reactions possible in this system are many, few were found to have measurably large rates. Figure 1 shows that for the reaction of O_2^+ with CH_4, there are at least 16 exothermic reaction channels. Of these, Franklin and Munson report only two:

$$O_2^+ (\tilde{X}\ ^2\Pi_g) + CH_4 \rightarrow CH_3O_2^+ + H \qquad k = 1.26 \times 10^{-11}\ cm^3/molec\text{-}sec$$
$$\rightarrow CH_2O^+ + H_2O \qquad 2.8 \times 10^{-11}$$

Ion-molecule reactions in general have rates which are comparable to elastic ion-molecule collision frequencies.[3] A much-quoted estimate for the collision frequency comes from the orbiting cross-section,[4] which is computed by assuming that all collisions with impact parameters up to a maximum value $b_m(E)$ lead to reaction. The maximum impact parameter $b_m(E)$ is the greatest value which leads to a trajectory in which the collision partners would pass through the origin, $r = 0$, if they moved under the ion-induced-dipole potential, $-\alpha e^2/2r^4$. This cross-section predicts reaction rate constants independent of the relative velocity of the encounter:

$$k = 2\pi e\left(\frac{\alpha}{\mu}\right)^{\frac{1}{2}} = 2.342 \times 10^{-9}\ cm^3/molec\text{-}sec \cdot \left(\frac{\alpha(\text{Å}^3)}{\mu(\text{AMU})}\right)^{\frac{1}{2}}, \qquad (1)$$

where α is the polarizability of the neutral and μ is the reduced mass of the ion-neutral pair. For estimation, polarizability data from dielectric constant measurement is normally used.[12] This approximation has been used successfully to rationalize the magnitude and energy dependence of the rates of many ion-molecule reactions at low relative kinetic energy of collision.[6] For the thermal $O_2^+ + CH_4$ interaction, Eq. 1 predicts a rate of $11.5 \times 10^{-10}\ cm^3/molec\text{-}sec$, while Franklin and Munson observe a total of about 0.4×10^{-10}. The very large rate

0 0 0 0 3 6 0 3 / 8 6

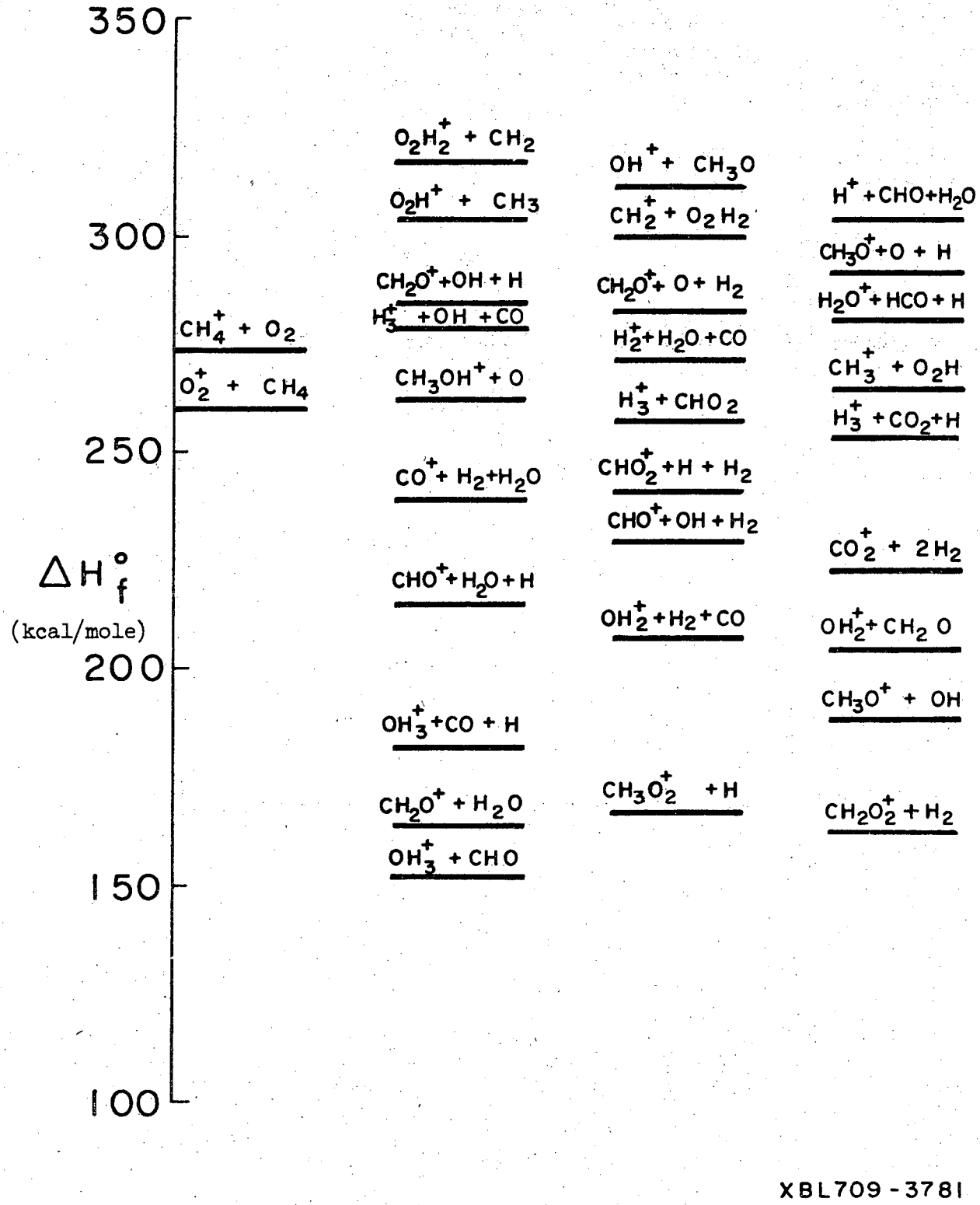

Fig. 1. Thermodynamic data on the system of stoichiometry $CH_4O_2^+$.

constants observed for a large number of ion-molecule reactions is generally attributed to an absence of activation energy, inasmuch as ions "are themselves free radicals and might be expected to react rapidly and with little or no activation energy."[5] Cassuto[7] has proved that the activation energy of

$$CH_4^+ + CH_4 \rightarrow CH_5^+ + CH_3 , \qquad (11)$$

is zero to within 0.2 kcal/mole by measuring its rate over the temperature range between -150°C and +200°C. While we cannot perform a comparable series of measurements, the question of whether or not an activation barrier explains the relative slowness of the reactions in the methane-oxygen system will be one of the main questions to be addressed in this dissertation.

If each of the many exothermic reactions occurs with a rate on the order of 10^{-12} or 10^{-11} cm^3/molec-sec, the total could approach the 11.5×10^{-10} predicted by the orbiting reaction rate (Eq. 1). The occurrence of fast reactions of methane ions with methane could in some cases mask these slow reactions. We shall examine the question of whether this might be the case.

The high pressure mass spectrometer used by Franklin and Munson is not ideally suited for determining which ions are the reactant precursors of each product ion. The techniques which were employed are:

1. appearance potential measurements
2. determining the effect of each neutral partial pressure
3. and determining the effect of the ion extracting field strength.

The measurement of an appearance potential is as follows: in pure methane, for example, when the ionizing electron energy is 70 volts,

0 0 0 0 3 6 0 5 7 8 7

strong signals can be observed for primary ions, CH_4^+, CH_3^+, CH_2^+, CH^+, and C^+, as well as for a number of secondary ions if the methane pressure is high enough to allow ion-molecule reactions to proceed rapidly; as the ionizing electron energy is reduced to below the appearance potential of C^+ ions from methane (19.5 eV) the formation of that ion and any ions which it produced upon reaction with methane will cease. That the appearance potential of $C_2H_3^+$ is the same as that of CH_2^+ establishes the ion-molecule reaction $CH_2^+ + CH_4 \rightarrow C_2H_3^+ + H_2 + H$ as <u>one</u> source of mass 27 ions. The appearance potential of CH^+ is greater than that of CH_2^+ and therefore mass 27 ions produced from the above reaction will persist to a lower ionizing electron energy than will those produced from $CH^+ + CH_4 \rightarrow C_2H_3^+ + H_2$. In order to establish the occurrence of such competing reactions by means of the appearance potential method one must either use a virtually mono-energetic electron beam, or carefully deconvolute the energy spread there is in the beam. Since the spread in energy of the electron beam in Franklin and Munson's spectrometer was about 1 eV there will be some uncertainty involved in the appearance potentials he reported. Obviously the weaknesses of this method can become accentuated in a system such as the methane-oxygen system, since the two major reactants CH_4^+ and O_2^+ ($\tilde{X}\ ^2\Pi_g$) have appearance potentials within 0.7 eV and since most of the reactions are very slow and the product ion signals are at best very small. Furthermore, when the reaction of a minority species is in competition with that of a majority species, such as

$$CH^+ + O_2 \rightarrow HCO^+ + O \qquad \text{slow (?)}$$
$$CH_3^+ + CH_4 \rightarrow C_2H_5^+ + H_2 \qquad \text{fast,}$$

it is very easy for the appearance potential method to overlook the

former reaction, especially if its rate be slow. This is also true for the ion cyclotron resonance technique, but to a much smaller extent. We expect to be able to describe more nearly completely what reactions occur.

The effect of varying the ion extracting field strength is to alter the kinetic energy of the ions in the ion source. When the extracting field is continuously applied, as it was in the 1965 study, the ions never have an opportunity to thermalize. The minimum extracting potential used was 14.5 volts, so that the average center of mass kinetic energy for reactant ions was probably around 3 to 5 eV. This kinetic energy range can be reached with the ion cyclotron resonance apparatus, but the attendant experimental difficulties are great; consequently, a direct comparison of the results of the 1965 study with the present will suffer from the fact that ion-molecule reaction chemistry is distinctly different in the two energy ranges. The 3 eV center of mass kinetic energy is sufficient to drive a large number of endothermic reactions and surmount most activation barriers. The difficulty in learning how efficiently this kinetic energy can be converted into internal energy renders uncertain many arguments based on thermodynamic data and the conservation of energy principle.

The length of time during which ions react is about 10^3 times longer in the ICR than in the HPMS, even though the product of the reaction time and reactant neutral density is comparable in the two instruments. Appreciable populations of electronicly excited ions are produced by electron impact[8] in both instruments, but in the ICR, all but a fraction of the longest-lived excited ions probably relax to the ground state via spontaneous emission before appreciable reaction has

occurred. The $\tilde{A}\ ^2\Pi_u$ state of O_2^+, for example, has about 100 kcal/mole more internal energy than the $\tilde{X}\ ^2\Pi_g$ ground state, and is expected to be highly reactive. Franklin and Munson reported no reaction of this excited species with methane, and with oxygen only the following:

$$O_2^+ (\tilde{A}\ ^2\Pi_u,\ v=0 \text{ to } 2) + O_2 \rightarrow O_3^+ + O.$$

The same product is seen in the ICR experiments, but not from the above reaction, since that excited state will have relaxed to the ground state and insufficient energy will be available to drive the reaction. The $O_3^+ + O$ product is seen in the ICR spectrometer produced from the reaction of $O_2^+ (\tilde{a}\ ^4\Pi_u)$ with O_2. This excited state appears to have sufficient lifetime to persist through the typical reaction times used in these experiments.

The data of Franklin and Munson seems to indicate that methane quite rapidly reduces the population of excited oxygen ions available to produce O_3^+ because upon going from 25 microns (μ) O_2 plus 25μ CH_4 to 53μ O_2 plus 53μ CH_4 the mass 48 peak intensity (O_3^+) drops by about 30%. Their failure to point out this fact may indicate that there is a typographical error in the data reported. No reaction of excited oxygen ions with methane is reported; and no marked differences in the rates of reaction of excited oxygen ions with methane compared with those of ground state oxygen ions with methane have been observed here. This surprising result will be considered in some detail in subsequent chapters.

The final motivation for this study centers about the role of potentially long-lived complexes. Two models of ion-molecule reaction dynamics currently receiving attention are reaction through complex formation and stripping. In the former case the projectile and target

are assumed to coalesce into a moiety of sufficient lifetime to allow equilibration of vibrational energy throughout the complex. In the other model, the projectile strips away part of the target molecule and little or no momentum is transferred to what remains of the target. A long-lived complex mechanism is most likely to be found when the total energy is relatively low, the ground state of the assumed complex is very stable, and there are many vibrational modes to participate in sharing the energy. Henglein[9] has demonstrated that a long-lived complex mechanism persists for the reaction

$$CH_3OH^+ + D_2 \rightarrow [CH_3 - \underset{H\ D}{O} - D^+]^* \rightarrow CH_3OHD^+ + D$$

up to about 4 eV initial relative kinetic energy. The most persuasive proof of a long-lived complex is to show that the complex rotates many times before it decomposes, so that the products come off with equal probability at all center-of-mass angles. If all bonds in the collision complex share the internal energy of the complex, the theories of unimolecular decomposition[10, 11] can be used to predict the relative rates of reaction into each open channel. Unfortunately even the simplest such theory requires more detailed knowledge of the structure of the complex than is available at present for the complexes we may encounter in the methane-oxygen system. Nevertheless we can reasonably expect to make some conclusions as to the role of a complex in these reactions and if so, the structure of the complex.

SUMMARY

Earlier studies of ion-molecule reactions suggest that some of the reactions in methane-oxygen mixtures are considerably slower than expected. The present study is motivated by a desire to verify the

0 0 0 0 3 6 0 3 7 8 9

earlier results, more firmly establish the precursor-product ion relationships, and discuss what conclusions can be reached concerning the dynamics of the reactions which occur.

References - Chapter I

1. R. J. Myers, private communication, 1970.

2. J. L. Franklin and M. S. B. Munson, Tenth Symposium on Combustion, 561 (1965).

3. F. W. Lampe, J. L. Franklin and F. H. Field, Progress in Reaction Kinetics, 1, 68 (1961).

4. G. Gioumousis and D. P. Stevenson, J. Chem. Physics 29, 294 (1958).

5. L. Friedman and B. G. Reuben, "Review of Ion-molecule Reaction," Adv. in Chem. Phys. 19, to be published.

6. E. W. McDaniel, V. Cermak, A. Dalgarno, E. E. Ferguson, and L. Friedman, Ion Molecule Reactions (Wiley-Interscience, New York, 1970).

7. A. Cassuto, Adv. in Mass Spectrometry, 2, (Pergamon Press, New York, 1963), p. 296.

8. B. R. Turner, J. A. Rutherford, and D. M. J. Compton, J. Chem. Phys. 48, 1603(1968).

9. A. Ding, A. Henglein, and K. Lacmans, Z. Naturforsch. 23A, 799 (1968).

10. H. S. Johnston, Gas Phase Reaction Rate Theory (Ronald Press, New York, 1966).

11. H. M. Rosenstock, M. B. Wallenstein, A. L. Wahrhaftig, and H. Eyring, Proc. Natl. Acad. Sci. 38, 667 (1952).

12. E. W. Rothe and R. B. Bernstein, J. Chem. Phys., 31, 1619 (1959).

0 0 0 0 3 6 0 3 7 9 0

II. ION CYCLOTRON RESONANCE MASS SPECTROMETRY

A. General Basis of the Technique

1. The Cyclotron Frequency

Ion cyclotron resonance mass spectrometry is based on the classical motion of charged particles in magnetic and electric fields. In a uniform magnetic field, $\vec{B}$, an ion moves in a circular orbit with angular frequency ω_c in the plane perpendicular to $\vec{B}$; its motion parallel to $\vec{B}$ is unconstrained. The cyclotron frequency ω_c is dependent only on the field strength $|\vec{B}|$ and the charge-to-mass ratio of the ion:

$$\omega_c = \frac{|q||B|}{m} = 1.53557 \text{ MHz} \cdot \frac{B(\text{kgauss})}{m/q(\text{AMU/charge})} , \qquad (1)$$

where q is the ion charge, B is the magnetic field strength, and m is the ion mass. For CD_4^+ ions at 14 kgauss (the maximum field obtainable with our instrument) the cyclotron frequency is about 1 MHz. Equation (1) is derived from equating the centripetal force of the particle moving in a circular orbit, $\frac{mv^2}{r}$, to the force which causes it, $q\vec{v} \times \vec{B}$, the force exerted on an ion of mass m, charge q, and velocity $\vec{v}$ in a magnetic field of intensity B.

$$\frac{mv^2}{r} = q\vec{v} \times \vec{B} \qquad (2)$$

This implies the constancy of the angular frequency of the ions' orbit.

$$\frac{v_\perp}{r} = \omega_c = \frac{qB}{m} . \qquad (3)$$

where $v_\perp$ is the ion velocity perpendicular to $\vec{B}$.

For thermal kinetic energy CD_4^+ ions at 14 kgauss, the average speed is 559 m/sec; hence the orbital radii will be only .0559 cm.

2. Cyclotron Resonance

When an alternating electric field $\vec{E}_1(t)$ at frequency ω_1 is applied perpendicular to $\vec{B}$ so that the changing electric field is in phase with an ion's cyclotron orbital motion, the ion will be accelerated by the electric field. If the frequency of the electric field ω_1 is the same as the ion's cyclotron frequency, the ion's motion will continue to be in phase with the electric field and the ion's acceleration will be continuous. Figure 1 shows that a mass 15 ion initially at rest for which $\omega_1 = \omega_c$ has an orbit which spirals outward and a kinetic energy which increases as t^2. Figure 2 shows a similar ion for which $\omega_1 \neq \omega_c$. The orbit spirals outward while the ion's orbital motion stays in phase with the electric field but later it spirals inward when out of phase. The average kinetic energy is constant.

For a group of thermal ions moving with random phase with respect to the alternating electric field, the net power absorption for non-resonant ions ($\omega_1 \neq \omega_c$) will be zero; the net power absorption for resonant ions will increase as the square of the time during which absorption occurs.

B. The Development of Cyclotron Resonance Instrumentation

Perhaps the earliest ion cyclotron resonance instrument was described by Lawrence in 1930.[1] Application of cyclotron resonance to the study of the electrons in solids and flames also dates back about forty years. An ion cyclotron resonance device was reported in 1949[2]

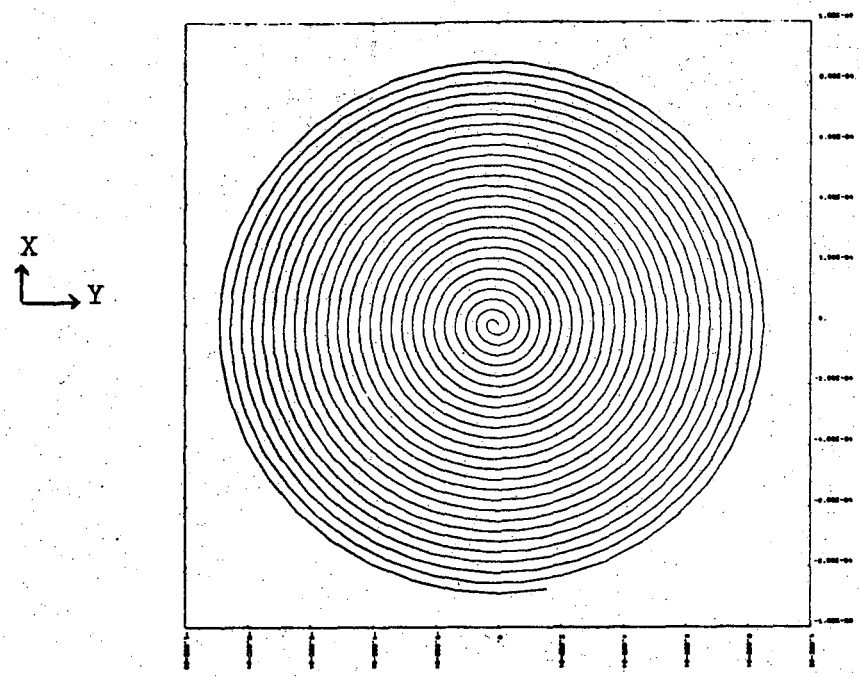

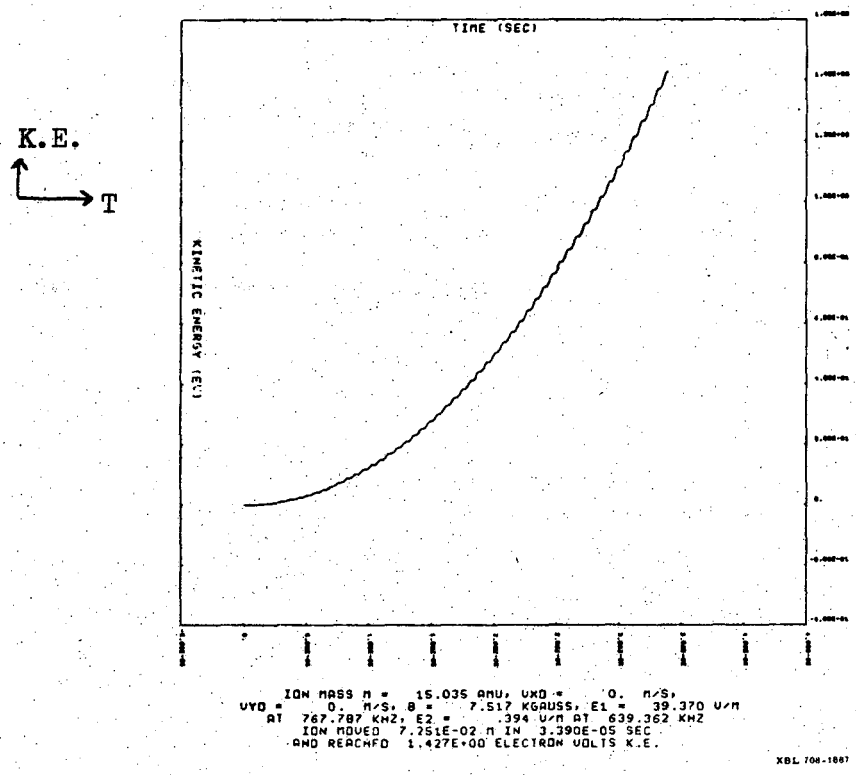

Fig. 1. Resonant ion motion.

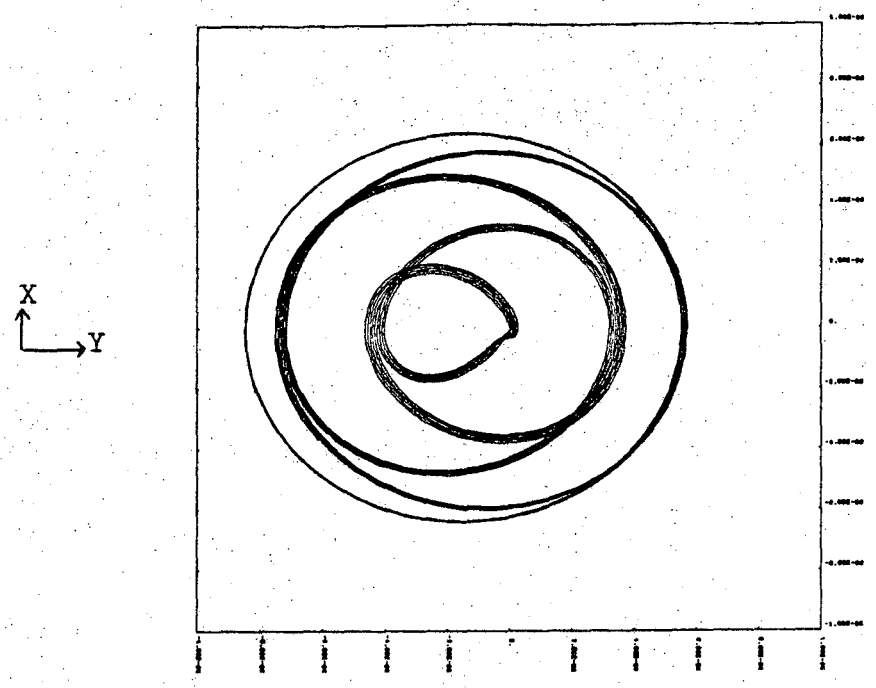

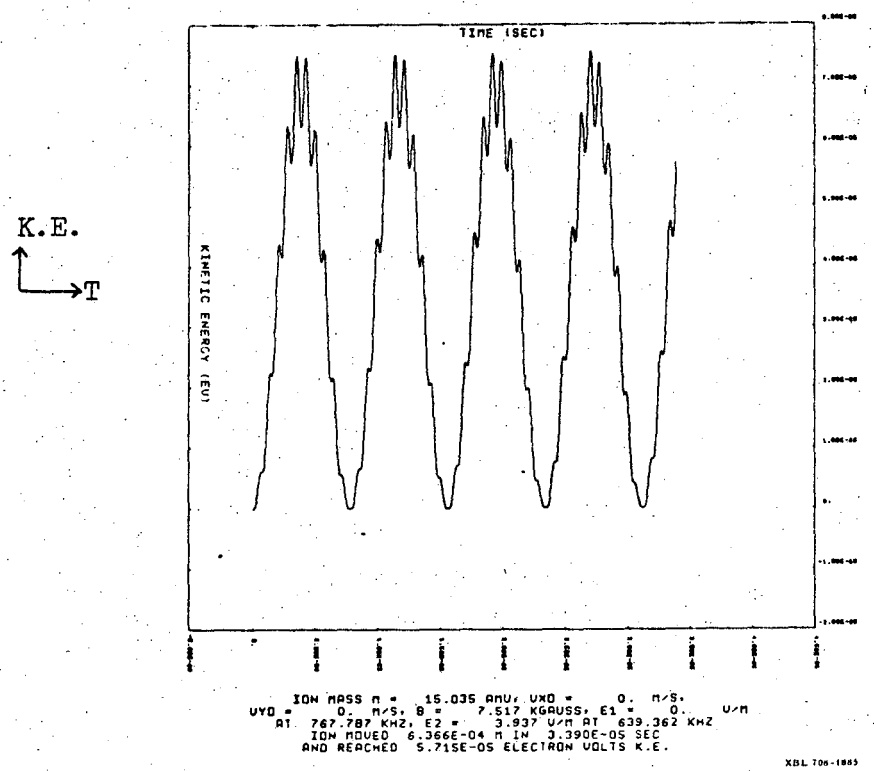

Fig. 2. Non-resonant ion motion.

as an independent way to measure the magnetic field in a NMR experiment. By measuring for protons the ratio of the nuclear magnetic resonance frequency to the ion cyclotron resonance frequency one can determine the proton magnetic moment. This experiment has become today the technique of choice for determining the proton magnetic moment to a high degree of accuracy.[3-5] Almost identical to Lawrence's original particle accelerator design, the modern omegatron gauge[6] is primarily used as a medium to low resolution partial pressure gauge for analyzing residual gases in vacuum systems in the 10^{-5} to 10^{-9} torr pressure range. Ions are formed at the center of the gauge by electron impact upon the gas in the gauge; non-resonant ions remain largely near the center but resonant ions eventually spiral out to the ion collector about a centimeter from the source after having been accelerated to a kinetic energy on the order of hundreds of eV.

A high resolution cyclotron resonance mass spectrometer has recently become available commercially.[7] Its sensitivity is sufficient to detect 8 ions (with signal-to-noise ratio of 1).[8] Its resolution ranges up to about 5000 ($=\frac{M}{\Delta M}$), permitting, for example, satisfactory resolution of O_2^+ and $C_2D_4^+$ peaks when the ions are of comparable abundance. This greater sensitivity stems from two technological advancements which grew out of the development of nuclear magnetic resonance in the 1950's. The first is the application of the marginal oscillator as an energy absorption detector, capable of sensing very small changes in the energy of the ions without having to accelerate them so greatly as in the omegatron. The other development was that of magnetic fields which are intense and highly uniform over

a sufficiently large area to permit separation of the source and detection regions and to allow ions to be drifted slowly but under precise control through the detection region. The mechanism and details of ion drift will be discussed below (sect. II). Separation of the source and analyzer regions largely eliminates the shifting and broadening of the cyclotron resonance absorption caused by the electron beam;[9-11] however, keeping the emission current at about .05 μA or lower is necessary to obtain optimal signal shape and good quantitative data.[11-12]

C. Ion Cyclotron Double Resonance

An additional and powerful method for the identification of ion-molecule reactions which is unique to ion cyclotron resonance is the double resonance technique.[13] Consider a cyclotron resonance experiment in which primary ions P react with neutrals N to form secondary ions S and other products,

$$P \text{ ions} + N \text{ neutrals} \rightarrow S \text{ ions} + \text{other products}.$$

Ion cyclotron double resonance can be performed by applying an electric field $\vec{E}(t)$ with two frequency components instead of one. One component is of low amplitude and of frequency equal to the cyclotron frequency of the product ion S. This is the detector component of $\vec{E}(t)$. The frequency of the other component, called the irradiation component of $\vec{E}(t)$, is swept through a range which includes the cyclotron frequency of the reactant ion P. When these reactant ions are non-resonant, they will have a thermal distribution of kinetic energies and a certain spacial distribution through the cell; but when they are resonant both energy and spacial distributions will change, because upon acceleration

0 0 0 0 3 6 0 3 7 9 3

both v_1 and r will change for each ion. These changes in the reactant ions' distributions alter the distributions for the product ions. The resulting change in signal is taken as indication of the existence of an ion-molecule reaction connecting P with S. The effect is shown schematically in Fig. 3.

The effect of double resonance upon the energy distribution of reactant and product ions has been examined in some detail by Beauchamp.[14,15] He has shown the double resonance signals due to changing reactant ion energies to be proportional to $\frac{dk}{dE}$, the rate of change of the reaction rate coefficient with energy. When changing the reactant ion energies causes the double resonance signal, the signal can be negative only for those reactions which are occurring at thermal energies. Such reactions must be exothermic or thermoneutral. On the other hand endothermic reactions cannot occur at thermal energies (by definition of the term endothermic) hence an endothermic reaction must give a positive double resonance signal or no signal. The relationship between ΔH for a reaction and $\frac{dk}{dE}$ can be summarized as follows:[15]

if $\frac{dk}{dE}$ is	positive or zero	negative
then ΔH	any value	negative or zero
if ΔH is	positive	negative or zero
then $\frac{dk}{dE}$	positive or zero	any value.

Thus in some cases the sign of ΔH can be inferred from the sign of the double resonance signals when the signals are caused solely by increasing the kinetic energy of reactant ions.

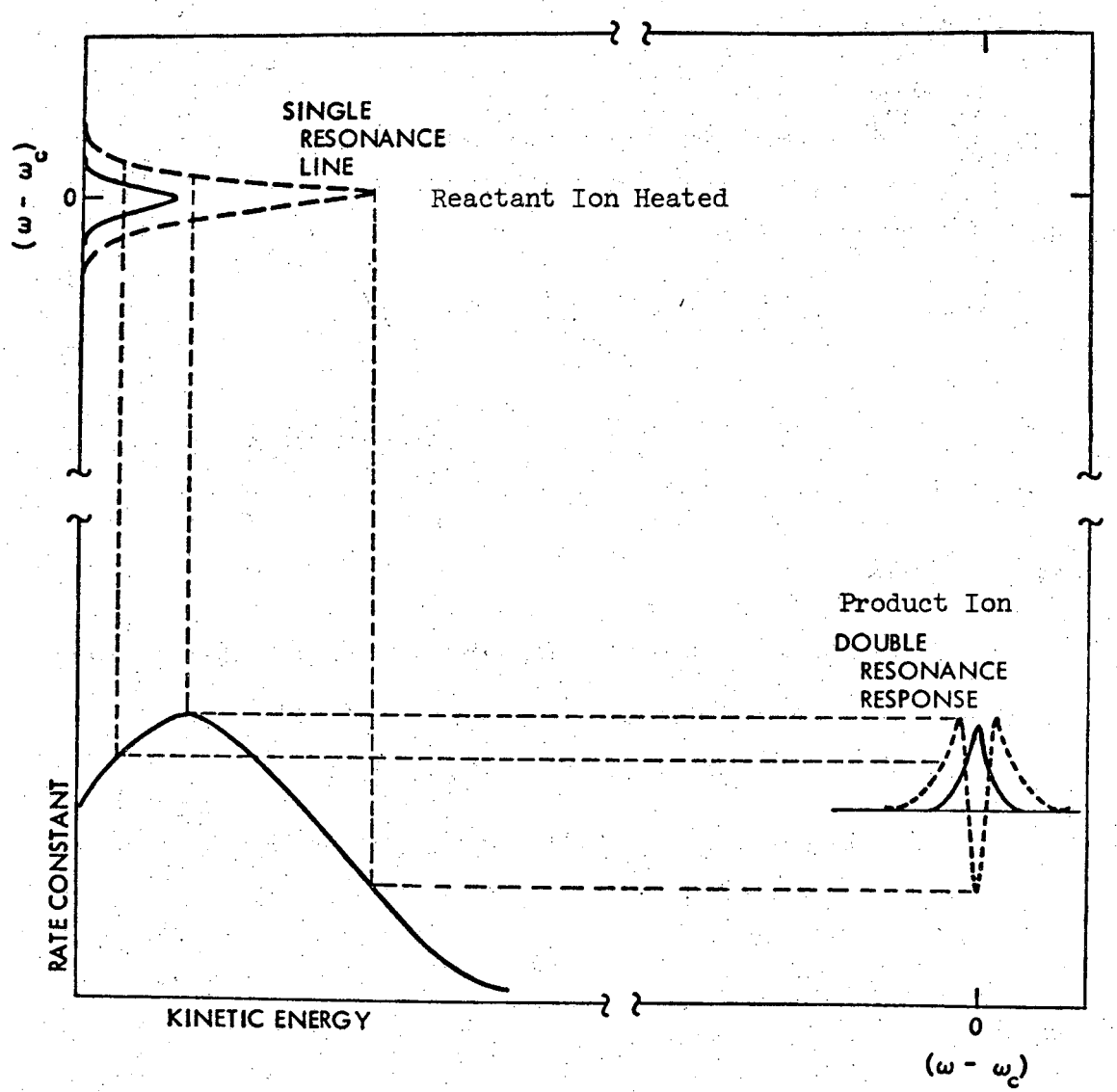

XBL 708-1863

Fig. 3. Absorption of power by a reactant ion increases its kinetic energy. A double resonance response depends on how much effect on the rate of reaction results from heating the reactant ions.

0 0 0 0 3 6 0 3 7 9 4

The effect on the product ion distributions due to altering the spacial distribution of reactant ions is termed "sweep out." If reactant ions are driven from the cell, the smaller number of reactant ions will be reflected in a smaller number of product ions, in proportion to the size of k, rather than $\frac{dk}{dE}$. Unfortunately, sweep-out will give a double resonance signal if the two ions P and S are coupled by the chemical reaction or by some non-chemical effect such as space-charge. Goode, et al.,[16,17] have shown sweep-out effects of both chemical and non-chemical origins are significant relative to the effects dependent on $\frac{dk}{dE}$ over a very wide range of experimental conditions. In spite of these short-comings, however, ion cyclotron double resonance is the most powerful technique available today for establishing what precursor ions are responsible for each product ion species in a system of ion-molecule reactions.

D. Description of the Apparatus

1. Gas Inlet and Flow

Figure 4 shows a schematic of the apparatus. Gas mixtures are prepared on a separate apparatus consisting of a manifold with oil diffusion pump, a mercury manometer for measuring pressures in the 1 to 76 cm range, and a mercury-filled Toeppler pump used to move volumes of gas from one container to another. Detailed discussion of this apparatus will be omitted because the relative portions of each gas comprising a mixture, including contaminants, is determined from low pressure mass spectra obtained from the ICR spectrometer. The container of gas is transferred to the gas storage manifold. If the

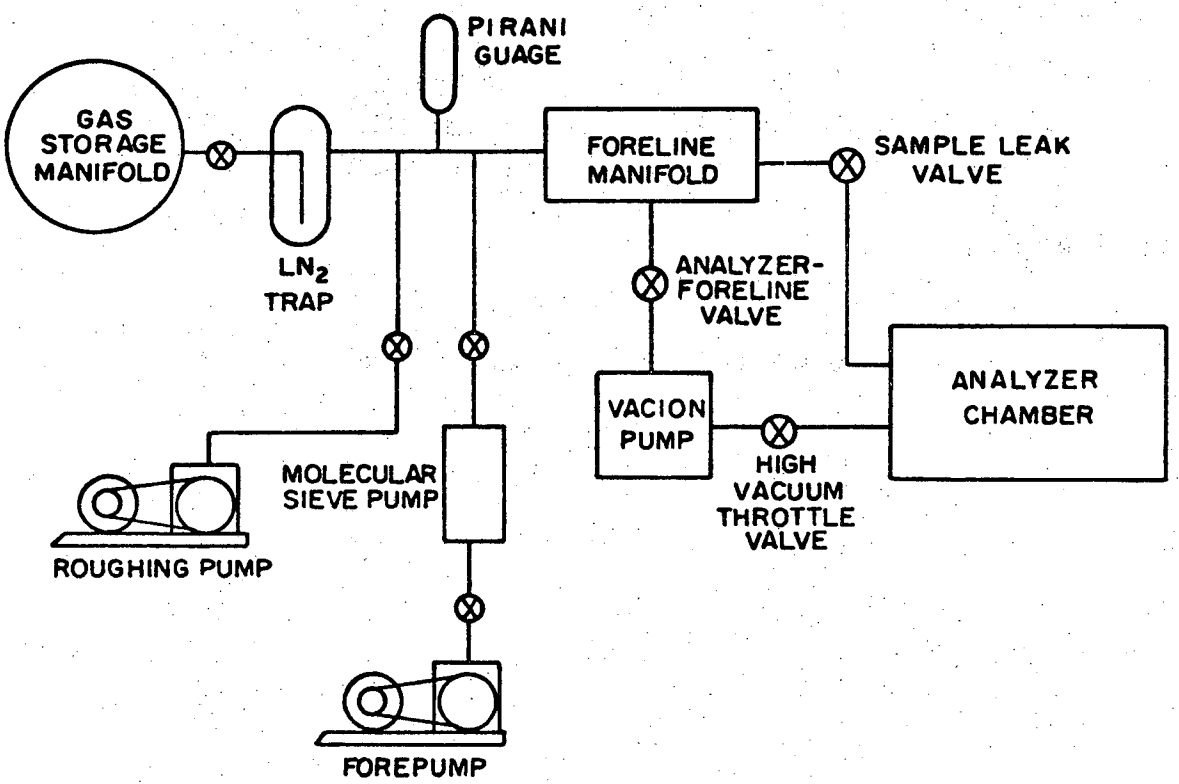

Fig. 4. Schematic of the apparatus.

0 0 0 0 3 6 0 3 7 9 5

container valve is opened slowly, gas will flow hydrodynamicly into the foreline manifold but condensible gases will be most effectively removed by the stainless-steel-wool-filled $1N_2$ trap. A roughing pump and molecular sieve pump are provided to pump out the foreline manifold to 10^{-3} and 10^{-5} torr, respectively. When pumping is shut off the foreline pressure will rise on the order of 10^{-3} torr during the duration of a typical experiment (4-8 hours). This leakage is negligible compared with the 10 to 40 torr typical sample pressure; methane begins to condense in the $1N_2$ trap above 40 torr. The analyzer foreline valve is shut except during maintenance and bake-out procedures. Gas effuses through the sample leak valve into the analyzer chamber; however, since flow out of the analyzer into the Vac-Ion R pump is also effusive, the relative portions of each gas comprising the mixture in the analyzer chamber is the same as that in the foreline manifold. The stainless steel analyzer chamber sits between the poles of the electromagnet. The entire ICR cell is within the analyzer chamber; consequently the gas mixture pervades both source and detector regions of the cell, unlike conventional high pressure mass spectrometers in which only the source contains gas.

2. The ICR Cell

Figures 5 and 6 show the configuration of the ion cyclotron resonance cell. The dimensions are $\frac{1}{2}$ inch by 1 inch by $6\frac{1}{2}$ inches. The electron beam is parallel to the magnetic field $\vec{B}$. The cyclotron frequency of the electron at 14 kgauss is 3.919×10^{10} Hz; therefore

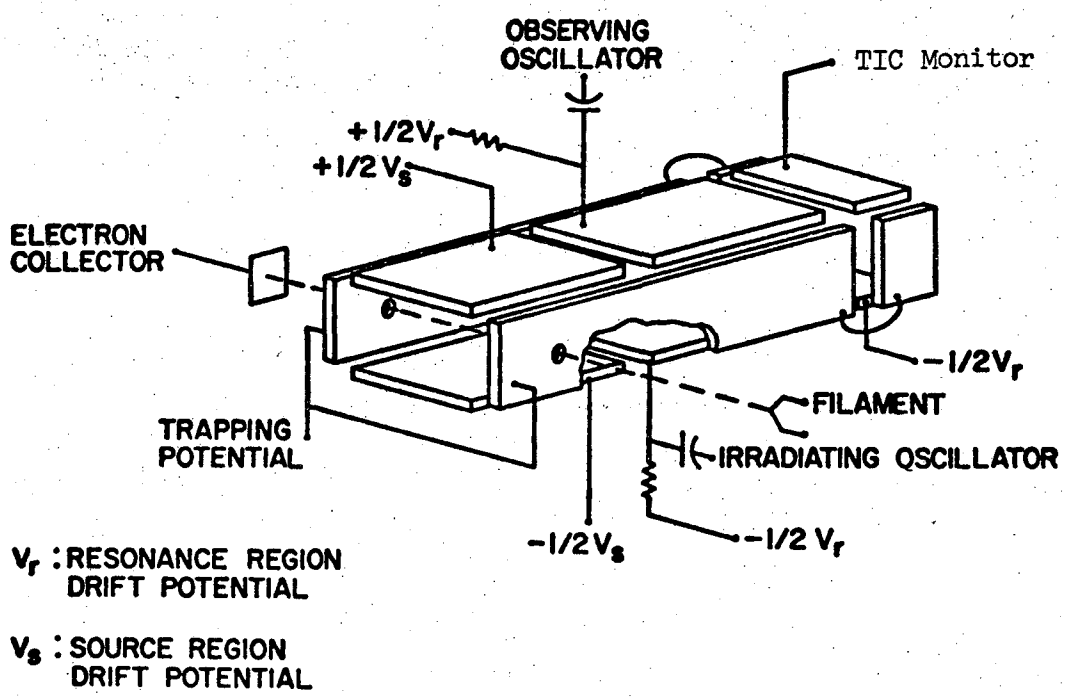

XBL 708-1862

Fig. 5. The ion cyclotron resonance cell.

Typically V_s and V_r are equal.

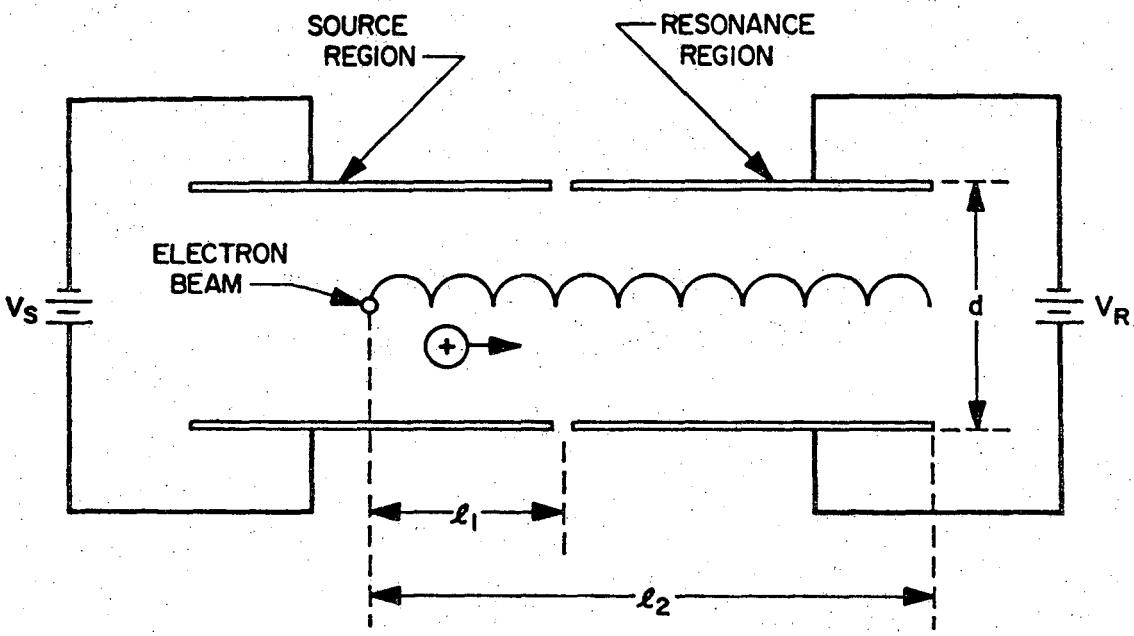

XBL 708-1865

Fig. 6. Side view of ion cyclotron resonance cell, showing exaggerated cycloidal ion drift orbit.

even electrons with $v_\perp = 5.6 \times 10^8$ cm/sec (~70eV) will have orbital radii no more than .0015 cm. A reasonable estimate for the average electron orbit is 2×10^{-4} cm; hence, the electrons' trajectories deviate negligibly from straight lines parallel to the magnetic field. The electron beam is produced by thermal emission from a thorium-oxide-coated irridium filament;[27] the beam is accelerated to the desired ionization energy and collimated by a circular aperture $\frac{1}{64}$ inch in diameter. This narrow cylindrical beam drifts freely through the cell, ionizing some of the gas in its path, and out of the cell to an electron collector. While the ions produced have a $\overset{\text{kinetic}}{\wedge}$ energy distribution which is largely the same as that of the neutral gas (at 300°K), in oxygen as much as a third of the O^+ ions are formed with kinetic energy greater than $\frac{1}{4}$ eV.[18] This is due in large part to dissociative ionization of O_2 to produce fast O^+.[18] That a much larger fraction of such fast ions is lost from conventional mass spectrometers than from the ICR instrument is shown by the fact that the number of O^+ ions relative to O_2^+ ions is about three times as great in the ICR as in a conventional spectrometer. Furthermore about 30% of the O_2^+ ions produced are in the meta-stable $\tilde{a}\,^4\Pi_u$ excited electronic state and about 30% of the O^+ are in the meta-stable ^2D state.[19] Other excited states are produced but they relax to the above-mentioned meta-stable states or the ground state in less than 20 μsec.[19]

Figure 6 shows, greatly exaggerated, the cycloidal drift of ions through the cell. This drift is accomplished by placing dc potentials on the plates which are parallel to the plane defined by the electron beam direction and the desired direction of ion drift. During half

0 0 0 0 3 6 0 3 7 9 7

of an ion's cyclotron orbit this dc potential accelerates the ion and consequently increases the radius of the orbit slightly. During the other half orbit, deceleration reduces the orbital radius. The net result is that the center of curvature of the orbit translates at constant velocity v_d given by

$$v_d = \frac{E_d}{B} \tag{4}$$

where E_d is the dc electric field and B is the magnetic field. Note that the drift velocity is independent of ion mass, velocity, or charge. One can get an idea of the relative magnitude of the ion drift velocity by observing that in order to have a mass resolution on the order of a thousand, the ions must execute on the order of thousands of cyclotron orbits during the time they drift through the detector region. Typically, the 3.5 inch distance l_2 is traversed in .2 to 2 msec. The drift velocity vector will follow a line of equal potential; it is therefore necessary to set the plane of zero potential so that it passes through the electron beam. The effects of electric field fringing on the drift of ions will be discussed later.

A quadrupole trapping potential is applied to the cell to prevent ions from escaping the cell by moving parallel to the magnetic field; ions of the wrong polarity are immediately ejected by the trapping potential. One can see in Fig. 5 that with positive and negative drift potentials applied to the appropriate plates there will result a quadrupole trap when equal trapping potentials are applied to the plates normal to the magnetic field. The effect[20] of this potential

is such as to contribute a small amount to the ion drift velocity, to shift the ion cyclotron resonance absorption frequency by a small amount and to cause the ions in the cell to execute harmonic motion in the direction parallel to the magnetic field. All these effects have been calculated[20] assuming that the trapping potential creates near the center of the cell a simple harmonic oscillator potential. The characteristic frequency, ω_T, of this potential is given by

$$\frac{\omega_T}{2\pi} = \omega_T^o \left(\frac{V_T}{m}\right)^{\frac{1}{2}} \tag{5}$$

where ω_T^o is calculated to be 123.0 kHz when V_T is in practical volts and m in AMU. The shift in the cyclotron frequency is such that

$$\omega_{c,eff} \cong \omega_c(1 - \omega_T^2/2\omega_c^2) \; ; \tag{6}$$

consequently the effect is typically on the order of $\frac{1}{2}\%$. One can use the quadrupole trap as a quadrupole mass spectrometer. This experiment is termed "ion ejection" and is accomplished by adding an r.f. component V_{rf} to the trapping potential. The time required to eject an ion from the center of the cell is

$$\tau_e = 5 \; \mu\text{sec} \left(\frac{m \; V_T}{V_{rf}^2}\right)^{\frac{1}{2}}$$

where V_T and V_{rf} are in practical volts and m in AMU.[20] The resolution of the quadrupole mass spectrometer is very low because the characteristic frequency of motion, typically 20 to 40 kHz, is low, permitting few such oscillations during the 1 msec typical ion lifetime. The

width and center frequency appear to depend on V_{rf} among other things, although a detailed analysis of the parameters involved has not been undertaken. Figure 7 shows two ion ejection spectra in pure oxygen at 3.10×10^{-6} torr. The upper part of Fig. 7 shows the O^+ signal detected by the marginal oscillator at 614 Kc when the magnetic field is at 6.545 Kgauss. As the frequency of the ion ejection field is swept from 20 to 45 kHz, the signal due to O^+ drops at 39.50 KHz to about 79% of its value with no ejection. Similarly, O_2^+ detected at 614 Kc and 12.935 Kgauss drops at 27.93 KHz to about 61% of its value with no ejection. O_2^+ is relatively more strongly ejected because it drifts through the cell more slowly, and is therefore exposed to the ejecting field longer. The data obtained from Fig. 7 will be used later to identify reactants ions in an experiment analogous to ion cyclotron double resonance. One can see that by using an ejecting rf field of low intensity one can eject 20 to 40% of the ions of a given species without adding very much kinetic energy to the ions. Although the resolution is very low, the resulting ion ejection double resonance gives a decrease in product ion intensity that depends upon the rate of the reaction k (and not upon $\frac{dk}{dE}$).

Drift and trapping potentials are applied to a short third section of the icr cell. This is done so that the ions will not simply stop drifting when they move out of the analyzer region. Were they allowed to do so they would still be within sufficient proximity to the detector to produce signals; their space charge would shift and broaden the signals due to ions still within the detector region. Furthermore, drifting the ions into a collector plate provides a convenient monitor of the pressure in the cell. This plate is connected

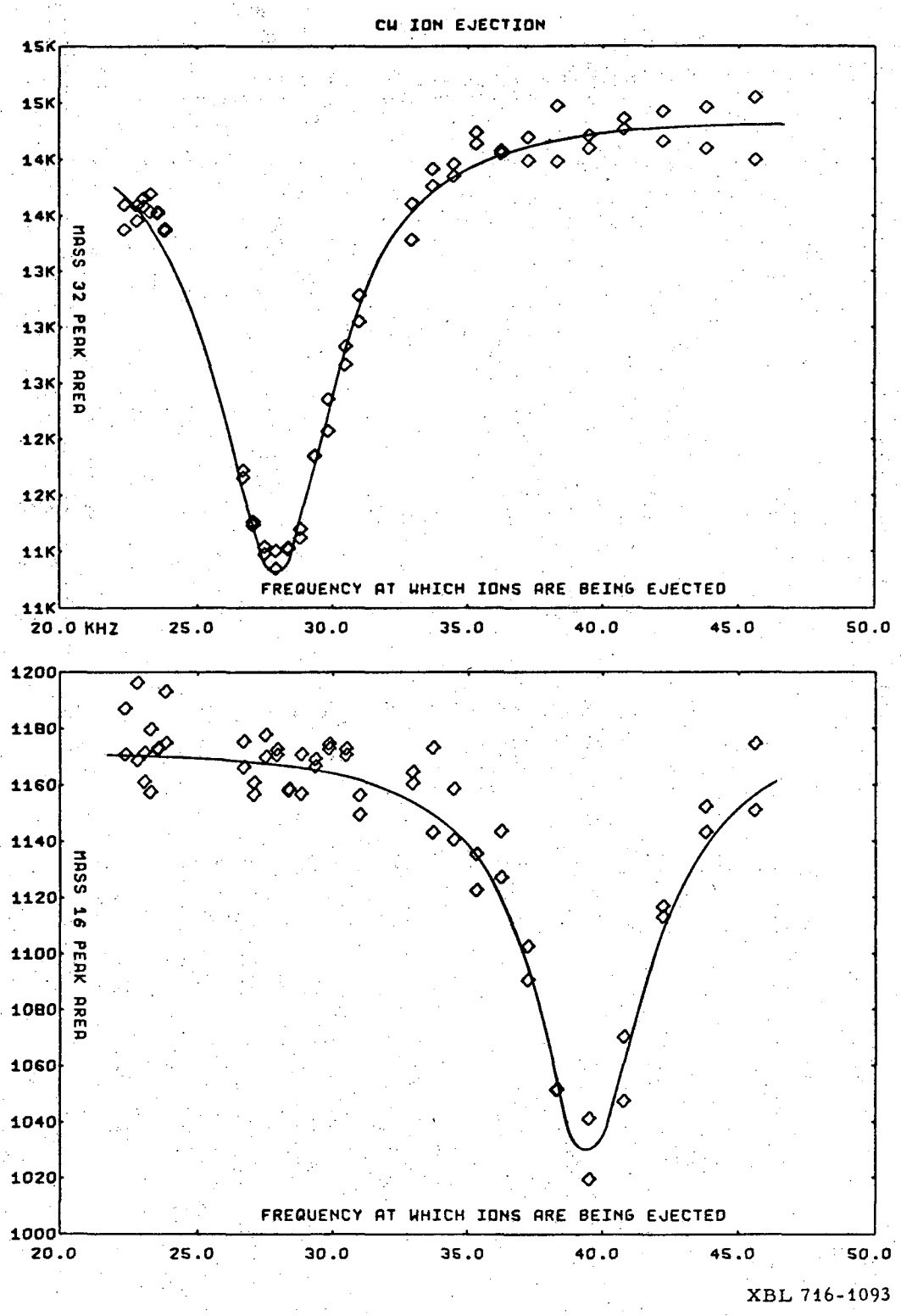

Fig. 7. Ion ejection spectra for O_2^+ (top) and O^+ (bottom) in pure oxygen.

0 3 0 0 3 6 0 3 7 9 9

through an electrometer to ground. Because the plate is thus essentially at ground potential all ions formed near ground potential will be collected. When the drift potentials are low so as to obtain good shape and resolution of the ion cyclotron resonance signals, one finds that large fractions of the ions formed in the ion source fail to be collected by the ion current monitoring plate. It appears that they simply drift past the plate without striking it; it does not seem likely that the low ion current measured at low drift and trapping potential is due to loss of ions to the cell walls because such ion losses would have been appreciable when the ions were passing through the detector region and would have been detectable. As drift and trapping potentials are increased the monitored ion current rapidly approaches an asymptote referred to as the "total ion current" (TIC). Figure 8 shows that the area under the mass 32 peak in pure oxygen is directly proportional to the TIC. In pure oxygen at pressures up to about 3×10^{-5} torr, O_2^+ is almost entirely a primary ion; addition or loss of O_2^+ due to ion-molecule reactions is negligible. Therefore the number of O_2^+ ions being detected is proportional to the pressure. That the peak area is proportional to the number of ions being detected will be shown later. Consequently, Peak Area (32) $\propto$ O_2 pressure, proves in Fig. 8 that the TIC is directly proportional to the O_2 pressure.

3. Techniques of Modulation

In order to provide needed enhancement of the signal over noise, the resonance power absorption is modulated at 200 Hz. Because the marginal oscillator senses this power absorption, the output of the marginal oscillator will be modulated at 200 Hz. This output is lock-in detected by a Princeton Applied Research JB-4 phase sensitive detector. By operating the JB-4 in the internal mode, the same 200 Hz

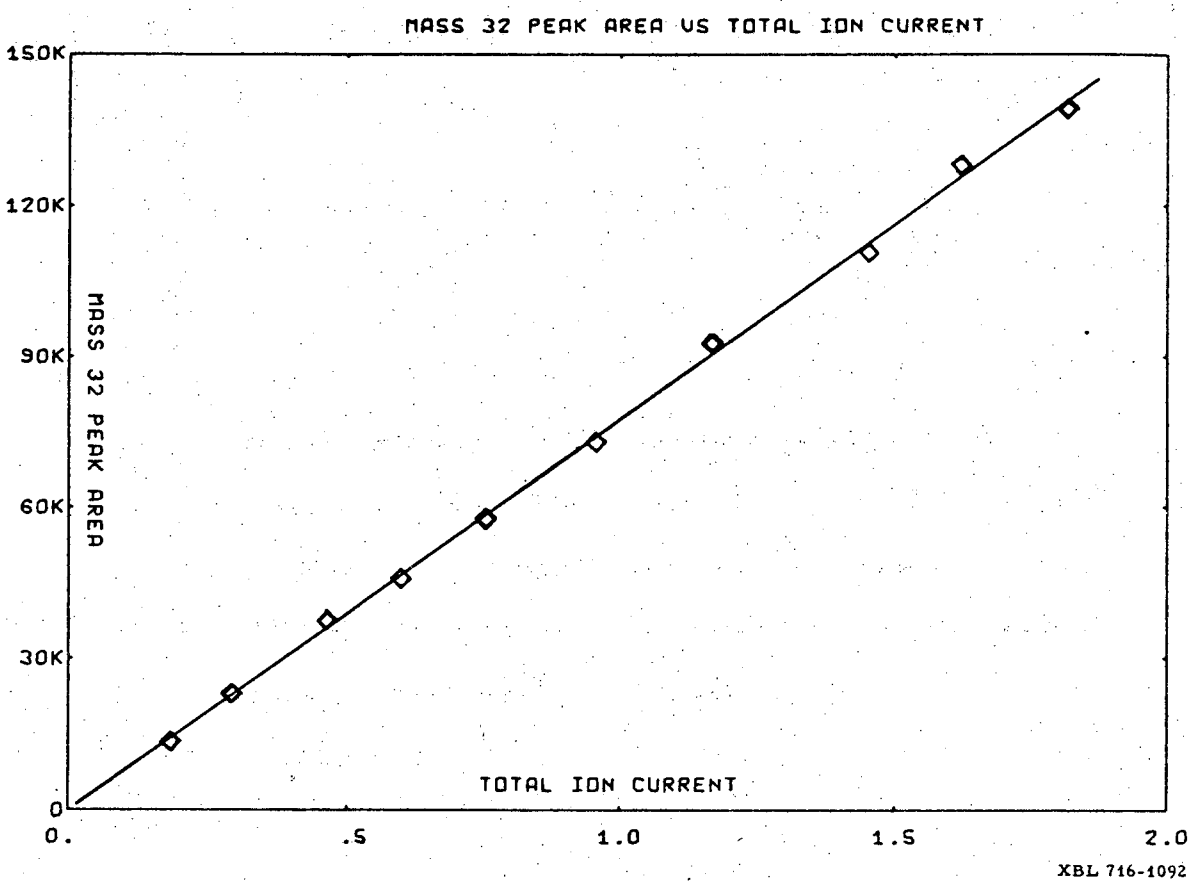

Figure 8. Mass 32 peak area versus TIC (in units of 10^{-10} Amp) in pure oxygen. Solid line is straight and has zero intercept. Mass 32 peak area is proportional to TIC because TIC is proportional to oxygen pressure. Peak area is derived from ICR mass spectra in the pressure range up to about 3×10^{-5} torr.

0 0 0 0 3 6 0 . 0 0 0

signal which references the JB-4 can be used to cause the modulation of the resonance power absorption. Any experimental parameter can be modulated in order to achieve modulation of the resonance power absorption but only a few will be discussed.

a. Magnetic Field Modulation

By placing two small magnetic field modulation coils on the pole caps of the large magnet which provides the intense d.c. field, and by passing the amplified reference signal (about 80 watts of power) through these coils, the d.c. magnetic field can be augmented by a small (0-25 gauss) ac component. With the ac component's amplitude fixed at some small fraction of the width of the cyclotron resonance absorption to be measured, the dc component is then swept at a fixed rate through the appropriate range. The resulting lock-in detected signal is the derivative of the actual bell-shaped cyclotron resonance absorption peak. One can achieve the bell-shaped peak rather than the derivative by fixing the dc magnetic field and sweeping the amplitude of the ac component; however, this method is impractical because the ac component should be a square wave, the range of sweep possible is limited and the dc magnetic field regulation circuitry tends to "track" with the modulation at high amplitude. There are difficulties attendant to normal magnetic field modulation as well. The derivative of the power absorption signal can easily be measured to determine the width and height of the signal itself, however, the product of width and height is related to the area only if the signal shape is consistent. Because the derivative of the peak is observed, small deviations of the peak itself are accentuated. The derivative of the peak is not easily integrated electronicly. The amplitude of the derivative of the peak is dependent on the rate at which the dc magnetic field is swept.

b. Drift Potential Modulation

By drifting ions very rapidly through the cell half of the time, one can obtain a peak which is the difference between power absorption when the ions spend a lot of time in the cell and very little time. For practical reasons it is not possible to drift the ions through the cell so fast that negligible power absorption occurs. Consequently signal shape is complex and it is difficult to extract data from the signals one gets.

c. Electron Energy Modulation

The modulation method of choice is electron energy modulation.[21] Typically, the kinetic energy which electrons have as they enter through the beam collimating aperture is square wave modulated between 70 eV and about 14 eV. Because 14 eV is below the appearance potential of all positive ions in the methane-oxygen system, the electrons pass through the cell without producing any ions and without causing other excitation except in a quite negligible minority of the neutral molecules. The square wave rises and falls in about 2% of the time it is constant at 70 volts. The beam energy is modulated between 70 and 14 volts rather than say 70 and 4 volts in order to minimize any pile-up of electrons in the region outside the cell between the filament and the beam collimating aperture. Even so, a space charge does build up and causes a slight modulation of the emission current. However since virtually all ionization occurs during the 70 volt portion of the cycle, only the emission current of electrons having this energy is important; consequently the slight modulation of the emission current is very easy to correct for.

0 0 0 0 3 6 0 3 0 1

d. Pulsed Ion Cyclotron Double Resonance

The cyclotron double resonance experiment has been described earlier. Proper conditions are found which center on the cyclotron resonance absorption of power from the marginal oscillator at frequency ω_{MO} by a given product ion S, then modulation stops. Now a second r.f. electric field is added to that which ions experience and the amplitude of this field is modulated so that when a species of reactant ions P absorbs energy from the field, the kinetic energy or spacial distribution of that species is modulated. Finally the ion-molecule reaction communicates the modulation to product ions so that the resonance power absorption from the marginal oscillator is modulated. Cyclotron double resonance in which the second r.f. field is operated continuous wave (CW) while another parameter, say electron energy, is modulated carries precisely the same information as pulsed double resonance. Figure 9 shows a CW cyclotron double resonance experiment in which electron energy is modulated, while the irradiating oscillator frequency is swept from 250 to 1000 KHz. The ions being detected by the marginal oscillator at 614 KHz are mass 15 in pure methane. While mass 15 is predominantly a primary ion, CH_3^+, one can easily see that it has other components. The deduced assignments are:

Signal	Freq.	Reaction	ΔH
17 → 15	542 KHz	$CH_5^{+*} + CH_4 \rightarrow CH_3^+ + H_2 + CH_4$	See ref. 22
16 → 15	576 KHz	$^{13}CH_3^+ + CH_4 \rightarrow CH_3^+ + {}^{13}CH_4$	0
14 → 15	658 KHz	$CH_2^+ + CH_4 \rightarrow CH_3^+ + CH_3$	-22 kcal /mole

One can see sharp artifacts when the irradiating oscillator is at various harmonics of the marginal oscillator. It is clear from Fig. 9 that double resonance does not have to have amplitude modulation of the

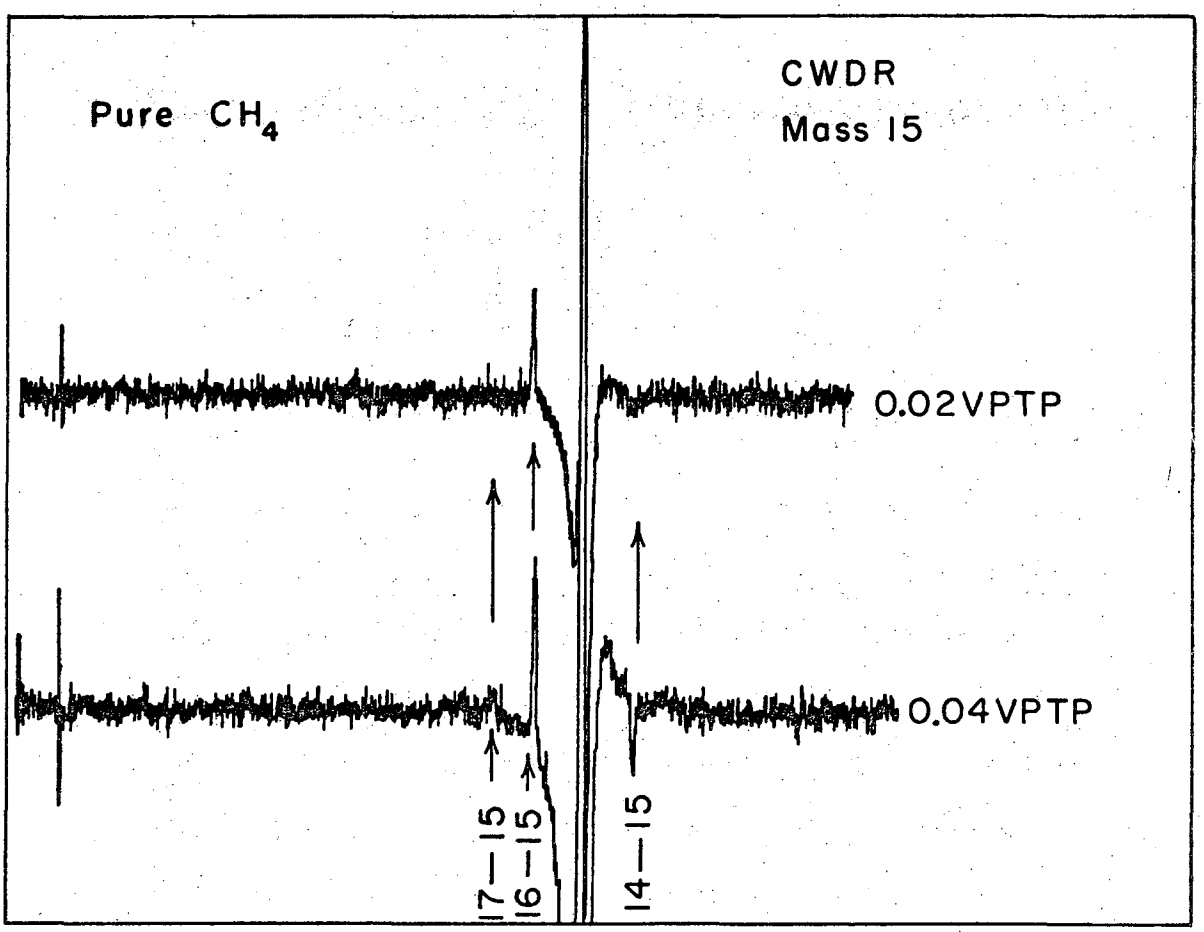

XBL716-3725

Fig. 9. Cyclotron double resonance. While detecting mass 15 ions in methane with marginal oscillator at 614 KHz, irradiating oscillator is swept from 250 to 1000 KHz. Irradiating oscillator amplitude is 0.02 practical volts peak-to-peak (VPTP) and 0.04 VPTP for the two scans. Irradiation gives reactant ions average center of mass kinetic energy on the order of 1/2 and 1 eV, respectively.[16]

0 0 0 0 3 6 0 3 8 0 2

irradiating electric field.

e. Pulsed Ion Ejection

Ion ejection double resonance experiments as discussed above have been performed in both CW and pulsed modes in this laboratory and elsewhere.[23] As with cyclotron double resonance, both modes convey the same information. Figure 7 really should be called ion ejection self double resonance, inasmuch as some O^+ ions are resonance ejected by a r.f. trapping field of 39.50 KHz while the marginal oscillator cyclotron resonance detects O^+ ions at 614 KHz.

E. Quantitative Measurement of Thermal Ion-Molecule Reaction Rates

This section describes the experimental parameters which govern the shape and intensity of the signals observed for each ion and how the parameters are measured.

1. Theory of Ion Cyclotron Resonance Lineshape

While an ion is absorbing power in resonance with the r.f. electric field, the rate at which its kinetic energy changes $\frac{dE}{dt}$ is given by the power (A) which is absorbed:

$$A = \frac{dE}{dt} \tag{8}$$

If n^+ ions are initially thermal and absorb energy during the course of time τ then we can integrate (8) to get,

$$E = \frac{A \cdot \tau}{n^+} + \frac{3}{2} KT \tag{9}$$

where K is Boltzmann's constant and T is the temperature. If power

absorption continued for a very long time the absorption by non-resonant ions would average to zero. Any process which interrupts the absorption of power broadens the frequency range for which the average power absorption will be non-zero. Beauchamp[14] has derived the equation for the linewidth when collisions of ions with neutral gas molecules interrupts the power absorption. He has shown that

$$A(\omega) = \frac{n^+ q^2 \mathcal{E}_o^2 \tau}{4m} \frac{1}{1 + \tau^2(\omega-\omega_c)^2} = \frac{n^+ q^2 \mathcal{E}_o^2 \tau}{4m} L(\omega,\omega_c,\tau) \qquad (10)$$

where $A(\omega)$ is the power absorption by n^+ ions of mass m, charge q, and cyclotron frequency ω_c from the r.f. electric field of amplitude $\mathcal{E}_o$ and frequency ω and where τ is the mean free time between collisions. The function $L(\omega,\omega_c,\tau)$ is a Lorentzian lineshape function whose maximum, Lo, is unity when $\omega=\omega_c$, and which has half width at half height of $1/\tau$ and area π Lo/τ. Combining (9) and (10) at $\omega=\omega_c$ we get

$$E = \frac{3}{2} KT + \frac{q^2 \mathcal{E}_o^2 \tau^2}{4m} \quad , \qquad (11)$$

which is the energy a resonant ion reaches after being heated for time τ. In order to detect thermal ions $\mathcal{E}_o$ must be kept small so that the second term in 11 is negligible. Butrill[24] has examined the broadening which results from interrupting power absorption by drifting the ions out of the cell. He found that the signals retained the Lorentzian line shape but that the width increase linearly with the drift velocity of the ions in the resonance region of the cell. At low drift velocity he found that the linewidth became constant and he attributes this intrinsic width to stray electric fields in the cell. Thus the width of the ion cyclotron resonance lines $\frac{1}{\tau}$ depends upon elastic and reactive collision frequency, ion drift velocity, and any other parameter which interrupts power absorption. We can get n^+/m from (10) by determining the area

0 0 0 0 3 6 0 3 0 3

under the absorption curve or the product of peak height $A(\omega=\omega_c)$ and width $1/\tau$:

$$\frac{A(\omega=\omega_c)}{\tau} = \frac{n^+ q^2 \mathcal{E}_o^2}{4m} \propto \frac{n^+}{m} \quad .$$

That the area under the absorption peaks is proportional to n^+/m when the peak shapes deviate somewhat from the Lorentzian line shape has been well established (Refs. 8, 11, 12, 16; see also Fig. 8).

2. Chemical Kinetics

The number of ions of each species i in the cell can be gotten as the integral of the current of that sort of ions j_i over the length of time the ions spend in the cell:

$$n_i^+ = \int_{\tau}^{\tau'} j_i(t)dt \quad ,$$

where τ and τ' are respectively the time at which the ions enter and leave the analyzer region of the cell. The rate at which the current of a given sort of ion changes is gotten by balancing the loss and gain processes for that ion due to reaction:

$$\frac{dj_i(t)}{dt} = -j_i(t) \sum_{l}^{\substack{\text{all} \\ \text{neutrals}}} n_l \sum_{m}^{\substack{\text{all} \\ \text{ions}}} k_{ilm} + \sum_{l}^{\substack{\text{all} \\ \text{neutrals}}} n_l \sum_{m}^{\substack{\text{all} \\ \text{ions}}} j_m(t) k_{mli} \qquad (12)$$

where k_{abc} is the rate coefficient for the reaction of ion a with neutral b, having number density n_b, to produce product ion c. j_i is an ion current in units of ions per second; if k_{ilm} be expressed in units of cm^3/molec-sec then n_l will have units of number of neutral molecules per cm^3. In the simple case in which a single reaction is the only source of product s and the only loss of reactant p, (12) can be integrated immediately to give

$$n_p^+ = \frac{j_p(t=0)}{nk}\left[\exp(-nk\tau_p) - \exp(-nk\tau'_p)\right]$$

and (13)

$$n_s^+ = \frac{j_p(t=0)}{nk}\left[nk(\tau'_s - \tau_s) + \exp(-nk\tau'_s) - \exp(-nk\tau_s)\right] ,$$

where n_p^+ is the total number of primary ions in the cell, n_s^+ is the number of secondary ions and n is the number density of neutral reactants. Equation (4) gives drift velocity inversely proportional to magnetic field; hence for fixed magnetic field drift time will be proportional to mass:

$$\frac{\tau_s}{m_s} = \frac{\tau_p}{m_p} \quad \text{and} \quad \frac{\tau'_s}{m_s} = \frac{\tau'_p}{m_p} \tag{14}$$

When the arguments of the exponentials are small, 13 can be simplified by using 14 to get

$$\frac{m_p^2 n_s^+}{m_p^2 n_s^+ + m_s^2 n_p^+} = \frac{m_p A_s}{m_p A_s + m_s A_p} \approx \frac{1}{2} nk(\tau_p' + \tau_p) , \tag{15}$$

where A_s and A_p are areas under the secondary and primary ions peaks, respectively. Equation (15) has been used extensively to extract thermal ion-molecule reaction rate coefficients from ion cyclotron resonance data.[11,17,23,24] Figure 10 shows data from this laboratory for the reaction $N_2^+ + D_2 \rightarrow N_2D^+ + D$ for which we determine $k = 1.60 \times 10^{-9}$ cm^3/molec-sec by a least squares fit of Eq. (13) to the data. The solid curve in Figure 10 is determined from Equations (13); the slope of this curve near the origin, $\frac{1}{2}$ nk, is much different

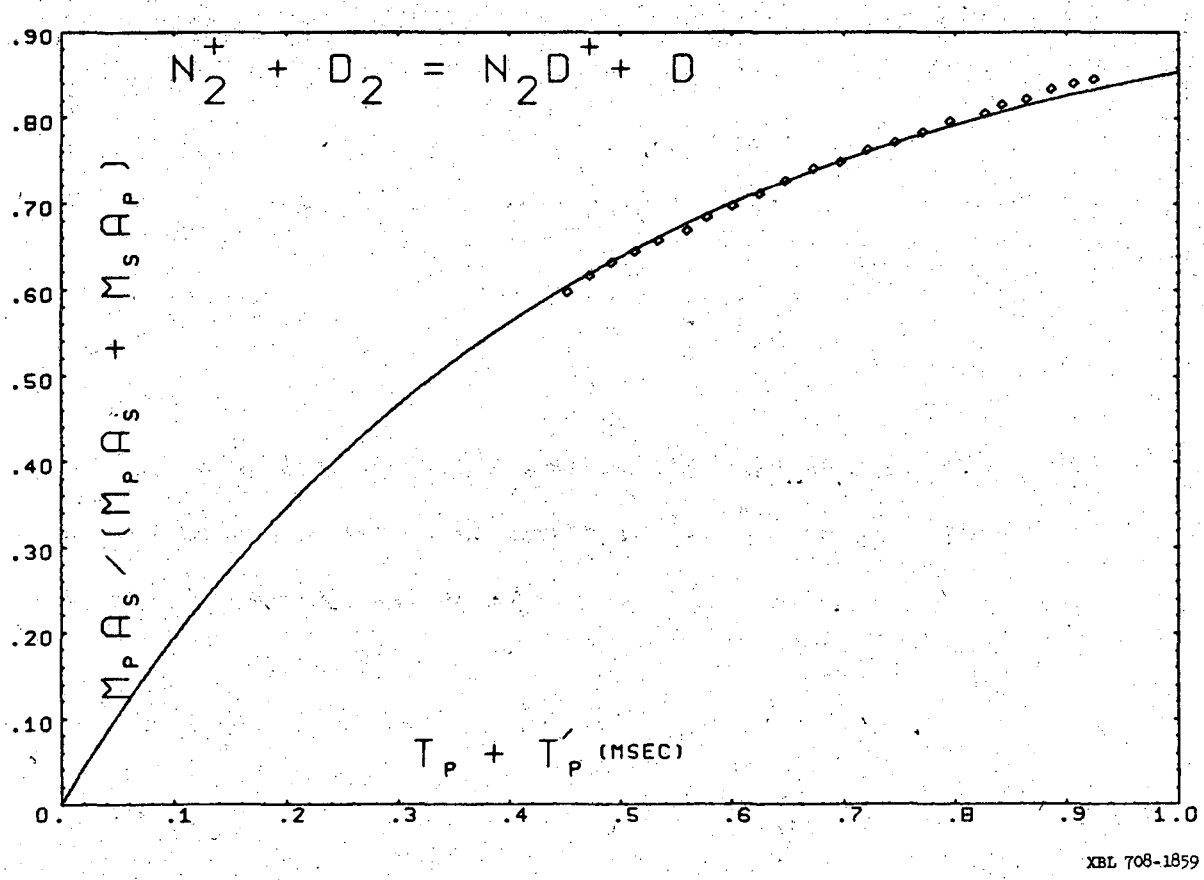

Fig. 10. Quantitative measurement of the rate of $N_2^+ + D_2 \rightarrow N_2D^+ + D$. The rate is determined to be 1.60×10^{-9} cm^3/molec-sec, in good agreement with earlier determinations.[29a-e]

from the slope of a straight line fitted to the data, showing that the approximation (15) should be limited to data for which $m_p A_s/(m_p A_s + m_s A_p)$ is less than about 0.3. Equation (15) does make it clear that the relative size of primary and secondary peak areas is governed by the two variables, reactant neutral density and reaction time.

3. How Ion Drift Time Is Determined

Fringing of electric fields within the cell results from the fact that potentials are applied to finite plates rather than infinitely extended planes. We examine in this section the effect on the ion drift times on the fringing of the electric fields used to drift ions through the cell.

Figures (11-13) show calculated contours of equal drift electric field. These contours are calculated by numerically solving Poisson's equation in two dimensions:

$$\vec{\nabla}^2 \phi + \rho = 0 \qquad (16)$$

where ϕ is the scalar electric potential at each point (x,y) and ρ is the charge density distribution. Also shown is a narrow rectangle near the horizontal center line of the cell, showing the relative position of most of the ions. This rectangle is actually the "shadow" of the electron beam which passes through the source region, but since thermal ions' orbits are small relative to the size of this rectangle we can take it as a good estimate of the height and width of the sheet of ions which drifts out of the source region and through the analyzer region. Solving (16) in two dimensions makes the incorrect assumption

0 0 0 0 3 6 0 8 5

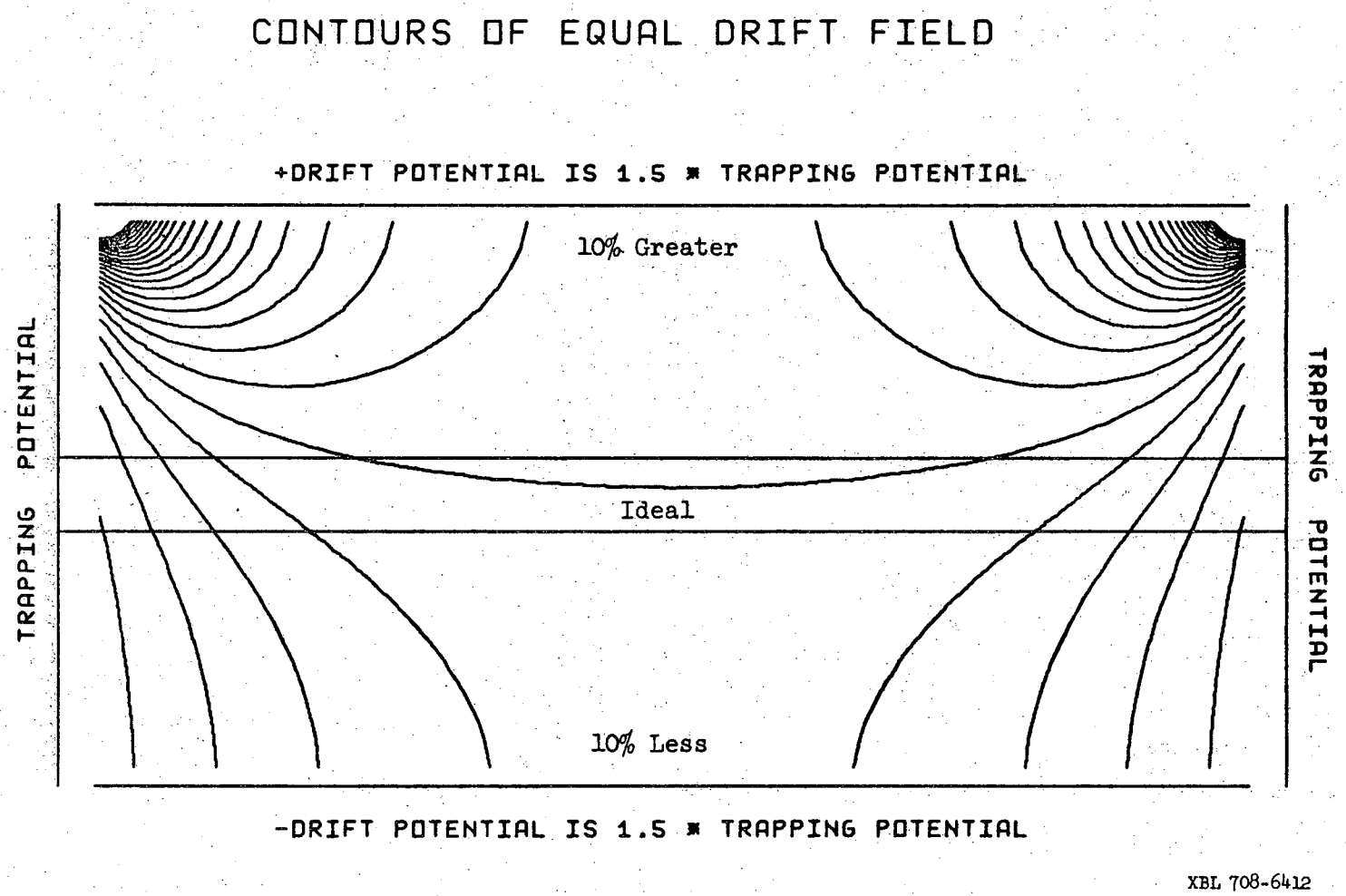

Fig. 11. The dc electric field which causes ions to drift through the cell is nearly ideal for ions near the center of the cell.

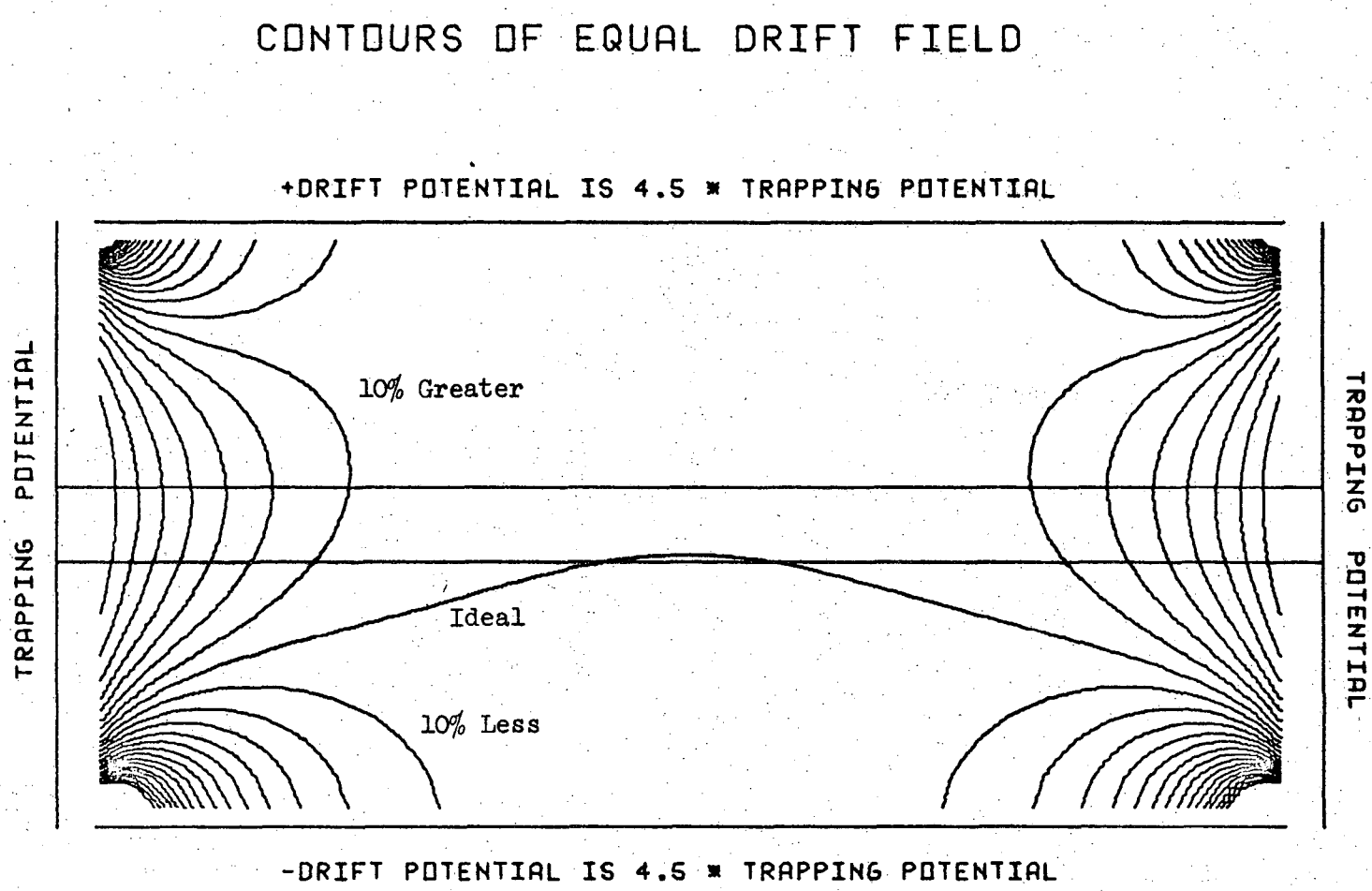

Fig. 12. The dc electric field which causes ions to drift through the cell.

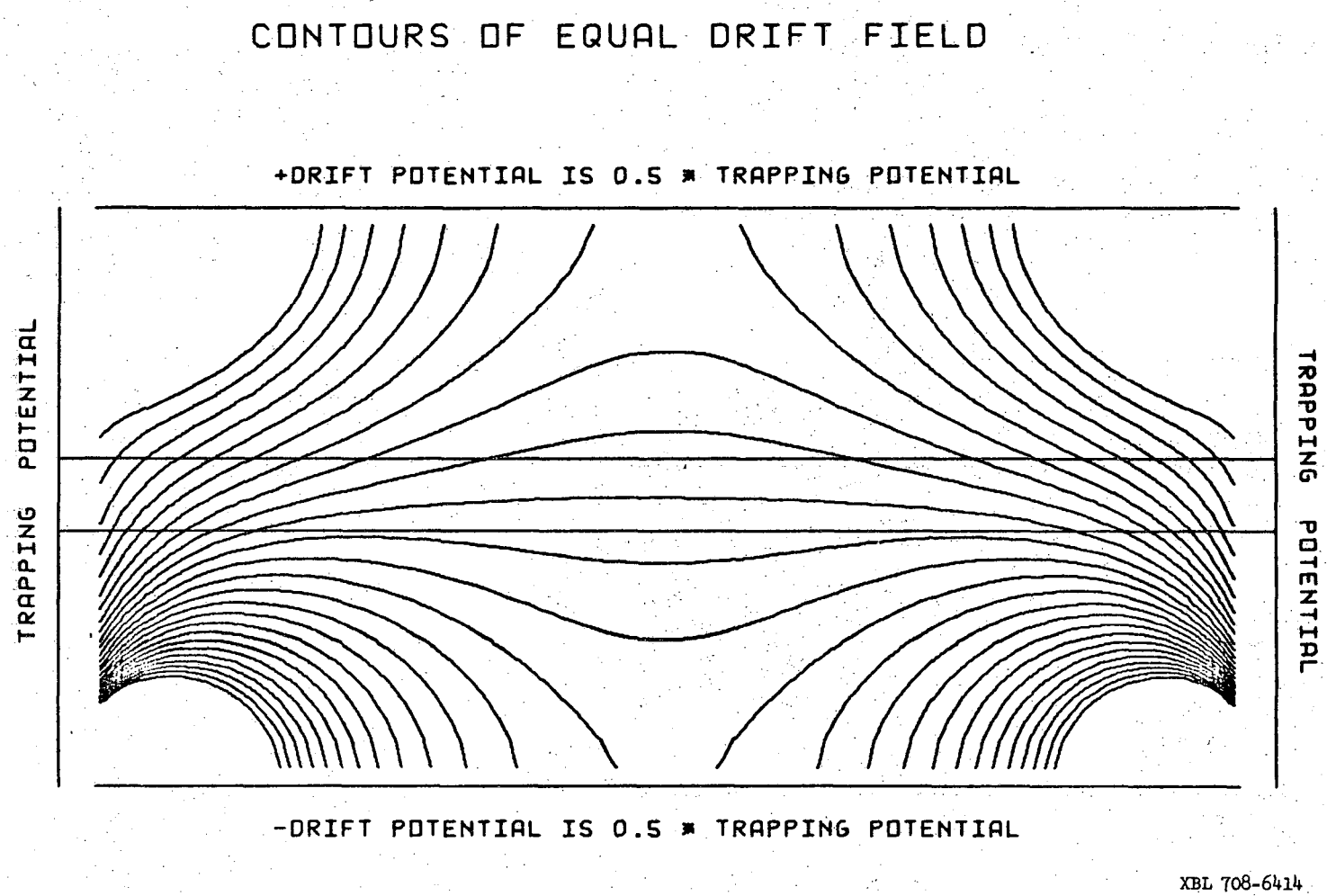

Fig. 12. The dc electric field which causes ions to drift through the cell.

that the cell is $\frac{1}{2}$ inch thick, 1 inch wide and infinitely long. However, because the cell extends 1 inch at each end beyond the actual path which ions follow from electron beam through analyzer region, the actual potentials the ions experience are well approximated by the infinitely long cell of finite width and thickness. So long as the electron beam emission current is kept at about .05 μA or lower, the calculated effect of any non-zero charge density is negligible. Figures 11-13 are calculations for $\rho \equiv 0$. The drift electric field is determined as the gradient of the potential in the direction normal to the drift plate. As expected, the contour which passes near the center of the cell in Figs. 11-13 is the value of the electric field which the infinitely-extended-planes ideal predicts. Since the thin rectangle half-way between the drift plates is the approximate extent of the sheet of ions, one can see from these figures that for the most part, ions experience drift fields which are approximately the ideal.

We can determine empirically what drift fields the ions experience on the average. Figure 14 shows a schematic of the experiment we used. A square wave is generated by an Exact Model 255 wave generator. This square wave is used as a timing reference for a brief pulse of ionizing electrons. The resulting pulse of ions are allowed to drift down the cell under the influence of measured potentials applied to each plate on the cell. Because the ions experience different drift

0 0 0 0 3 6 0 3 8 0 7

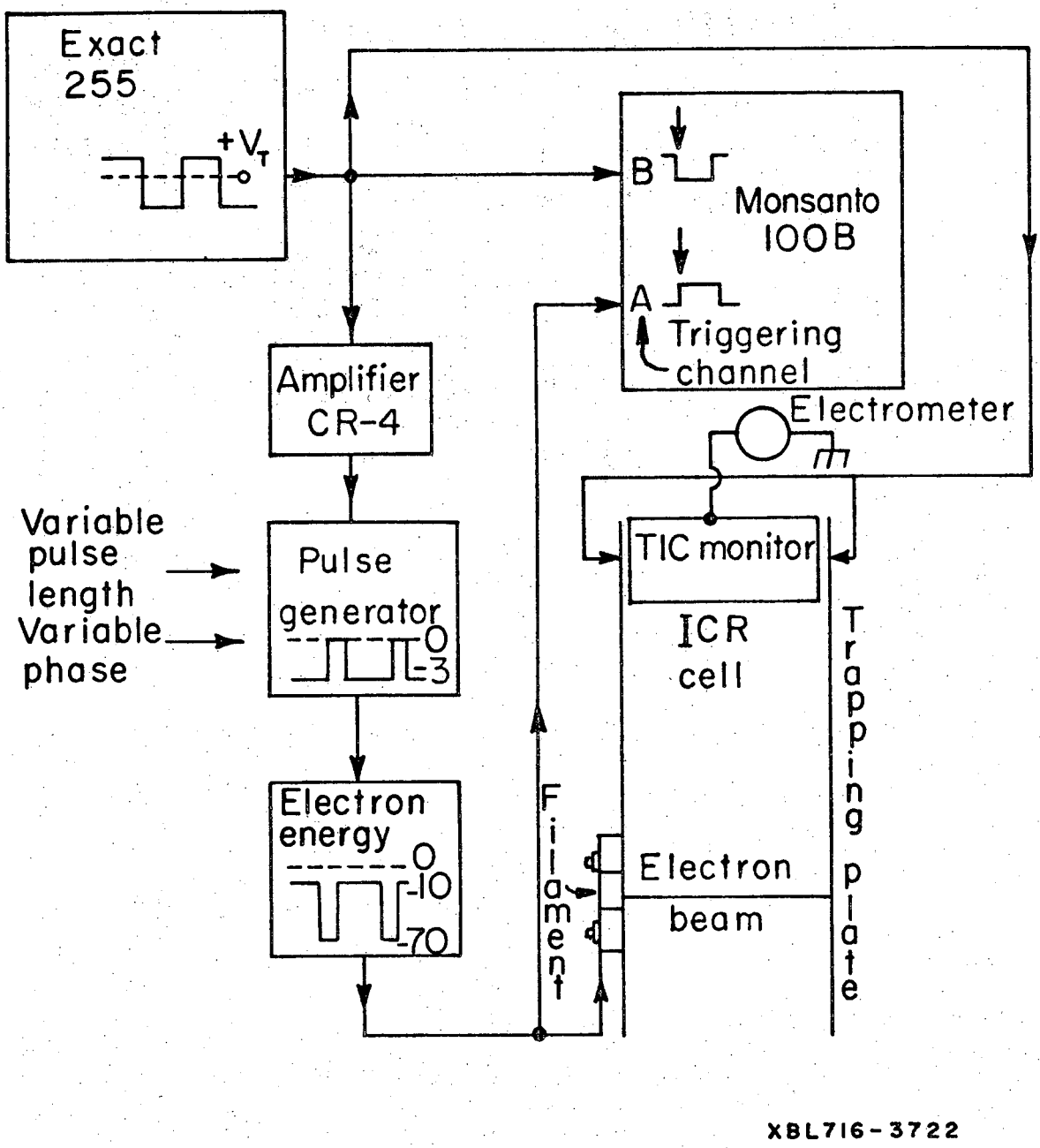

Fig. 14. Experimental determination of ion drift time. Trapping voltage $+V_T$ is maintained while short pulse of ions drift from electron beam to TIC monitor. When trapping potential goes suddenly negative, any ions still in the cell are swept out to trapping plates.

fields depending on the precise trajectory each follows through the cell, some ions will arrive at the TIC monitoring plate early and some late. When half the ions have arrived, the trapping potential (supplied by the Exact 255) drops suddenly to a negative value and ions are immediately swept out of the cell without reaching the TIC monitoring plate. A Monsanto 100B counter is used to keep track of the length of time it required for half the ions to drift from source to TIC monitoring plate. Figure 15 shows the results one such experiment. The solid line is the prediction assuming that the average potential experienced is the infinite-plane ideal. Since we are interested in studying ion-molecule reactions over the entire range shown in Fig. 15 we shall have to use empirically determined drift times rather than calculate them. The experiment above was also used to determine how broad is the distribution of drift times about the average value. The half width at half height of the distributions is about 50 μsec at 211 μsec average, about 31 μsec at 577 μsec and about 24 μsec at 965 μsec. Thus the distribution is sharpest at the greatest drift times and the width of the distribution drops from about 50%(FWHM) at short drift time to only about 1% at long drift time.

4. How the Neutral Density is Determined.

We now have two methods for determining the density of neutrals in the cell:

1. We measure the total ion current, TIC, and the electron emission current, je, and relate them to n by 17:

$$n = \frac{j_{ion}}{j_e \sigma \ell} \qquad (17)$$

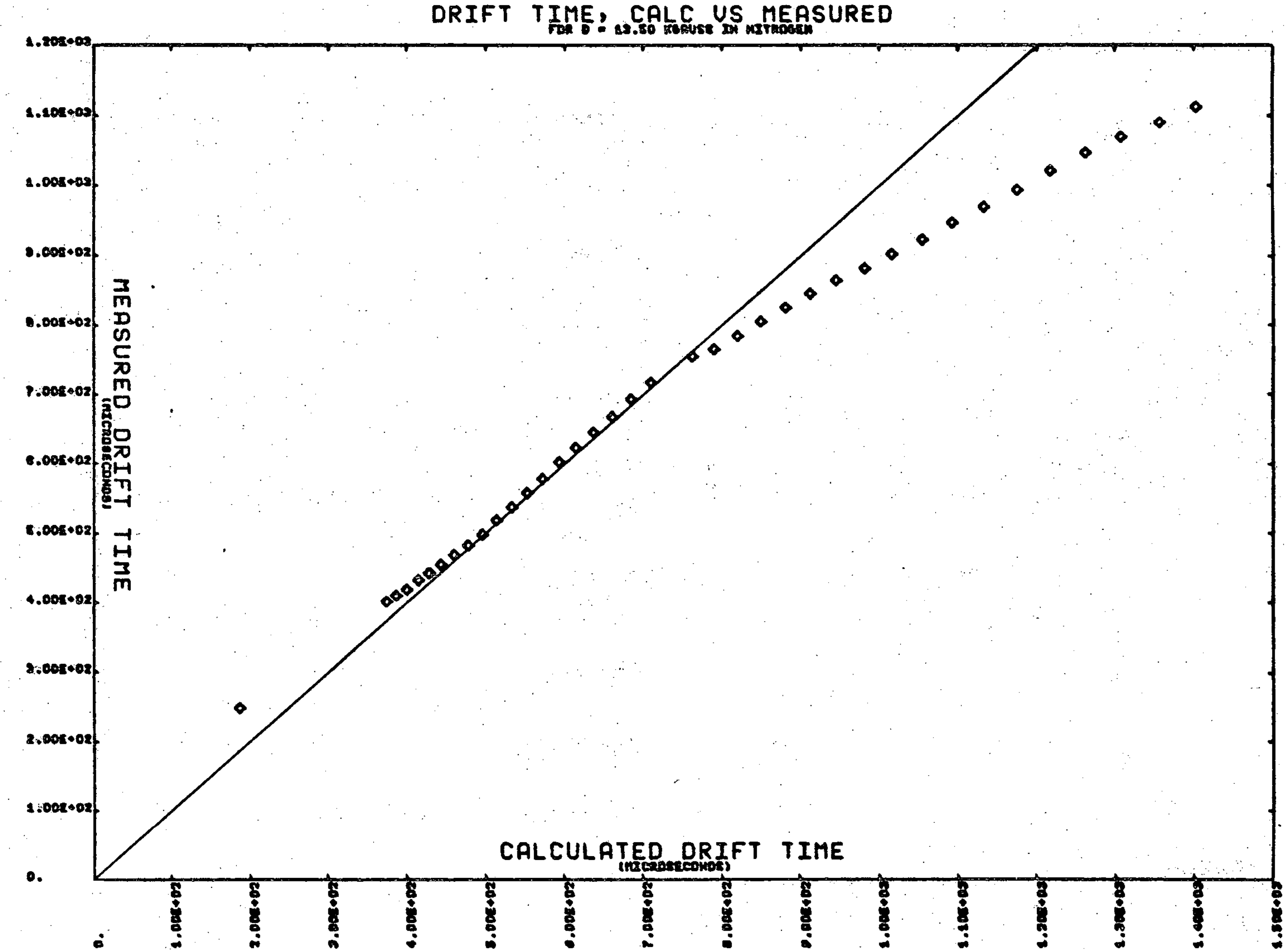

XBL 708-6410

Fig. 15. The average drift time for ions should be determined empirically for quantitative rate constant measurements.

0 0 0 0 3 6 0 0 8 0 8

2. We find a system for which the rate of reaction is well known and determine for a given n the relative size of primary and secondary peak areas in that system, for a given ion drift time, using Equation (12) or (13).

The first method is most direct but it relies for its accuracy on published values for the electron impact ionization cross sections, σ. Some data of this sort is available for the total cross section for formation of all ions from a given neutral gas by electrons of a given energy.[25] The data for 70 volt electrons is

Table I

Neutral	$\sigma(X10^{-16}\ cm^2)$
CH_4	3.66
H_2	0.98
O_2	2.65
CO	2.90
CO_2	3.20
H_2O	1.98.

This table does not supply quite enough information, however, because we need the cross section for producing each species of ion, not simply the total. Because little such data is available we augment the above table with our own data giving the relative current of each ion species produced at neutral pressure low enough that ion-molecule reactions cause no appreciable loss of any species. Table II gives the data derived in this manner from Table I.

0 0 0 0 3 6 0 3 8 0 9

Table II. Ionization cross section for impact of 70 volt electrons

Neutral	Ion	$\sigma(10^{-16}$ cm$^2)$
CH_4	C^+	.0451
	CH^+	.161
	CH_2^+	.350
	CH_3^+	1.43
	CH_4^+	1.68
CD_4	C^+	.0400
	CD^+	.171
	CD_2^+	.274
	CD_3^+	1.41
	CD_4^+	1.77
O_2	O^+	.367
	O_2^+	2.28
CO	C^+	.129
	O^+	.0455
	CO^+	2.73
CO_2	C^+	.172
	O^+	.242
	CO^+	.211
	CO_2^+	2.58
H_2O	H_2O^+	1.64
	HO^+	.242

We use the second method for determining neutral density as an independent assessment of the data in Table II. The reaction which appears most often to have been studied is

$$CH_4^+ + CH_4 \rightarrow CH_5^+ + CH_3.^{26} \qquad (17)$$

Recently the consensus on the rate of this reaction seems to have become 11.8×10^{-10} cm^3/molec-sec.[26h,i] We have used this value and a methane pressure of 3.30×10^{-5} torr to produce the curves in Fig. 16. The mass 17 curve has to be corrected for a small amount of $^{13}CH_4^+$, but the natural ratio of ^{13}C to ^{12}C gives this correction accurately. The drift time for this experiment was determined by the method discussed earlier. From Eq. (17) we calculate a methane pressure of 3.10×10^{-5} torr. Considering the poor agreement for the CH_4^+ production cross-section data of Table II with reference 25, and further considering that one publish ICR-determined[24] rate for 17 is 20% lower than the consensus, one must regard the agreement of our data to within 7% for the two methods for determining n_{CH_4} as somewhat fortuitous.

F. Summary

For determining the thermal ion-molecule reactions occurring in a given sample mixture, we shall employ the following procedure:

1. First we determine what primary species, ions and neutrals, there are to react by using the following techniques:

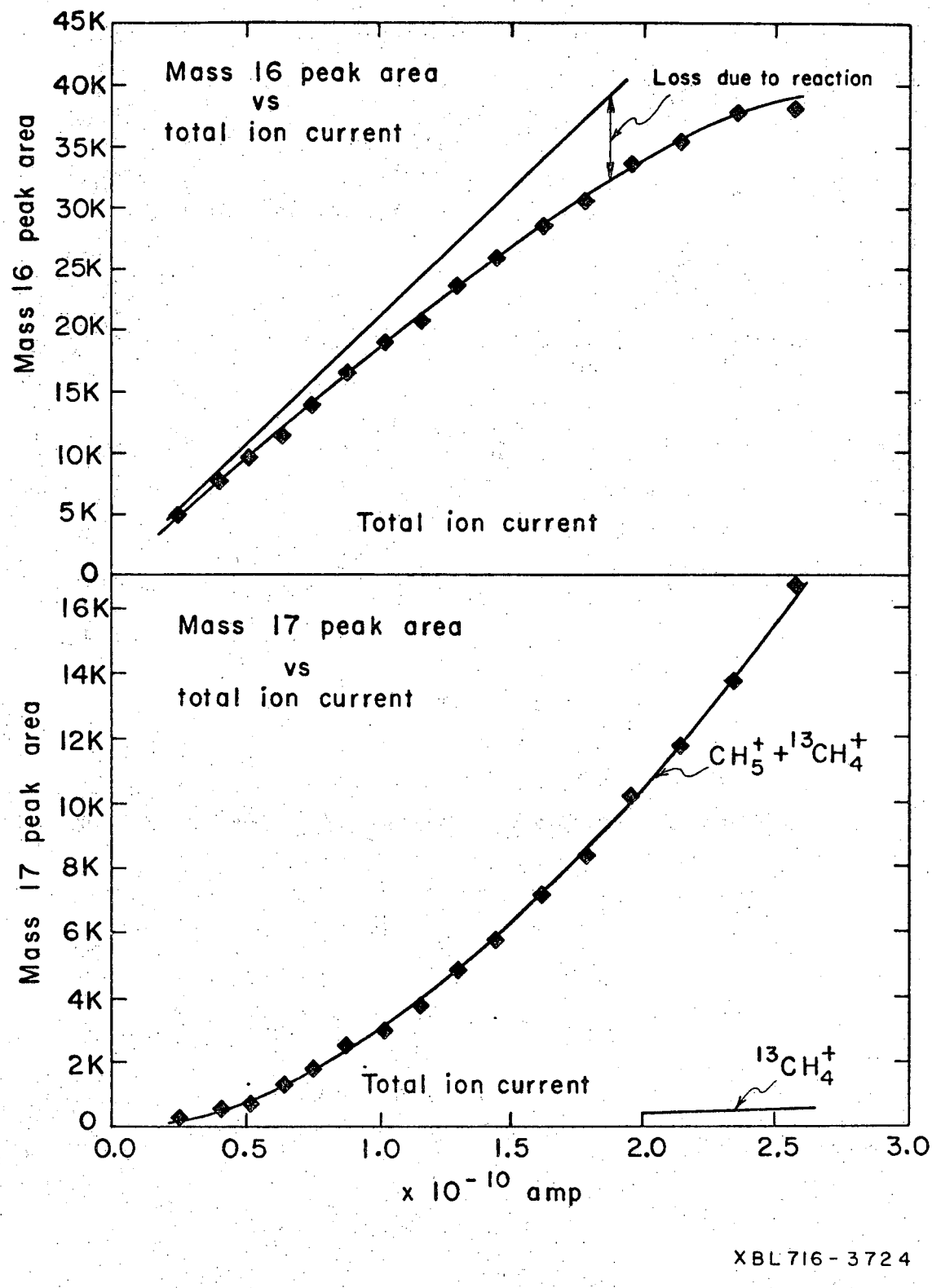

XBL716-3724

Fig. 16. Comparison of two methods for measuring methane partial pressure. For a measured drift time, fitting the solid curve to the data determines nk. Measured total ion current to electron beam emission current ratio determines nσ. Literature values of k and σ give values of n which agree to within 7%.

a. low pressure ion cyclotron resonance mass spectra.

b. log-log plots of peak area data versus TIC or inverse analyzer drift voltage; data approximates straight lines of integral slope, with unity slope for primary ions. (This data is tabulated in the Appendix, Tables III and IV.)

c. manufacturer's specifications on contaminants.

d. high pressure ICR mass spectra to determine contaminants on the order of 100 ppm or greater when an ion is produced which is not masked by other ions.

2. The remaining species are products of ion-molecule reactions; for each we determine which species are precursors by using techniques including the following:

a. varying the partial pressure of each component of the sample. (In the methane-oxygen system, for example, this shows a given secondary species is produced from the reaction of ions produced from methane reacting with neutral methane molecules, oxygen ions reacting with oxygen, or cross reactions.)

b. ion cyclotron double resonance and ion ejection double resonance.

c. appearance potential measurements.

d. thermodynamic data and the principles of energy and electron spin conservation. (Energy conservation limitations are often mitigated by the existence of kineticly or internally hot species; the spin selection rule is not without violations.)

3. For each primary species Eq. (12) takes the simple form:

$$\frac{d}{dt}\left(\ln j_i(t)\right) = \text{sum of loss terms.}$$

0 0 0 0 3 6 0 3 8 1

Thus for each primary species a least squares fit of the solution of the above equation determines the total rate of loss of that species. The independent variables are reactant neutral partial pressures and ion drift time; the sole parameter is the total loss rate.

4. Finally, using the total rate of loss of each primary species determined in 3 as an auxiliary constraint, another least squares fit is performed. For secondary species Eq. (12) cannot be uncoupled in general. Therefore the mutually coupled system of differential equations (Eq. 12) is solved numerically. The resulting coupled system of solutions is fit using reactant neutral pressure and ion drift time again as independent variables and the rate coefficients for the system of ion-molecule reactions determined in step 2 above as adjustable parameters. This calculation is accomplished with programmer intervention (rather than random search) to obtain convergence. The analysis of the data described in this thesis was done on the CDC 7600 in about 2 hours (total central processor time).[28]

Ion cyclotron resonance mass spectrometry has two powerful techniques, ion cyclotron and ion ejection double resonance, for establishing the reactant ion which produces each product ion. Quantitative rates for thermal ion-molecule reactions determined using ICR spectrometry is of comparable quality to conventional techniques.

REFERENCES

1. E. O. Lawrence and N. E. Edlefsen, Science, 72, 376(1930).
2. H. Sommer, H. A. Thomas, and J. A. Hipple, Phys Rev., 76, 1877 (1949); 80, 806(1950; 82, 697(1951).
3. D. O. Fystrom, "Redetermining the Magnetic Moment of Protons," Phys Rev Let., 25, 1469(1970).
4. M. A. Haney and D. L. Vander Hart, private communication, 1970.
5. B. N. Taylor, D. N. Langenberg and W. H. Parker, "Fundamental Physical Constants," Scientific American, October 1970, p. 62.
6. Fred Rosebury, Handbook of Electron Tube and Vacuum Techniques, (Addison-Wesley, 1965) page 402.
7. Syrotron (Trade Mark), Varian Assoc., Palo Alto, Calif.
8. L. R. Anders, Ph. D. Thesis, Harvard U. (1966).
9. D. Wobschall, J. R. Graham and D. P. Malone, Phys Rev., 131, 1565 (1963).
10. B. W. Petley and K. Morris, "An Omegatron Measurement of the Magnetic Moment of the Proton," Report QU7, Quantum Metrology Divn., National Physical Lab., Teddington England, Nov. 1969.
11. M. T. Bowers, D. D. Elleman, and J. L. Beauchamp, J. Phys. Chem., 72, 3509(1968). See especially section II.
12. R. M. Lambert, report to B. H. Mahan, June 1969.
13. L. R. Anders, J. L. Beauchamp, R. C. Dunbar and J. D. Baldeschwieler J. Chem Phys., 45, 1062(1966).
14. J. L. Beauchamp, J. Chem. Phys., 46, 1231(1967).
15. J. L. Beauchamp and S. E. Butrill, J. Chem. Phys., 48, 1783(1968); Equation 20 should be corrected to read:
... x $[\exp(-nk^{\circ}\tau)(1+nk^{\circ}\tau) - \exp(-nk^{\circ}\tau')(1+nk^{\circ}\tau')]$.

0 0 0 0 3 6 0 5 8 1 2

16. J. H. Futrell, private communication, Second Winter Course in Gas Kinetics, 1970.

17. J. H. Futrell, G. C. Goode, et al., Int. J. Mass Spect. and Ion Physics, 4, 165(1970); 5, 229(1971); 5, 393(1971).

18. L. J. Kieffer and Gordon H. Dunn, Rev. Mod. Phys., 38, 1(1966); see their Figures 17 and 31.

19. B. R. Turner, J. A. Rutherford, and D. M. J. Compton, J. Chem. Phys., 48, 1602(1968).

20. J. L. Beauchamp and J. T. Armstrong, Rev. Sci. Instr, 40, 123(1969).

21. J. Henis and W. Frasure, Rev. Sci. Instr., 39, 1772(1968).

22. A. Giardini-Guidoni, J. Chem. Phys., 45, 937(1966).

23. M. T. Bowers, D. D. Elleman, and J. King, J. Chem. Phys., 50, 4787 (1969).

24. S. E. Buttrill, Jr., J. Chem. Phys., 50, 4125(1969).

25. L. J. Kieffer, "Compilation of Low Energy Electron Collision Cross Section Data," JILA Report No. 6, 1969.

26. a) A. G. Harrison, J. J. Myher and J. C. J. Thynne, Ion Molecule Reactions in the Gas Phase, Adv. in Chem, No. 58, Chapter 10 (1966).

b) Ref. 24.

c) F. H. Field and F. W. Lampe, J. Am. Chem. Soc., 80, 5583(1958).

d) K. R. Ryan, J. H. Futrell and C. D. Miller, Rev. Sci. Instr., 37, 107(1966).

e) K. R. Ryan, J. H. Futrell and C. D. Miller, J. Chem Phys, 42 824(1965).

f) C. W. Hand, H. Von Weyssenhaff, Can J. Chem. 42, 195(1964).

g) F. H. Field, J. L. Franklin, F. W. Lampe, J. Am. Chem. Soc., 79 2419(1957).

h) F. H. Field, J. L. Franklin, and F. W. Lampe, 85, 3575(1963)

i) Shuang-Ling Chong and J. L. Franklin, J. Chem Phys., 54, 1487 (1971).

27. Produced by Electron Technology, Inc., 626 Schuyler Avenue, Kearny, N. J., 07032 to specifications as follows: Irridium wire 1 inch long by .005 inch diameter to be coated with thoria. Active surface to be about $\frac{1}{2}$ inch long near the center of the wire. Cost: 8 filaments for $50.00 total.

28. Donation of this time by Control Data Corporation is gratefully acknowledged.

29. a) D.O. Schissler and D.P. Stevenson, J. Chem. Phys., 24, 926 (1956)

b) J.B. Homer, R.S. Lehrle, J.C. Robb, and D.W. Thomas, Nature, 795 (1964).

c) C.F. Giese, and W.B. Maier, J. Chem. Phys., 39, 739 (1963).

d) B.R. Turner, M.A. Fineman, and R.F. Stebbings, J. Chem. Phys., 42, 4088 (1965).

e) D.A. Kubose and W.H. Hamill, J. Am. Chem. Soc., 85, 125 (1963).

0 0 0 0 3 6 0 3 8 1 3

III. RESULTS FOR THE METHANE SYSTEM

In order to evaluate the rates of ion-molecule reactions in mixtures of methane and oxygen, it is important to have as much information as possible on the reactions in the two pure components. We discuss the methane system here first and the oxygen system in Chapter V.

The procedure given at the end of Chapter II will be followed here. First we determine the ion and neutral species which will be present before much reaction has occurred. Then for each secondary ion species we try to determine the precursor ion and finally quantitative rate coefficients are extracted by data fitting.

The question of sample purity is one which frequently recurs. Table I gives the manufacturer's specifications. Sample purity is determined chromatographically and, of course, is always equal to or better than specification. Table I also tabulates the observed composition. In the composition column, for example, is shown less than about 300 ppm H_2O. This simply means that a high total pressure experiment was performed, in which the methane partial pressure was 3.08×10^{-5} torr. If the H_2O partial pressure had been 9×10^{-9} torr (300 ppm) it would have given a mass 18 signal at the threshold of detectability. The observed amounts of CO, N_2, and C_2H_4 are lumped together in the 0.850% shown for CO. It is reasonable to conclude that the N_2 partial pressure is no more than 1/20 of this 0.850% since N_2 is not very abundant in the sample initially and the observed total of CO, N_2 and C_2H_4 does not increase appreciably over the course of leaving the sample in the foreline manifold 8 hours as it would be expected to do as a result of leaks in the foreline manifold. That C_2H_4 is lacking

Table I

Component	Specification[1]	Observed Composition
Methane	99.999%	≥(98% CH_4 and 1.11% $^{13}CH_4$)
N_2	50 ppm	
O_2	2 ppm	< 100 ppm
CO	10 ppm	0.850%
CO_2	10 ppm	< 100 ppm
C_2H_6	30 ppm	< 100 ppm
C_2H_4	1 ppm	
H_2O	1.5 ppm	< 300 ppm

from the sample leads one to assign the majority of this 0.850% to CO. We find the source of this gas is the filament. If methane is admitted to the analyzer chamber and if both sample leak valve and high vacuum throttle valve are shut simultaneously, one can observe continuous slow oxidation of CH_4 to CO, presumably by the hot thorium oxide-coated iridium filament. The resulting rate of increase of mass 28 is at least three orders of magnitude greater than the rate of production of $C_2H_4^+$ from ion-molecule reations. Table II gives the purity determined for perdeuteromethane (CD_4).

0 0 0 0 3 6 0 3 8 1 4

Table II

Component	Observed Partial Pressure
$CD_4 + {}^{13}CD_4$	94.8%
CHD_3	2.31%
$CO + N_2$	2.93%
CO_2	$\lesssim$ 100 ppm
C_2D_4	$\lesssim$ 100 ppm
C_2D_6	$\lesssim$ 100 ppm
H_2O	?
D_2O	$\lesssim$ 900 ppm
O_2	$\lesssim$ 100 ppm

The sample of CD_4 as supplied contained about ten times as much CO and/or N_2 as shown in Table II, but was purified somewhat by distillation at ℓN_2 temperature using the Toeppler pump to draw off several uncondensed portions of the CD_4 sample. This purification was somewhat more effective than Table II shows since there is some oxidation of CD_4 to produce CO within the cell as there was with CH_4.

Tables III and IV of the Appendix show the results of a convenient preliminary analysis which readily reveals much about the chemistry of a system. Almost all peaks can be described as either primary or secondary and therefore the log-log plot of peak area versus reaction time or reactant neutral density (see Chapter 2, Eqs. 12-15) will give approximately linear behavior with slope 1 or 2, respectively. However, we need not go to so much trouble because we seek a quick,

convenient answer. We make log-log plots of peak area versus the inverse of the drift potential and versus TIC instead of carefully determining the reaction time for each drift potential or neutral density for each TIC. Observe in Table III of the Appendix how the primary ions in the mass 12-16 range (C^+, CH^+, CH_2^+, CH_3^+ CH_4^+) exhibit slopes in the 0.8 to 0.9 range and the secondary peaks (CH_5^+, $C_2H_2^+$, $C_2H_3^+$, $C_2H_4^+$, $C_2H_5^+$) except mass 28 exhibit slopes which are approximately double that, 1.8 to 2.0. Mass 28 has an intermediate slope because its two sources, primary CO^+ and secondary $C_2H_4^+$, are comparable. We shall show that mass 14, for example, has a slight secondary contribution but its effect is not evident from these tables. Likewise mass 17 has a few-percent contribution from the primary ion, $^{13}CH_4^+$, but this fact is obscured. The RMS deviations for the data of Table III, Appendix, is slightly less than for those of Table IV, Appendix, because of the greater number of points which determine the line rather than because the inverse of the drift potential is less noisy than the total ion current. It is not surprising that the slopes determined from reciprocal drift potentials are comparable to those determined from TIC, since each of these quantities is proportional to the independent variables in Eq. (13) of Chapter II and these variables always appear as the product, $n\tau$.

For those peaks which are indicated as primary we shall examine all loss mechanisms and try to account for them by means of gain mechanisms for the secondary peaks. Table III gives the observed rate of loss of the six primary ions. The reactions of CO^+ with methane will be considered in Chapter IV.

0 0 0 0 3 6 0 3 0 5

Table III

Rate of Loss of Primary Ions in Methane*

Reaction Number	Primary Ion Species	Reactant Neutral	Loss Rate Coefficient ($\frac{\times 10^{-10}\ cm^3}{molec\text{-}sec}$)	Orbiting Reaction Rate Coefficient ($\frac{\times 10^{-10}\ cm^3}{molec\text{-}sec}$)
1,2,3)	C^+	CH_4	14.2	14.3***
	C^+	CD_4	13.5	13.7
4,5,6)	CH^+	CH_4	13.4	14.0
	CD^+	CD_4	13.0	13.0
7,8,9)	CH_2^+	CH_4	14.6	13.7
	CD_2^+	CD_4	13.4	12.6
10)	CH_3^+	CH_4	9.92	13.7
	CD_3^+	CD_4	8.97	12.6
11)	CH_4^+	CH_4	12.0	13.2
	CD_4^+	CD_4	10.7	11.8
**	CO^+	CH_4	12	11.7
	CO^+	CD_4	11	11.0

*Corrections for ^{13}C have been made; the corrections are generally quite small except for the contribution to mass 17 due to $^{13}CH_4^+$, which is 11% at 7.7×10^{-6} torr and 2.7% at 3.08×10^{-5} torr.

**See Chapter IV.

***Based on polarizability data from Chapter I, Ref. 12.

Table III points our an additional feature which is very much used in our analysis of cyclotron double resonance spectra: the rates of ion-molecule reactions in perhydromethane are comparable to those in perdeute perdeutero-methane. Of course, we might expect isotope effects to be seen in such hydrogen atom transfer reactions as

$$C^+ + CH_4 \rightarrow CH_3^+ + CH; \qquad C^+ + CD_4 \rightarrow CD_3^+ + CD, \tag{3}$$

but we do not expect the rates to differ by as much as an order of magnitude, especially if the rates approach the orbiting reaction rate. Therefore in analyzing cyclotron double resonance spectra we shall always expect a reaction to show double resonance signals of roughly comparable size in perhydromethane and in perdeutero-methane. If such corroboration is not found, the credibility in a given reaction's occurrence will be greatly weakened.

A. The Reactions of C^+ with Methane

The thermodynamic data of the Appendix Table III indicates that the $C^+ + CH_4$ interaction has three exothermic reaction channels:

Table IV

		in CH_4		in CD_4	
	ΔH (kcal/mole)	Double Resonance	k ($\times 10^{-10}$)	Double Resonance	k
1) $C_2H_2^+ + H_2$	-96	12 → 26	5.2	12 → 28	5.2
2) $C_2H_3^+ + H$	-92	12 → 27	4.0	12 → 30	3.8
3) $CH_3^+ + CH$	-11	12 → 15	∿ 5.0	12 → 18	∿ 4.5
			14.2		13.5

0 0 0 0 3 6 0 3 8 1 6

The observed rate of loss of C^+ in methane is 14.2×10^{-10} cm^3/molec-sec; in CD_4, 13.5×10^{-10}. These rates agree well with the orbiting cross section (Chapter I, Eq. 1) prediction of rates of 14.30 and 13.68×10^{-10} cm^3/molec-sec, respectively. Reactions 1-3 have recently been studied in the 2-200 eV range of initial relative kinetic energy.[2] This study showed that in the low energy range the total cross section for loss of C^+ agrees quite well with the orbiting cross section. The cross sections for reactions 1-3 were all large, and each individually showed approximately the orbiting cross section energy dependency. These observations lead one to expect small negative cyclotron double resonance signals for 1-3 while none are observed for 1 and 3 and a large negative signal is seen for 2.

The ion ejection double resonance data presented in Tables V and VI are not very informative because of the relatively small signal-to-noise ratio. Table V shows the results of ejecting primarily mass 12, for example in methane and Table VI, of ejecting mass 12 in perdeutero-methane. The second and third columns show the observed mass spectra without and with ion ejection. In order to understand column four a brief aside is necessary. Recall from Chapter II, Fig. 7, that the ion ejection double resonance of O^+ and O_2^+ in pure oxygen occurred over a broad frequency range around the center frequency determined approximately by Eq. (5) of Chapter II:

$$\frac{\omega_T}{2\pi} = \omega_T^\circ \left(\frac{V_T}{m}\right)^{\frac{1}{2}} ,$$

where ω_T° is calcualted to be 123.0 kHz when V_T is in practical volts and m in AMU; the measured value of ω_T° is 158 kHz, determined by

Table V. Expt. 158 Pure Methane CW Ejection Centered at Mass 12

Ion Detected	Peak Area w/o Ejection	Peak Area with Ejection	Calculated	Difference	Ratio (%)
12	835	687	684	3	+.5
13	3143	3027	3035	-8	-.3
14	7483	7362	7395	-33	-.5
15	34280	34550	34060	487	+1.4
16	39270	38530	39100	-575	-1.5
17	16470	16620	16420	197	+1.2
18	194	193	193	0	.0
26	1487	1356	1485	-128	-9.5
27	5105	4943	5098	-154	-3.1
28	2709	2653	2705	-51	-2.0
29	32800	32230	32760	-523	-1.6
30	751	753	750	3	+.3

Table VI. Expt 164 Pure Methane-D_4 CW Ion Ejection at Mass 12

Ion Detected	Peak Area w/o Ejection	Peak Area with Ejection	Calculated	Difference	Ratio (%)
12	822	676	673	3	.5
14	3568	3550	3526	24	.7
15	107	106	106	0	.0
16	6947	6795	6917	-122	-1.8
17	754	742	752	-9	-1.3
18	39850	40010	39740	272	.7
19	1563	1541	1559	-17	-1.2
20	48920	48450	48820	-373	-.8
21	958	965	956	9	.9
22	25430	24770	25390	-619	-2.5
23	287	285	287	-1	-.7
28	4275	4210	4269	-59	-1.4
29	170	162	170	-7	-4.8
30	8219	8103	8209	-105	-1.3
31	168	170	168	2	1.3
32	1855	1782	1853	-69	-3.9
33	476	471	475	-4	-1.0
34	38450	39560	38400	1162	2.9
35	907	901	906	-4	-.5

0 0 3 6 9 3 1 7

using an approximately Lorentzian function

$$E(\omega,\omega_T^{\circ}) = \frac{1}{1+\left(\frac{\omega-\omega_T^{\circ}}{WIDTH}\right)}\left[1+\sum_{M=1}^{4} B_M(\omega-\omega_T^{\circ})^M\right] \qquad (3a)$$

to determine the rate at which ions are ejected,

$$\frac{d\, j_i(t)}{dt} = -\, j_i(t)\cdot E(\omega,\omega_T^{\circ}) \ . \qquad (3b)$$

The solution to 3b is simply

$$j_i(t) = j_i(t=0)\ \exp(-E(\omega,\omega_T^{\circ})t) \ , \qquad (3c)$$

which can be integrated over the length of time ions of the ith type spend in the cell:

$$A_i \propto n_i^+ = \int_{\tau_i}^{\tau_i'} j_i(t)dt = \frac{j_i(t=0)}{E(\omega,\omega_T^{\circ})}\left\{\exp(-E\tau_i) - \exp(-E\tau_i')\right\} \qquad (3d)$$

A least squares fit of Eq. (3d) to the data in Fig. 7 of Chapter II generated the solid curves. This least squares fitting determines the six parameters in Eq. (3a). The most important of these are ω_T°, the center frequency, and WIDTH, the half width at half height if the B_M's were zero. The sums of the B_M terms are generally less than 1 in the 20 to 50 kHz range but are never negligible except for $\omega \approx \omega_T^{\circ}$. These same parameters were used in Eq. (3d) to determine the calculated data in the fourth column of Table V. Notice that Eq (3b) is similar

0 0 0 0 3 6 0 . 0 1 8

to Eq. (12) of Chapter II, which can be written as

$$\frac{dj_i(t)}{dt} = -j_i(t) \sum_{l}^{\substack{\text{all}\\\text{neutrals}}} n_l \sum_{m}^{\substack{\text{all}\\\text{ions}}} k_{ilm} + \sum_{l}^{\substack{\text{all}\\\text{neutrals}}} n_l \sum_{m}^{\substack{\text{all}\\\text{ions}}} j_m(t) k_{mli} \qquad (3e)$$

$$-j_1(t) \cdot E(\omega, \omega_T^{\circ}).$$

For an ion such as $C_2H_2^+$ the first term in 3e will be negligible in the range of n_1's and t's of these experiments; if ejection is centered at mass 12, the third term is 3e will also be quite small. The second term in 3e is mostly responsible for the loss of $C_2H_2^+$ which accompanies ejection of C^+; this difference is given in column five of Table V. Column six shows the ratio of numbers in column five to those in column three. Experience has shown that a value in column six which is no less than about -2% may not be significant relative to noise. Tables V and VI clearly show the occurrence of Reactions 1 and 2.

An additional source of information is fortuitous and comes from Experiments 179 and 180, to be discussed in Chapter 4, in which the addition of small amounts of CO and CO_2, respectively, to methane adds about 20% more C^+. This added C^+ gives rise in turn to additional peak area at mass 26 and 27. The effect of Reaction 3 in response to this additional C^+ would be to contribute 43 units to the observed total mass 15 peak area of 34,280 units in pure methane at 3.05×10^{-5} torr; therefore we cannot prove Reaction 3 occurs but simply hypothesize a rate of about 5×10^{-10} to agree with reference 2 and to account for the observed rate of loss of C^+.

B. The Reactions of CH^+ with Methane

Conservation of energy allows the following product channels for the interaction of $CH^+ + CH_4$:

Table VII

Product	ΔH (kcal/mole)	in CH_4 Double resonance	in CH_4 k ($\times 10^{-10}$) cm^3/molec-sec	in CD_4 Double Res.	in CD_4 k (10^{-10}) cm^3/molec-sec
4a) $C_2H_3^+ + H_2$	-112	13 → 27	3.1	14 → 30	2.9
4b) $C_2H_4^+ + H$	-75	13 → 28	<.5	14 → 32	<.5
4c) $CH_3^+ + CH_2$	-27	13 → 15	∿0	14 → 18	∿0
5) $CH_2^+ + CH_3$	-15	13 → 14	∿6	14 → 16	∿6
6) $C_2H_2^+ + H_2 + H$	-12	13 → 26	4.0	14 → 28	3.8
			13.4		13.0

Reaction 4a shows a strong cyclotron double resonance signal while 4b-6 show none; however, 4a accounts for only a quarter of the observed CH^+ loss. 4b-6 may show no signals simply because dk/dE is small while k is not. It can be shown that only about half the observed loss of $C_2H_2^+$ in Table V is due to Reaction 1; the remainder is due to Reaction 6 and the fact that when ion ejection removes 20% of the C^+, it also removes about 8% of the CH^+. Tables V and VI also show about 2% loss of CH_2^+ (or CD_2^+). This effect is probably also due to the fact that CH^+(or CD^+) are lost due to direct ejection when

0 0 0 0 3 6 0 . 3 1 9

ejecting C^+. The direct ejection of all ions, including CH^+ and CH_2^+ is corrected for in Tables V and VI; the additional 2% loss of CH_2^+ (or CD_2^+) shows the occurrence of Reaction 5. Reaction 4c, however, would have to have a rate on the order of 3×10^{-9} cm^3/molec-sec to produce a comparable percantage loss of CH_3^+ (or CD_3^+). Therefore while we tend to believe 4c has a very small rate because it is spin forbidden* and shows no double resonance signals, the rate coefficient could be nearly the full orbiting reaction rate without seriously altering any observables. Since virtually all $C_2H_4^+$ is produced from Reaction 7, to be discussed later, the rate of 4b can be no greater than 5×10^{11} cm^3/molec-sec. Complete data analysis gives us good confidence in this upper limit and in the rates for 4a and 6, we can only guess at the rates for 4c and 5.

C. The Reactions of CH_2^+ with Methane

The reaction channels which may be open at thermal energies for the interaction of CH_2^+ with CH_4 are:

---

*The reaction, 4c, $CH^+(\tilde{X}^1\Sigma^+) + CH_4(\tilde{X}^1 A_1) \rightarrow CH_3^+(\tilde{X}^1 A_1') + CH_2(\tilde{X}^3\Sigma_g^-)$ is spin forbidden; excited states of the producets exist for which 4c is allowed by spin but not by energy conservation.

Table VIII

Product	ΔH (kcal/mole)	in CH_4 Double resonance	in CH_4 k ($\times 10^{-10}$)	in CD_4 Double. Res.	in CD_4 k (10^{-10})
7a) $C_2H_4^+ + H_2$	-62	14 → 28	2.75	16 → 32	2.50
7b) $C_2H_5^+ + H$	-44	14 → 29	?	16 → 34	?
8a) $CH_3^+ + CH_3$	-22	14 → 15	5.8	16 → 18	5.3
8b) $C_2H_2^+ + 2H_2$	+ 2	14 → 26	<.1	16 → 28	<.1
9) $C_2H_3^+ + H_2 + H$	+ 6	14 → 27	6.1	16 → 30	5.6
			14.6		13.4

After increasing the rate of loss of CH_2^+ by about 7% to correct for gain of CH_2^+ due to reaction 5, the loss rate becomes 14.6×10^{-10} cm^3/molec-sec. Similarly correcting the rate of loss of CD_2^+ in methane-d_4 gives 13.4×10^{-10} cm^3/molec-sec. These corrections make the rates about 7% higher than the orbiting reaction predictions of 13.70 and 12.55×10^{-10} cm^3/molec-sec; however, the corrected loss rates agree well with the total of the fairly accurately determined rates for reactions 7a, 8a, and 9a

Figure 1 shows the dependency of the mass 28 peak on TIC. At low pressure the peak is largely primary and due to CO^+. At high pressure some CO^+ is lost due to reactions which will be discussed in Chapter 4. The peak thus becomes predominantly secondary and due to $C_2H_4^+$. These two sources of mass 28 ions are thus very easy to distinguish. The calculated rate of formation of $C_2H_4^+$ is predominantly

0 0 0 0 3 6 0 , 8 2 0

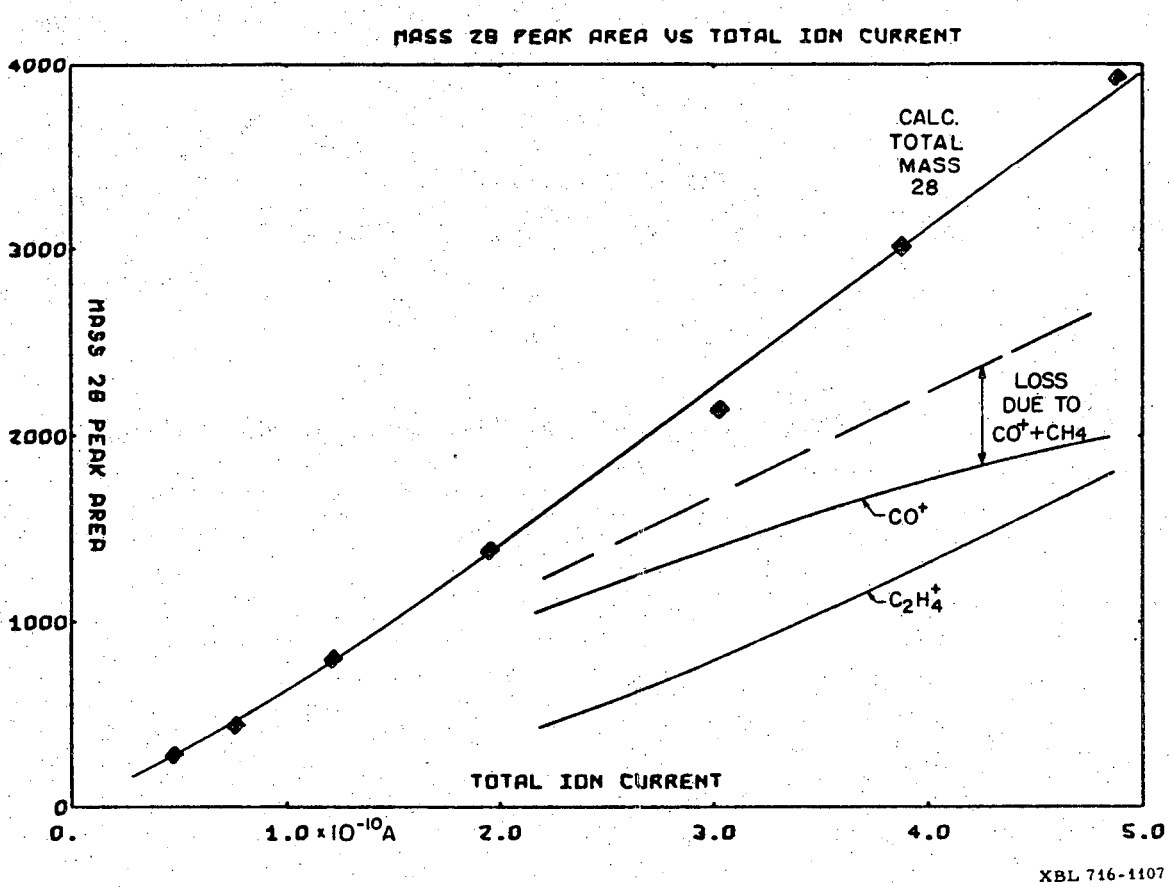

Fig. 1. Mass 28 peak area vs. total ion current.

due to reaction 7a. It has been mentioned that a harmonic effect appears in cyclotron double resonance when irradiating at twice the frequency of the detecting oscillator; however, the very large negative signal due to reaction 7a easily overshelms the harmonic effect in both CH_4 and CD_4. The appearance potential measured by Franklin[7] for $C_2H_4^+$ coicides with that of CH_4^+, but the rate of this reaction

$$CH_4^+ + CH_4 \rightarrow C_2H_4^+ + 2H_2 \qquad (11b)$$

is three orders of magnitude lower than the orbiting reaction rate. Therefore, the occurrence of Reaction 7a is not madked by reaction 11b in Franklin's appearance potential measurement because a sharp break in the $C_2H_4^+$ appearance occurs at 15.5 volts, coincident with the threshold for production of CH_2^+ from methane.

Small positive cyclotron double resonance signals are seen for Reactions 8a and 9. As mentioned in Chapter II, the sign of the cyclotron double resonance signal indicates the sign of $\frac{dk}{dE}$; we expect Reaction 9 to show a positive $\frac{dk}{dE}$ because it is within about $\frac{1}{2}$ eV of threshold. Indeed CH_2^+ ions in the ground electronic and vibrational states cannot react via Reaction 9; however, it seems most reasonable to suppose that the average CH_2^+ ion in these experiments has sufficient internal energy that Reaction 9 is an open, exothermic channel. Of course, Reaction 8a does not necessarily have a positive $\frac{dk}{dE}$ because it is endothermic, for that it is not; by the same measure, that Reaction 9 has a positive $\frac{dk}{dE}$ does not imply that Reaction 9 is endothermic. Reaction 8b is also endothermic for ground state CH_2^+, but 8b shows a very weak <u>negative</u> cyclotron double resonance signal.

0 0 0 0 3 6 0 3 3 2 1

Reaction 8b has a lot of similarity with Reaction 11b:

8b) $CH_2^+ + CH_4 \rightarrow C_2H_2^+ + H_2 + H_2$ $\quad \Delta H = +6$ kcal/mole

11b) $CH_4^+ + CH_4 \rightarrow C_2H_4^+ + H_2 + H_2$ $\quad \Delta H = -3$

Both are nearly thermoneutral; both involve condensation (C-C bonding) between projectile and target molecules; and both require that pairs of hydrogen atoms be ejected concertedly in order that the reaction not be highly endothermic. Our data indicates rates of less than 10^{-11} for both reactions; Franklin[7] observes a rate of less than 3×10^{-13} for 11b and less than 5×10^{-12} for 8b.

Nothing definitive can be said about Reaction 7b. It shows no double resonance signal but this may not prove the reaction does not occur. It could have a moderate rate without causing serious downward revision of the rate of reaction 10, which is the major source of $C_2H_5^+$:

$$CH_3^+ + CH_4 \rightarrow C_2H_5^+ + H_2 \quad . \qquad (10)$$

Reaction 10 is fast and completely masks any break in the appearance potential measurement for $C_2H_5^+$ which might show the onset of Reaction 7b at 15.5 eV (the appearance potential for $C_2H_5^+$ is 14.2 eV, which coincides with that of CH_3^+).[7]

D. The Reaction of CH_3^+ with Methane

The only exothermic product of reaction of thermal $CH_3^+ + CH_4$ is given in Table IX:

Table IX

Product	ΔH (kcal/mole)	in CH_4 Double res.	in CH_4 $k(\times 10^{-10})$	in CD_4 Double res.	in CD_4 $k(\times 10^{-10})$
10) $C_2H_5^+ + H_2$	-23	15 → 29	9.92	18 → 34	8.97

These reaction rates are in reasonable agreement with the prediction of the orbiting reaction model, 13.46 and 12.16 × 10^{-10} cm^3/molec-sec respectively. The apparent rate of loss of CH_3^+ is about 10% lower than the rate of formation of $C_2H_5^+$ because of the relatively high rate of reaction 8. Correcting for Reaction 8 brings into good agreement the rate of loss of CH_3^+ with the rate of formation of $C_2H_5^+$. The above result agrees well with previous measurements.[3,5,6]

E. The Reactions of CH_4^+ with Methane

As pointed out in Chapter 2, reaction 11 is the most thoroughly examined ion-molecule reaction of all.[8] There are, however, two allowed reaction channels of almost identical exoergicity:

Table X

Product	ΔH (kcal/mole)	in CH_4 Double res.	in CH_4 $k(\times 10^{-10})$	in CD_4 Double res.	in CD_4 $k(\times 10^{-10})$
11a) $CH_5^+ + CH_3$	-2	16 → 17	12.0	20 → 22	10.7
11b) $C_2H_4^+ + 2H2$	-3	16 → 28	<.1	20 → 32	<.1

The rate of loss of CH_4^+ accurately matches the rate of formation of CH_5^+ and agrees well with the orbiting reaction prediction of 13.24 × 10^{-10} cm^3/molec-sec (11.83 for perdeutero-methane reaction). Since most of the $C_2H_4^+$ observed is accounted for by means of reaction 7

0 0 0 0 3 6 0 3 8 2 2

the rate of formation of $C_2H_4^+$ from a major ion such as CH_4^+ with a rate greater than 10^{-11} cm^3/molec-sec would require serious downward revision of the rate of Reaction 7. Franklin[7] reports a rate for 11b of less than 3×10^{-13} cm^3/molec-sec. Because of this and because the cyclotron double resonance signal due to reaction 11b is very small considering the great abundance of CH_4^+ ions, this reaction seems a reasonable candidate for future investigations aimed at setting an upper limit on the magnitude of effects such as sweep out which were discussed in Chapter 2. It seems likely to assume that most of the 16 → 28 and 20 → 32 double resonance signals is due such non-chemical effects.

A number of studies of the energy dependence of the rate of Reaction 11 have been made and predict that dk/dE will be small in the energy range below an eV, center-of-mass energy. Taht the $CH_4^+ + CH_4 \rightarrow C_2H_4^+$ cyclotron double resonance signal is small and may be due totally or in part to non-chemical effects indicates that at relative kinetice energy up to about one eV, this reaction channel is largely closed. Apparently because the hydrogen atom exchange, Reaction 11, can be accomplished without so much rearrangement and because the two competing channels are of similar exothermicity, the condensation reaction virtually never occurs. At higher relative kinetic energy of interaction, the atom transfer mechanism begins to invest sufficient internal energy in CH_5^+ that it quickly decomposes to $CH_3^+ + H_2$, but the condensation mechanism still does not play a part in reaction.[9]

Summary

Generally good agreement of the rates of loss of the various primary ions in methane with the orbiting reaction estimate indicate that this system is highly reactive. In two cases in order to bring into accord the rate of loss of a primary ion with the rate of formation of product ions, it was necessary to invoke reactions which cannot be proven directly. However, where this was done, firm double resonance evidence is available to justify the invoked reactions. Table XI gives a summary of the conclusions reached concerning the thermal ion-molecule reactions in methane. Consideration of CO^+ and CO have been deferred to the next chapter. Good quantitative agreement between the calculated and observed peak areas provides a satisfactory foundation on which to assess the additional peak areas found in the more complex methane-oxygen system.

0 0 0 0 3 6 0 0 8 2 3

Table XI. The Reactions of Methane Ions with Methane

Reaction*	ΔH (kcal/mole)	k(×10^{-10}cm^3/molec-sec) in CH_4	k(×10^{-10}cm^3/molec-sec) in CD_4
1) $C^+ + CH_4 \rightarrow C_2H_2^+ + H_2$	-96	5.2	5.2
2) $C_2H_3^+ + H$	-92	4.0	3.8
3) $CH_3^+ + CH$	-11	~5.0	~4.5
4a) $CH^+ + CH_4 \rightarrow C_2H_3^+ + H_2$	-112	3.1	2.9
b) $C_2H_4^+ + H$	-75	<.5	<.5
c) $CH_3^+ + CH_2$	-27	~ 0	~ 0
5) $CH_2^+ + CH_3$	-15	~ 6	~ 6
6) $C_2H_2^+ + H_2 + H$	-12	4.0	3.8
7a) $CH_2^+ + CH_4 \rightarrow C_2H_4^+ + H_2$	-62	2.75	2.50
b) $C_2H_5^+ + H$	-44	?	?
8a) $CH_3^+ + CH_3$	-22	5.8	5.3
b) $C_2H_2^+ + 2H_2$	+2	<.1	<.1
9) $C_2H_3^+ + H_2 + H$	+6	6.1	5.6
10) $CH_3^+ + CH_4 \rightarrow C_2H_5^+ + H_2$	-23	9.92	8.97
11a) $CH_4^+ + CH_4 \rightarrow CH_5^+ + CH_3$	-2	12.0	10.7
b) $C_2H_4^+ + 2H_2$	-3	<.1	<.1

IV. THE FAST REACTIONS OF IMPURITY AND CONTAMINANT SPECIES

Brief mention in Chapter II was made of the fact that methane is apparently oxidized by the hot thoriated irridium filament. Experiments similar to the one described there were performed with a number of gases. In these experiments portions of gas were trapped in the analyzer chamber and the mass spectrum was monitored as a function of time. The samples trapped were at pressures of about 3×10^{-5} torr, so that the nature of the sample slowly evolved over the course of about four hours under the influeence of ion-molecule reactions. Methane, for example, initially showed secondary product ions as described in Chapter III. Four hours later, however, substantial peaks at masses 41 and 42 indicated that neutral molecules containing two or more carbon atoms had come to make up a few percent of the sample. A considerably more dramatic increase had occurred at mass 28, which had doubled in the course of about 50 minutes. This increase was probably the oxidation of methane to carbon monoxide, whose partial pressure had risen five-fold in 50 minutes. A similar experiment in CO_2 shows that CO_2 is reduced to CO at a rate comparable to methane oxidation, and O_2 is liberated at about 20% of that rate. Pure oxygen, on the other hand, is completely absorbed in the course of about 3 minutes. These observations indicate that the filament is quite active chemically. Further experiments are needed to show this effect is not due to filament out-gassing or pump regurgitation. At first sight these effects seem negligibly slow inasmuch as the fastest has a half-life on the order to a minute while the ion-molecule reactions we are studying have half-lives on the order of milliseconds (taking $p \approx 3 \times 10^{-5}$ torr and $k \approx 10^{-9}$ cm^3/molec-sec gives $nk \approx 5000$ persecond) for the fast reactions and perhaps as long as a second for the very slowest. However, one must recall that gases are pumped from the analyzer chamber by a Vac-Ion R

0 0 0 0 3 6 0 3 2 4

pump whose ultimate background pressure is about 5×10^{-9} torr under the best of circumstances. Typically, this pump's pumping rate is virtually zero for partial pressures in the 10^{-8} to 10^{-7} torr range. The maximum pumping speed is only 8 liters per second, this rate being achieved with no throttling and an analyzer chamber pressure of about 10^{-5} to 10^{-3} torr; however, the experiments reported here are performed with the high vacuum throttle valve at least 95% closed and with analyzer chamber pressures in the 10^{-6} to 3×10^{-5} torr range. It is thus not surprising that these low rate processes lead to contaminants in the 1 to 5×10^{-7} torr range. Table I gives some partial pressure data for selected experiments. While "pure" methane (and methane-d_4) becomes contaminated with nearly a percent of CO, "pure" oxygen generates hydrogen, carbon monoxide and carbon dioxide, while a mixture of methane and oxygen exhibits synergism; that is, the mixture produces more contamination than either component separately produces. Observe, furthermore, that a mixture of CD_4 and oxygen produces H_2, not D_2.

Since there may be instances in which the fast ion-molecule reactions of impurity species in the mixtures of methane and oxygen produce product ion peaks of size comparable to those of the slow reactions of methane with oxygen species, it will be the purpose of this chapter to discover and assess these fast reactions.

A. Hydrogen Species

No attempt has been made to determine the source of hydrogen except to note that it is produced when the filament is in oxygen or methane-oxygen mixtures. The methane-hydrogen system has been studied extensively in this laboratory and elsewhere.[2-4] Approximate rates of the important reactions are given in Table II.[2]

TABLE I[1]

Typical Observed Partial Pressures*

Expt. / Gas	158 "pure CH_4"	164 "pure CD_4"	170 "pure O_2"	184 $CH_4/O_2 \approx 1$	197 $CD_4/O_2 \approx 1$
H_2			8.4×10^{-8}	2.9×10^{-7}	2.5×10^{-7}
D_2					
CH_4	3.08×10^{-5}			3.10×10^{-5}	
CD_4		3.10×10^{-5}			3.20×10^{-5}
O_2			3.00×10^{-5}	3.70×10^{-5}	3.50×10^{-5}
CO	2.62×10^{-7}	9.08×10^{-7}	2.22×10^{-7}	5.32×10^{-7}	4.22×10^{-7}
CO_2			9.21×10^{-7}	4.70×10^{-7}	2.43×10^{-7}
H_2O				1.33×10^{-7}	?

* No experiments were run sooner than 30 minutes after start-up. Although most of the electronics remains on continuously, start-up refers to switching on the full complement of electronics, including drift voltage power supplies, magnet power supply, phase sensitive detector, and electron beam power supply, and then adjusting the sample leak valve so that the pressure in the analyzer chamber is approximately the desired value. After 30 minutes and a few minor adjustments of the experimental parameters, conditions will have achieved a steady state.

0 0 0 0 3 6 0 , 8 2 5

Table II

Reaction (where H may be H or D)	Approx. k (cm^3/molec-sec)	ΔH (kcal/mole)
$CH_4^+ + H_2 \rightarrow CH_5^+ + H$	3×10^{-10}	-1
$\searrow CH_4^+ + H_2$	1×10^{-11}	≈0
$CH_3^+ + H_2 \rightarrow CH_3^+ + H_2$	1.7×10^{-10}	≈0
$CH_2^+ + H_2 \rightarrow CH_3^+ + H$	3×10^{-10}	-21
$CH^+ + H_2 \rightarrow CH_2^+ + H$	5×10^{-10}	-14
$H_2^+ + CH_4 \rightarrow CH_4^+ + H_2$	small	-64
$\searrow CH_3^+ + H_2 + H$	small	-26

In CH_4-O_2 mixtures the partial pressure of H_2 is never large enough to permit any of the reactions in Table II to produce measurably large changes in the CH_2^+, CH_3^+, CH_4^+, or CH_5^+ peak areas. In CD_4-O_2 mixtures the effects would contribute, for example, a few percent to the CD_2H^+ peak area, but have been ignored because detailed analysis of the present data has been confined to the isotopically pure peak data.

All reactions of ground state O_2^+ with hydrogen are endothermic. The reactions of H_2^+ have several exothermic product channels:

	Product	ΔH (kcal/mole)	Double Resonance	k ($\times 10^{-10}$ cm^3/molec-sec)
	$HO^+ + OH$	-35	2 → 17	<1
19a)	$H_2O^+ + O$	-63	2 → 18	≲2
	$O^+ + H_2O$	-40	2 → 16	<1
19)	$HO_2^+ + H$	-33	2 → 33	80

This system was studied in experiments 182 and 183, in which oxygen

partial pressures were 3.20×10^{-5} torr and 3.00×10^{-6} torr, respectively, and hydrogen partial pressures were 6.7×10^{-7} and 6×10^{-8} torr, respectively. In 183, the H_2O partial pressure was found to be 1.9×10^{-7} torr; since the ratio of mass 18 to mass 32 peak areas is approximately the same in both experiments, it was concluded that H_2O^+ is almost entirely a primary ion as is O_2^+. There is a loss mechanism for H_2O^+ in this system:[5,6]

27) $H_2O^+ + O_2 \rightarrow O_2^+ + H_2O$ $\quad k \sim 2 \times 10^{-10}$ cm^3/molec-sec

Consequently, the rate of 19a is less than about 2×10^{-10}. The extremely high rate observed for 19 agrees well with published data.[6,7,8,21] Moran and Friedman[20] point out that what the observed amount of HO_2^+ really reflects is not just Reaction 19 alone but the total of 19 and 19b:

19b) $O_2^+ (\tilde{a}\ ^4\Pi_u) + H_2 \rightarrow HO_2^+ + H$ $\quad \Delta H = -48$ kcal/mole.

They feel that no more than the orbiting collision rate (21.3×10^{-10} cm^3 per molec-sec) should be assigned to 19 and the remaining HO_2^+ must be due to 19b. Actually they have measured not rate constants but the cross sections for these reactions in the relative kinetic energy range down to about $\frac{1}{4}$ eV; however, since they show the energy dependence agrees almost perfectly with the orbiting model one can affirm the relationship that

$$k \propto E^{\frac{1}{2}}\sigma(E) = \text{a constant independent of E,}$$

where E is the relative collision kinetic energy. They estimate that the O_2^+ ions comprise about 39% $\tilde{X}\ ^2\Pi_g$ and 61% $\tilde{a}\ ^4\Pi_u$ and on this basis determine that 19b occurs at a rate 69% of the theoretical rate; a recent measurement[21] shows that O_2^+ ions produced by electron impact at about 70 eV are 68% $\tilde{X}\ ^2\Pi_g$ and 32% $\tilde{a}\ ^4\Pi_u$. On this basis Moran and Friedman would determine a rate for 19b which is 31% greater than the orbiting collision rate, in contradiction to their original assumption about 19. Probably this contradiction indicates that the orbiting collision model, like all theoretical models, should <u>not</u> be expected to be perfect, especially

0 0 0 0 3 6 0 . 3 2 6

considering that it is based on the perturbation and point dipole limits and that the polarizability of widely separated and unperturbed molecules (as in gas phase Rayleigh scattering experiments) may be much different from that of a molecule with an ion only a few Ångstroms away. Indeed, stating a rate for 19 which is only four times the orbiting reaction rate should not be such a heresy. Most of the available data indicates that 19 is dominant over 19b. The appearance potential for HO_2^+ (15.4 eV) coincides with that of H_2^+ [6,7,8,20,21] and all reported measurements show 19 has a rate several times the orbiting reaction rate in the range of electron energies greater than the appearance potential of H_2^+ but less than that of O_2^+ ($\tilde{a}\ ^4\Pi_u$), 16.1 eV. The cyclotron double resonance signal which would correspond to 19b (32 → 33 in O_2-H_2 mixtures and 32 → 34 in O_2-D_2 mixtures) is almost exactly the same in oxygen-hydrogen mixtures as it is in pure oxygen. On the basis of this observation one must ascribe these signals to charge exchange among isotopes of oxygen and such non-chemical effects as sweep-out and the over-lap of the tail of the very strong mass 32 peak into the mass 33 and 34 peak region; however, on the basis of Moran and Friedman's observation[19] that k is almost entirely independent of E (hence $dk/dE = 0$) one does not expect to see a double resonance signal for 19b. Similarly one would not expect to see a cyclotron double resonance signal for 19 (2 → 33 in H_2-O_2 mixtures and 4 → 34 in O_2-D_2 mixtures) but a moderate signal can be seen. Furthermore, ion ejection double resonance indicates a rate for 19 in the range of 60 to 90 x 10^{-10} cm^3/molec-sec in agreement with the present quantitative measurement and all previous experimental measurements[6,7,8,21] except that of Moran and Friedman.[21] We should not lose sight of the central issue here, however,which is not how HO_2^+ is produced in oxygen-hydrogen mixtures but whether the amount of HO_2^+ seen in the mixtures is large, reproducible

and capable of being calculated for the experimental conditions we used for the slightly hydrogen-contaminated methane-oxygen mixtures. The agreement in answering this question in the affirmative is quite good among all measurements reported, including that of Moran and Friedman. Furthermore, it is clear that <u>all</u> HO_2^+ seen in mixtures of methane and oxygen can be accounted for on the basis of Reactions 19 and 19b from the observed hydrogen and oxygen partial pressures.

The products of the reactions of O^+ with H_2 are as follows:

	Reaction Product	Δ H* (kcal/mole)	Δ H** (kcal/mole)
a)	$OH^+ + H$	-10	-86
b)	$H^+ + OH$	- 1	-77
c)	$H_2^+ + O$	+42	-34
d)	$O^+ + H + H$	+104	+28
e)	$H^+ + O + H$	+104	+28

*Δ H for $O^+(\tilde{X}\ ^4S) + H_2(\tilde{X}\ ^1\Sigma_g^+)$

**Δ H for $O^+(\tilde{a}\ ^2D) + H_2(\tilde{X}\ ^1\Sigma_g^+)$

No products were observed for the above reactions in Experiment 182, in which $p(O_2)$ was 3.20×10^{-5} torr and $p(H_2)$ was 6.7×10^{-7} torr. This places an upper limit on b of about 5×10^{-10} cm^3/molec-sec and on a of about 2×10^{-10}. Fehsenfeld[6] has been alone in reporting a high rate (1×10^{-9}) for a, while several others have studied the $O^+ + H_2$ system without observing a.[7-10] This discrepancy may reflect different reactivity which results from the lower fraction of translationally and electronicly excited O^+ ions produced in the flowing afterglow experiment or incorrect assessment of the partial pressure of H_2O, which can give rise to OH^+ ions. Nevertheless, even if one assumes a rate of 10^{-9} for both

0 0 0 0 3 6 0 3 8 2 7

a and b, the H_2 partial pressure in methane-oxygen mixtures is never large enough to give measurably large effects from a or b.

B. Water Species

All reactions of H_2O^+ ions with O_2 are endothermic except charge exchange, Reaction 27, which has a rate of about 2×10^{-10} cm^3/molec-sec.[5,6] Likewise, all reactions of O_2^+ with H_2O are endothermic. Electronicly excited O_2^+ charge exchanges very rapidly with H_2O,[5] but because the partial pressure of H_2O is always relatively low in the experiments reported here, the fast reactions of a minor reactant ion species such as O_2^+* can not produce measurable effects. Charge exchange between O^+ and H_2O contributes[5] about 5% of the H_2O^+ observed in methane-oxygen mixtures.

The methane-water system is a complex and highly reactive system, although no measurements are to be found in the literature. Some of this high reactivity appears to be due to the fact that the permanent dipole moment of H_2O increases the long range forces between an ion and a water molecule. When the dipole moment is non-zero and stays alligned with the approaching ion in the most favorable manner, then the orbiting collision rate becomes:[11]

$$k_{thermal} = 2\pi e \left[\left(\frac{\alpha}{\mu}\right)^{\frac{1}{2}} + \left(\frac{2\mu_D^2}{\pi\mu KT}\right)^{\frac{1}{2}} \right]$$

where μ_D is the dipole moment of the neutral molecule, μ is the reduced mass, α is the polarizability of the neutral molecule, and K is Boltzmann's constant. If the dipole moment is zero or averages to zero because it fails of "track" with the incoming ion, the magnitude and energy dependence of the rate of the orbiting collisions will revert to the value discussed in Chapter I:[12,13]

$$k = 2\pi e \left(\frac{\alpha}{\mu}\right)^{\frac{1}{2}}.$$

For the reaction

$$H_2O^+ + H_2O \rightarrow H_3O^+ + OH \qquad (36$$

for example, the rate should fall between 51.04 and 9.40 x 10^{-10} cm^3 per molec-sec depending on the extent of tracking and the accuracy of this model for the reaction. Recent measurements have given 16.0 x 10^{-10} (Ref. 11), 26 x 10^{-10} (Ref. 14), and 25 x 10^{-10} (the present measurement) Many of the other reactions in the methane-water system have similarly large rates:

	Reaction	ΔH (kcal/mole)	k ($\frac{x10^{-10}\ cm^3}{molec\text{-}sec}$)	Ref.
14)	$H_2O^+ + CH_4 \rightarrow H_2O^+ + CH_3$	-16	~12	
33)	$CH_4^+ + H_2O \rightarrow H_2O^+ + CH_4$	- 1	~20	
34)	$\searrow H_3O^+ + CH_3$	-27	~30	
36)	$H_2O^+ + H_2O \rightarrow H_3O^+ + OH$	-10	25	14
37)	$HCO^+ + H_2O \rightarrow H_3O^+ + CO$	-33	25	15
35)	$CH_5^+ + H_2O \rightarrow H_3O^+ + CH_4$	-23	~50	

These reactions produce a relatively complex scheme when the partial pressures of CH_4 and H_2O are both on the order of 10^{-5} torr:

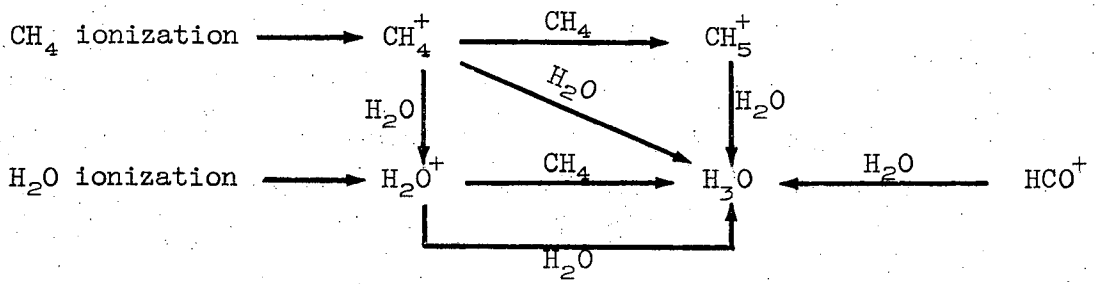

This scheme of reactions has been worked out from Experiments 176 and 177 to give the estimates shown in the above table; the observed rate for 36 agrees well with that of Ryan.[14] The rate of 35 appears comparable to that of 37, which was measured by Pritchard and Harrison.[15] When p_{CH_4}

0 0 0 0 3 6 0 . 3 2 8

is about 3×10^{-5} torr and p_{H_2O} is about 1.3×10^{-7} torr as they are in $CH_4:O_2 \approx 1$, the scheme simplifies:

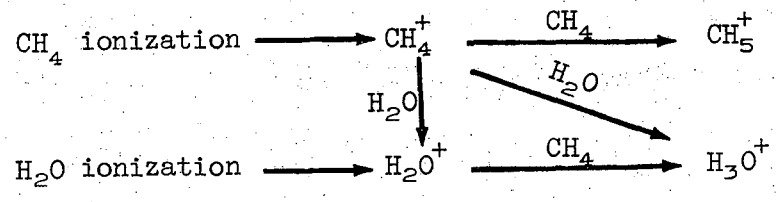

In this case H_2O^+ is produced about equally from ionization of H_2O and from Reaction 33; relatively little H_2O^+ is lost due to Reaction 14. The major source of H_3O^+ is Reaction 34. In $CH_4:O_2 \approx 1$ the mass 18 peak area comprises contributions due to $^{18}O^+$ and $^{13}CH_5^+$ which can be accurately corrected for; what remains of mass 18 and all of mass 19 are well accounted for by the reactions discussed above.

C. Carbon Monoxide Species

Probably the greatest difficulty and confusion in the study of the methane-oxygen system has centered about the questions which arise from carbon monoxide species contamination. A great deal of effort has been invested in trying to design experiments to show whether the primary ion contribution to mass 28 was due to ions of carbon monoxide, nitrogen, or ethylene. The primary ions of mass 28 were eventually shown to comprise predominantly CO^+ ions produced from oxidation of methane (Chapter III). Coincidence, the term used when two different ion species have the same mass number, plagues this system and clouds every issue. In every case the products of ion-molecule reactions involving carbon ions or neutrals is coincident with an important primary ion or a major secondary ion produced by other species. The exothermic reactions for the oxygen-carbon monoxide and methane-carbon monoxide systems are:

Reaction	ΔH (kcal/mole)	k ($\times 10^{-10}$ cm^3/molec-sec)	Ref.
28a) $CO^+ + O_2 \rightarrow O_2^+ + CO$	-45	2.0	16
28b) $\searrow CO_2^+ + O$	-14	< 1	
15a) $CO^+ + CH_4 \rightarrow HCO^+ + CH_3$	-53	12	17a,b,c
15b) $CO^+ + CH_4 \rightarrow CH_4^+ + CO$	-48	< 1	
15c) $\searrow CH_3^+ + HCO$	-23	< 1	
30) $CH_4^+ + CO \rightarrow HCO^+ + CH_3$	- 2	8.7	17b,c
31) $CH_5^+ + CO \rightarrow HCO^+ + CH_4$	-19	5.54	18

A small 28→32 cyclotron double resonance signal can be seen in "pure" O_2, CH_4-O_2 mixtures and CD_4-O_2 mixtures; Reaction 28a has been determined as the source of the signal. There is also a 32→28 signal which either indicates electronically excited O_2^+ charge exchanging with CO or sweep-out of O_2^+ accompanied by space charge coupling of CO^+ ions' spacial distribution to that of O_2^+ ions. No 28→44 signal has been observed; the observed rate of loss of CO_2^+ agrees well with the reactions to be discussed below; therefore, an upper limit on a source term for CO_2^+ such as

28b) $CO^+ + O_2 \rightarrow CO_2^+ + O$

can be set at less than 1×10^{-10} cm^3/molec-sec. The only exothermic reaction channel for $CH_4^+ + CO$ is reaction 30, for which the rate of 8.7×10^{-10} cm^3/molec-sec[17b,c] agrees reasonably well with the orbiting reaction model prediction of 10.22 to 20.21 $\times 10^{-10}$ cm^3/molec-sec, depending on the extent to which the dipole tracks with the ion.

Reaction 31 has been reported very recently[18] and may explain small cyclotron double resonance signals which connect mass 16 with mass 29 and mass 17 with mass 29 in "pure" methane. The intensity of the mass

29 signal due to COH^+ in "pure" methane is only a few thousandths that due to $C_2H_5^+$; therefore, the occurrence of Reaction 31 cannot be detected in the quantitative measurements of peak area versus TIC and the 17→29 double resonance signal is more likely explained by space charge coupling or some other non-chemical effect.

Reaction 15a is unexpectedly fast since the $CO^+ + CH_4$ interaction involves simply the ion-induced dipole long range force (which predicts a rate of 11.74×10^{-10} cm^3/molec-sec) and the two other exothermic reaction channels, 15b and c, appear to be completely ignored even though one differs from 15a simply by a matter of charge exchange. The ignored channels, 15b and c, are somewhat difficult to measure since the very important primary ion contributions to CH_3^+ and CH_4^+ interfere; in spite of this interference one can place an upper limit on 15b and c at about 3×10^{-10} cm^3/molec-sec on the basis of Experiments 178 and 179 and perhaps much lower than that on the basis of the high rate of 15a.

D. Carbon Dioxide Species

Because of the very low $\Delta H_f°$ of CO_2 few ion-molecule reactions of this neutral are exothermic; none are in the methane-oxygen system. A 32 → 44 double resonance signal occures in "pure" oxygen but most likely is explained by non-chemical means. Charge exchange between CO_2 and electronically excited O_2^+ is exothermic but these species are probably too rare to cause a measurable double resonance signal. The one exothermic channel for the interaction of CO_2^+ with oxygen or with methane is charge exchange:

	Reaction	ΔH (kcal/mole)	k ($\times 10^{-10}$ cm^3/molec-sec)	Ref.
	$CO_2^+ + O_2 \rightarrow O_2^+ + CO_2$	-39	< 1	
18a)	$CO_2^+ + CH_4 \rightarrow CH_4^+ + CO_2$	-25	< 1	
18)	$CO_2H^+ + CH_3$	+17	10	17a,b,18
18b)	$CH_3^+ + CO_2H$	+16	< 1	

However, no cyclotron double resonance signals originating with CO_2^+ (e.g., 44 → 32 or 44 → 15) have been observed in pure oxygen, pure methane or methane-oxygen mixtures; in Experiment 180, a mixture of 3.11×10^{-5} torr CH_4 with about 1.65×10^{-6} torr CO_2, a small 44 → 45 double resonance signal was observed but the absence of 44 → 16 or 44 → 15 signals substantiates the assignment of low rates for 18a and 18b. This assignment is further proven by the fact that the rate of loss of CO_2^+ is 1.0×10^{-9} cm^3/molec-sec in excellent agreement with the rate of formation of CO_2H^+, with Franklin's[18] determination of 1.05×10^{-9} and with the orbiting reaction prediction of 1.093×10^{-9} cm^3/molec-sec. All CO_2H^+ or CO_2D^+ observed in mixtures of methane and oxygen is accounted for by Reaction 18.

Summary

Table III shows an example of a mass spectrum obtained for a mixture of methane and oxygen. The various partial pressures for this experiment are:

O_2	3.70×10^{-5} torr
CH_4	3.10×10^{-5} torr
H_2	$.029 \times 10^{-5}$ torr

0 0 0 0 3 6 0 3 3 0

CO	$.052 \times 10^{-5}$ torr
CO_2	$.047 \times 10^{-5}$ torr
H_2O	$.013 \times 10^{-5}$ torr

The impurity neutrals listed above and the ion-molecule reactions discussed in this chapter account for all H_2^+, H_2O^+, H_3O^+, O_2H^+, CO_2^+, and CO_2H^+ shown in Table III and for most of the CO^+ ($C^+ + O_2$ produces a small amount of CO^+) and COH^+ ($CH^+ + O_2$ produces some COH^+). The product ion peaks from fast reactions of impurity species are more numerous and of comparable size to the product ion peaks from the slow reactions of methane and oxygen species.

Table III

Experiment 184

Mass	Total Peak Area	Ion Species	Assigned Peak Area
2		H_2^+	31
12	719	C^+	719
13	2465	CH^+	2456
		$^{13}C^+$	29
14	7205	CH_2^+	7170
		$^{13}CH^+$	35
15	36970	CH_3^+	36880
		$^{13}CH_2^+$	90
16	47530	O^+	13785
		CH_4^+	33310
		$^{13}CH_3^+$	435
17	15430	$^{17}O^+$	5
		OH^+	--
		CH_5^+	15030
		$^{13}CH_4^+$	390
18	489	$^{18}O^+$	52
		$^{13}CH_5^+$	180
		H_2O^+	257
19	381	H_3O^+	381
26	1184	$C_2H_2^+$	1184
27	4739	$C_2H_3^+$	4712
		$^{13}CCH_2^+$	27

0 0 0 0 3 6 0 3 8 3 1

Mass	Total Peak Area	Ion Species	Assigned Peak Area
28	3898	$C_2H_4^+$	1795
		$^{13}CCH_3^+$	111
		CO^+	1992
29	39190	$C_2H_5^+$	34300
		$^{13}CCH_4^+$	42
		$^{13}CO^+$	22
		COH^+	4828
30	1741	COH_2^+	881
		$^{13}CCH_5^+$	805
		$^{13}COH^+$	55
31	1781	COH_3^+	1781
32	181300	O_2^+	181300
33	719	$^{17}OO^+$	139
		O_2H^+	580
34	799	$^{18}OO^+$	799
44	1573	CO_2^+	1573
45	1865	CO_2H^+	1863
		$^{13}CO_2^+$	2
47	1352	$CO_2H_3^+$	1352
48	960	O_3^+	960

Chapter IV References

1. These data are inferred from mass spectrometric data. Partial pressures are calculated using data of Table II from Chapter II.
2. M. S. B. Munson, F. H. Field and J. L. Franklin, J. Am. Chem. Soc. 85, 3584 (1963).
3. S. Wexler, J. Am. Chem. Soc. 85, 272 (1963).
4. V. Aquilanti and G. G. Volpi, J. Chem. Phys. 44, 2307 (1966).
5. B. R. Turner and J. A. Rutherford, J. Geophys. Res. 73, 6751 (1968).
6. F. C. Fehsenfeld, A. L. Schmeltekopf, and E. E. Ferguson, J. Chem. Phys. 46, 2802 (1967).
7. D. P. Stevenson and D. O. Schissler, J. Chem. Phys. 29, 282 (1958).
8. D. P. Stevenson and D. O. Schissler, J. Chem. Phys. 24, 926 (1956).
9. A. Aquilanti, A. Galli, A. Giardini-Guidoni, G. G. Volpi, J. Chem. Phys. 43, 1969 (1965).
10. H. Gutbier, Z. Naturforsch 12A, 499 (1957).
11. S. K. Gupta, E. G. Jones, A. G. Harrison and J. J. Myher, Can. J. Chem. 45, 3107 (1967).
12. R. C. Dunbar, J. Chem. Phys. 52, 278 (1970).
13. J. V. Dugan and J. L. Magee, J. Chem. Phys. 47, 3103 (1967).
14. K. R. Ryan, J. Chem. Phys. 52, 6009 (1970).
15. H. Pritchard and A. G. Harrison, J. Chem. Phys. 48, 5623 (1968).
16. F. C. Fehsenfeld, A. L. Schmeltekopf and E. E. Ferguson, J. Chem. Phys. 45, 23 (1966).

17a. A. G. Harrison and J. J. Myher, J. Chem. Phys. 46, 3276 (1967).

b. T. W. Shannon and A. G. Harrison, J. Chem. Phys. 43, 4201 (1965).

c. A. G. Harrison, A. Ivko and T. W. Shannon, Can. J. Chem. 22, 974 (1966).

18. J. L. Franklin, J. Chem. Phys. 54, 1487 (1971).

0 0 0 0 3 6 0 2 3 2

19. T. F. Moran and L. Friedman, J. Chem. Phys. 42, 2391 (1965).

20. P. Dong and M. Cottin, J. Chim. Physique 57, 557 (1960).

21. B. R. Turner, J. A. Rutherford and D. M. J. Compton, J. Chem. Phys. 48, 1602 (1968).

V. THE OXYGEN SYSTEM

Most of the ion-molecule reactions occurring in "pure oxygen" have been discussed in Chapter IV. They are

19)	$H_2^+ + O_2 \rightarrow HO_2^+ + H$	$k = 80 \times 10^{-10}$ cm^3/molec-sec
	$CO^+ + O_2 \rightarrow O_2^+ + CO$	2
28)	$CO_2^+ + O_2 \rightarrow O_2^+ + CO_2$	< 1
27)	$H_2O^+ + O_2 \rightarrow O_2^+ + H_2O$	2.

There are but two additional reactions in pure oxygen:

	Reaction	k	ΔH
26)	$O^+ + O_2 \rightarrow O_2^+ + O$	$.169 \times 10^{-10}$ cm^3/molec-sec	-36 kcal/mole
29)	$O_2^+(\tilde{a}^4\Pi_u) + O_2 \rightarrow O_3^+ + O$	$\sim 7 \times 10^{-12}$	~0 kcal/mole.

Reaction 26 has received a great deal of attention[1] because of its great ionospheric importance. It was mentioned in Chapter II and IV that our experiments show about three times as much O^+, relative to O_2^+, as is observed in conventional mass spectrometers and this fact was attributed to the fact that the ICR spectrometer retains the translationally hot O^+ ions which are lost in conventional spectrometers. Reaction 26 has a low rate presumably because it is a non-resonant charge exchange. Rates for non-resonant charge exchange in atoms are very small for low velocities.[2] Rates of charge exchange increase as the energy defect diminishes toward zero and for resonance charge transfers observed rates approach the elastic collision rates.[3] Rates for charge exchange in polyatomic molecules presumably always resemble the resonance type because the near continuum of states generally guarantees a very small energy defect.[4,7] The behavior of charge

0 0 0 0 3 6 0 3 3 3 3

exchange in diatomic-diatomic systems and atom-diatomic systems such as (26) is intermediate between the polyatomic and atom-atom behavior.[4] The role of kinetic energy is crucial since at high kinetic energy charge transfer is always of the resonance form, occurring on the order of every collision.[5] At high kinetic energy the charge exchange cross section is small because the collision cross-section is small. The charge transfer cross section increases (in keeping with the increase in the collision cross-section), reaches a maximum near

$$v \approx p_o \Delta E/h$$

where v is the relative collision velocity, p_o is a collision parameter on the order of the range over which strong forces are exerted between ion and target, ΔE is the energy defect in the charge transfer, and h is Planck's constant.[6] ΔE is difficult to determine precisely for Reaction 26 because it is large (~1.3 eV) for transitions such as

26a) $O^+(\tilde{X}^4S) + O_2(\tilde{X}^3\Sigma_g^-, v=0) \rightarrow O(\tilde{X}^3P) + O_2^+(\tilde{X}^2\Pi_g, v=1)$

which have large Franck-Condon factors for the transition $O_2(\tilde{X}^3\Sigma_g^-, v=0) \rightarrow O_2^+(\tilde{X}^2\Pi_g, v=1)$ and small (~0.008 eV) for

26b) $O^+(\tilde{X}^4S) + O_2(\tilde{X}^3\Sigma_g^-, v=0) \rightarrow O(\tilde{X}^3P) + O_2^+(\tilde{X}^2\Pi_g, v=8)$,

which has a small Franck-Condon factor. Both 26a and 26b will be slow, one because ΔE is large and the other because the Franck-Condon factor is small; the processes intermediate between 26a and 26b will be somewhat faster. For example, much faster rates of charge exchange are found for

1) $N^+(\tilde{X}^3P) + O_2(\tilde{X}^3\Sigma_g^-) \rightarrow N(\tilde{a}^2D) + O_2^+(\tilde{X}^2\Pi_g)$

$$k = 5 \times 10^{-10} \text{ cm}^3/\text{molec-sec}$$

and

26c) $O^+(\tilde{a}^2D) + O_2(\tilde{X}^3\Sigma_g^-) \rightarrow O(\tilde{X}^3P) + O_2^+(\tilde{a}^4\Pi_u)$

$$k \gtrsim 10 \cdot (k \text{ for } 26)$$

both of which have small energy defect and large Franck-Condon factors.[8,1d]

Additional channels for the interaction of N^+ with O_2 are ion-atom interchange:

2) $N^+(\tilde{X}^3P) + O_2(\tilde{X}^3\Sigma_g^-) \rightarrow \begin{cases} NO^+(\tilde{a}^3\Sigma^+) + O(\tilde{X}^3P) & \Delta H = -48 \frac{\text{kcal}}{\text{mole}} \\ NO^+(\tilde{X}^1\Sigma^+) + O(\tilde{X}^3P) & \Delta H = -154 \frac{\text{kcal}}{\text{mole}} \end{cases}$

which proceed at a total rate equal to charge exchange, 5×10^{-10} cm^3/molec-sec. However, spin and electron orbital symmetry conservation arguments indicate that charge exchange of $O^+(^4S)$ with O_2 and $O^+(^2D)$ with O_2 probably do not involve atom exchange like 2.

The rate of 26 is sufficiently small that the additional O_2^+ produced is negligible relative to the primary O_2^+ concentration. Hence the plot of mass 32 peak area versus TIC (Figure 8 of Chapter II) is quite linear. Furthermore one can presume that the population of O^+ ions in the $\tilde{a}^2D$ state is small because 26c is fast and would cause a noticeable effect if the $\tilde{a}^2D$ population were as much as 10% of the total O^+.

Reaction 29 is established as the source of O_3^+ because its appearance potential, 17 volts, coincides with that of $O_2^+(\tilde{a}^4\Pi_u)$.[9] An additional source in high pressure mass spectrometers[10,11] is

29a) $O_2^+(\tilde{A}^2\Pi_u) + O_2 \rightarrow O_3^+ + O,$

0 0 0 0 3 6 0 3 8 3 4

but the $O_2^+(\tilde{A}^2\Pi_u)$ probably spontaneously relaxes to the ground state within a few microseconds of its formation. (cf. $NO(\tilde{B}^2\Pi)$ radiative lifetime of 3×10^{-6} sec.[12] Table I gives a comparison of NO and O_2^+ states.) Leventhal and Friedman[11] observe a rate for Reaction 29 of only about 2% the orbiting reaction rate and rationalize this low rate by showing that only a fraction of the $O_2^+(\tilde{a}^4\Pi_u)$ will have enough (v must be greater than about 5 to 7) but will not put so much energy into the O_3^+ that it will decompose to $O_2^+ + O$ (v must be less than about 9). The v = 7 to 9 states of $\tilde{a}^4\Pi_u$ comprise only about 25% of the total $\tilde{a}^4\Pi_u$ produced by electron impact.[13] Leventhal and Friedman estimated that about 10 μsec after formation, the O_2^+ would consist of 39% ground electronic state and 61% of the first metastable state ($\tilde{a}$). A recent measurement[14] gives these fractions as about 68% $\tilde{X}$ and 32% $\tilde{a}$. These fractions improve the agreement of Leventhal and Friedman's observations with their estimate of the v = 7 to 9 population in the $\tilde{a}^4\Pi_u$ state, giving the observed rate of formation of O_3^+ as more like 4% of the theoretical rate. However, assuming only 25% of the $O_2^+(\tilde{a}^4\Pi_u)$ can produce O_3^+, the rate of this process is still only 1/6 the theoretical rate; one must conclude that either the $\tilde{a}^4\Pi_u$ population is much less than 32% or that the state is much less reactive than expected.

The $\tilde{a}^4\Pi_u$ state might spontaneously relax to the ground state before reaction occurs. This possibility must be considered when noting that the present experiments show a much lower rate of formation of O_3^+, compared with the earlier experiments.[10,11] The essential difference between the experiments is that typical ion lifetimes were about 1 to 10 μsec in the earlier experiments while they are .1 to 1 msec in the present experiments. Spontaneous relaxation by emission of

Table I

Comparison of States of NO and O_2^+

	NO			O_2^+		
Electron Structure	State	T_e	r_e	State	T_e	r_e
$(3\sigma)^2(1\pi)^4(1\pi^*)^1$	$\tilde{X}\ ^2\Pi$	0 eV	1.16 Å	$\tilde{X}\ ^2\Pi_g$	0 eV	1.13 Å
$(3\sigma)^2(1\pi)^3(1\pi^*)^2$	$\tilde{a}\ ^4\Pi$	4.6	1.40	$\tilde{a}\ ^4\Pi_u$	4.0	1.38
$(3\sigma)^2(1\pi)^3(1\pi^*)^2$	$\tilde{B}\ ^2\Pi$	5.6	1.42	$\tilde{A}\ ^2\Pi_u$	4.8	1.42
$(3\sigma)^1(1\pi)^4(1\pi^*)^2$	$\tilde{b}\ ^4\Sigma^-$	5.8	1.30	$b\ ^4\Sigma_g^-$	6.2	1.28
$(3\sigma)^1(1\pi)^4(1\pi^*)^2$	$\tilde{B}'^2\Delta$	7.4	1.30	$^2\Delta_g$	7.9	1.3
$(3\sigma)^1(1\pi)^4(1\pi^*)^2$	$\tilde{G}\ ^2\Sigma^-$	7.7	1.34	$^2\Sigma_g^-$	8.2	1.34
$(3\sigma)^2(1\pi)^4(3s\sigma)^1$	$\tilde{A}\ ^2\Sigma^+$	5.4	1.06 *	comparable states		
$(3\sigma)^2(1\pi)^4(3p\pi)^1$	$\tilde{C}\ ^2\Pi$	6.3	1.06	not observed.		
$(3\sigma)^2(1\pi)^4(4p\sigma)^1$	$\tilde{D}\ ^2\Sigma^+$	6.4	1.06			
$(3\sigma)^2(1\pi)^4(4s\sigma)^1$	$\tilde{E}\ ^2\Sigma^+$	7.4	1.06			

* These states $\tilde{A}$, $\tilde{C}$, $\tilde{D}$, and $\tilde{E}$ are Rydberg states. Their structure is very much as if the molecule were NO^+ with a loosely bound electron orbiting about the ion. Consequently there is very little mixing of these states with the non-Rydberg states[18] and that NO has these Rydberg states has little effect on the lifetimes of the non-Rydberg states.[18,21] This is not true for the $\tilde{C}\ ^2\Pi$ state because its potential crosses that of the $\tilde{B}\ ^2\Pi$ state near r_e = 1.18 Å; near that point, the two states mix extensively and the crossing is avoided.[20]

0 0 0 0 3 6 0 0 3 3 5

vibrational quanta will have a very long (~1 second) radiative lifetime because O_2^+ has no dipole moment. Non-radiative transitions which are near resonance can be relatively fast. Probably the simplest molecule for which phosphorescence has been reported to date is formaldehyde,[15,16] and although the $\tilde{a}^3A_2$ is populated by direct absorption (oscillator strength is about 1.5×10^{-7}) radiationless transitions compete strongly with the phosphorescence,[15] which has a natural radiative lifetime of about 10 msec.[16] In O_2^+ the potential energy curves for $\tilde{X}^2\Pi_g$, $\tilde{a}^4\Pi_u$, and $\tilde{A}^2\Pi_u$ become nearly congruent for internuclear distances greater than about 1.7 Å;[20] therefore, for vibrational states greater than about v = 10 in $\tilde{a}^4\Pi_u$, one expects a great deal of mixing with the $\tilde{A}^2\Pi_u$. This mixing could lead to a non-radiative transition such as,

3) $O_2^+(\tilde{a}^4\Pi_u, v=10) \rightarrow O_2^+(\tilde{A}^2\Pi_u, v=5)$,

which has an energy defect of about 70 cm^{-1} (or about .009 eV)[17] and this state would rapidly relax,

4) $O_2^+(\tilde{A}^2\Pi_u, v=5) \rightarrow O_2^+(\tilde{X}^2\Pi_g, v=1 \text{ to } 3)$ - ~39000 cm^{-1}.

This mixing might also lead directly to phosphorescence:

5) $O_2^+(\tilde{a}^4\Pi_u) \rightarrow O_2^+(\tilde{X}^2\Pi_g) + h\nu$.

We can estimate the rate of this phosphorescence by comparison with similar processes in light diatomic molecules. Except for spin charge (5) is an allowed transition; since spin change is the weakest selection rule,[18] this process may be relatively fast. A recent measurement gives the radiative lifetime for CO $\tilde{a}^3\Pi \rightarrow \tilde{X}^1\Sigma^+$ as 1±.4 msec. This transition is also only spin forbidden and involves a spin change

transition in the same orbitals as for (5). The fact that the CO $\tilde{a}^3\Pi \rightarrow \tilde{X}^1\Sigma^+$ frequency ($T_e(\tilde{a}^3\Pi)$ = 48700 cm^{-1}) is very high would tend to make its lifetime relatively shorter than the $O_2^+(\tilde{a}^4\Pi_u \rightarrow \tilde{X}^2\Pi_u)$ lifetime (T_e = 32,600 cm^{-1}) if all other factors were equal.[18] On the other hand, the CO $\tilde{a}^3\Pi \rightarrow \tilde{X}^1\Sigma^+$ transition is allowed by mixing of the $\tilde{a}^3\Pi$ state with $\tilde{A}^1\Pi$ and other singlet states. Since the $\tilde{A}^1\Pi$ is 16,300 cm^{-1} higher than $\tilde{a}^3\Pi$ the mixing will be very small and the lifetime consequently will be long. Similar mixing in O_2^+ $\tilde{a}^4\Pi_u$ involves a doublet state only about 8000 cm^{-1} higher. A very similar transition to (5) is the $\tilde{a}^4\Pi$ to $\tilde{X}^2\Pi$ transition in NO, a molecule isoelectronic with O_2^+. A recent calculation[21] shows the $\tilde{a}^4\Pi_{5/2}$ has a lifetime of 100 msec due to spin-orbit mixing of the ground state $\tilde{X}^2\Pi_{3/2}$ with the $\tilde{b}^4\Sigma^-_{3/2}$; the lifetimes of the other members of the $\tilde{a}$ multiplet will be somewhat shorter. The $\tilde{a}^4\Pi_{3/2,1/2} \rightarrow \tilde{X}^2\Pi_{3/2,1/2}$ are mainly allowed through spin-orbit mixing of the $\tilde{a}^4\Pi$ and $\tilde{B}^2\Pi$ states (cf. earlier discussion here of similar mixing of $\tilde{a}^4\Pi_u$ and $\tilde{A}^2\Pi_u$ in O_2^+); the $\tilde{a}^4\Pi_{1/2} \rightarrow \tilde{X}^2\Pi_{3/2}$ is also allowed by spin orbit mixing of the $\tilde{a}^4\Pi_{1/2}$ and $\tilde{G}^2\Sigma^-_{1/2}$ states. These estimates lead one to conclude that the total lifetime of O_2^+ $\tilde{a}^4\Pi_u$ with respect to radiative and non-radiative relaxation is probably in the range of 1 to 1000 msec. Therefore the majority of the $O_2^+(\tilde{a}^4\Pi_u)$ produced at the electron beam survives spontaneous relaxation.

Thus far, we have examined non-collisional relaxation of O_2^{+*}. Considering, as well, the collisional processes we can rewrite equation 12, Chapter II as

$$6) \quad \frac{dj(O_2^{+*})}{dt} = -j(O_2^{+*}) \left\{ \sum_i A_i(O_2^{+*} \rightarrow O_2^+) + \sum_j n_j \sum_\ell k_{j\ell} \right\}$$

where $A_i(O_2^{+*} \rightarrow O_2^+)$ is the rate of the i^{th} type of non-collisional relaxation and $k_{j\ell}$ is the rate coefficient for the ℓ^{th} type of relaxation which occurs when O_2^{+*} collides with the j^{th} type of neutral species. Unfortunately the present experiments cannot get at the number of O_2^{+*} ions in the cell, but simply the total O_2^+, which is predominantly ground state. Therefore while we could in principle distinguish the relative rates of the two terms in (6) using the fact that the last term is of one higher order pressure dependence than the first, in practice we can measure no discernible loss of mass 32 ions (chapter II, Fig. 8). We do have direct measurement of the number of O_3^+ ions, for we can solve (6) and (7)

$$7) \quad \frac{dj(O_3^+)}{dt} = + j(O_2^{+*})\, k_{29}\, n(O_2)$$

to get

$$8) \quad j(O_2^{+*}) = j(O_2^{+*}, t=0)\exp(-Rt)$$

and

$$9) \quad j(O_3^+) = \frac{j(O_2^{+*}, t=0)n(O_2)k_{29}}{R} \left\{1 - \exp(-Rt)\right\}$$

where

$$R = \sum_i A_i(O_2^{+*} \rightarrow O_2^+) + \sum_j n_j \sum_\ell k_{j\ell} .$$

When R is small (9) becomes

$$10) \quad j(O_3^+) \approx j(O_2^{+*}, t=0)\; n(O_2)\; k_{29}(t - \tfrac{1}{2} Rt^2)$$

and

$$n^+(O_3^+) = \int_{\tau_{48}}^{\tau_{48}'} j(O_3^+)\,dt \approx$$

$$j(O_2^{+*},t=0)n(O_2)k_{29}\left\{t^2 - \frac{1}{6}\,n(O_2)k_{29}t^3 - \frac{1}{6}\underbrace{\left[R-n(O_2)k_{29}\right]}_{\text{small}}t^3\right\}_{t=\tau_{48}}^{t=\tau_{48}'}$$

Figure 1 shows the mass 48 peak versus O_2^+ ion current in various mixtures. The solid curve is a least squares fit of equation (11):

$$11)\quad n^+(O_3^+) = j(O_2^{+*},t=0)\; n(O_2)k_{29}\left\{t^2 - \frac{1}{6}\,n(O_2)k_{29}t^3\right\}_{t=\tau_{48}}^{t=\tau_{48}'}$$

From the fact that $R - n(O_2)k_{29}$ is small one can draw two conclusions:

a) $\sum_i A_i(O_2^{+*} \rightarrow O_2^+)$ is less than about 160 sec^{-1}, and

b) Methane and oxygen are not very efficient in collisionally depleting O_2^{+*}. The k's are less than about 5×10^{-10} cm^3/molec-sec.

Of course, the t^3 term in (11) is only 4.6% as large as the t^2 term at the highest pressure in Fig. 1 and this is the reason that the above conclusions cannot be any stronger.

A great deal of study of collisional quenching has been made to date. Electronic to translational energy conversion upon collision is inefficient for quenching.[22] Vibrational to vibrational energy conversion can be relatively efficient but drops off rapidly with increasing energy defect. The data of Millikan[23] and others, quoted by Burnett and North,[24] indicate that vibrational quenching of O_2^+ by O_2 will be 5 to 8 orders of magnitude less than gas kinetic; by CH_4, 2 to 5 orders less than gas kinetic. Burnett and North[25] briefly discussed electronic energy transfer in diatomic molecules. Their

0 0 0 0 3 6 0 5 8 3 7

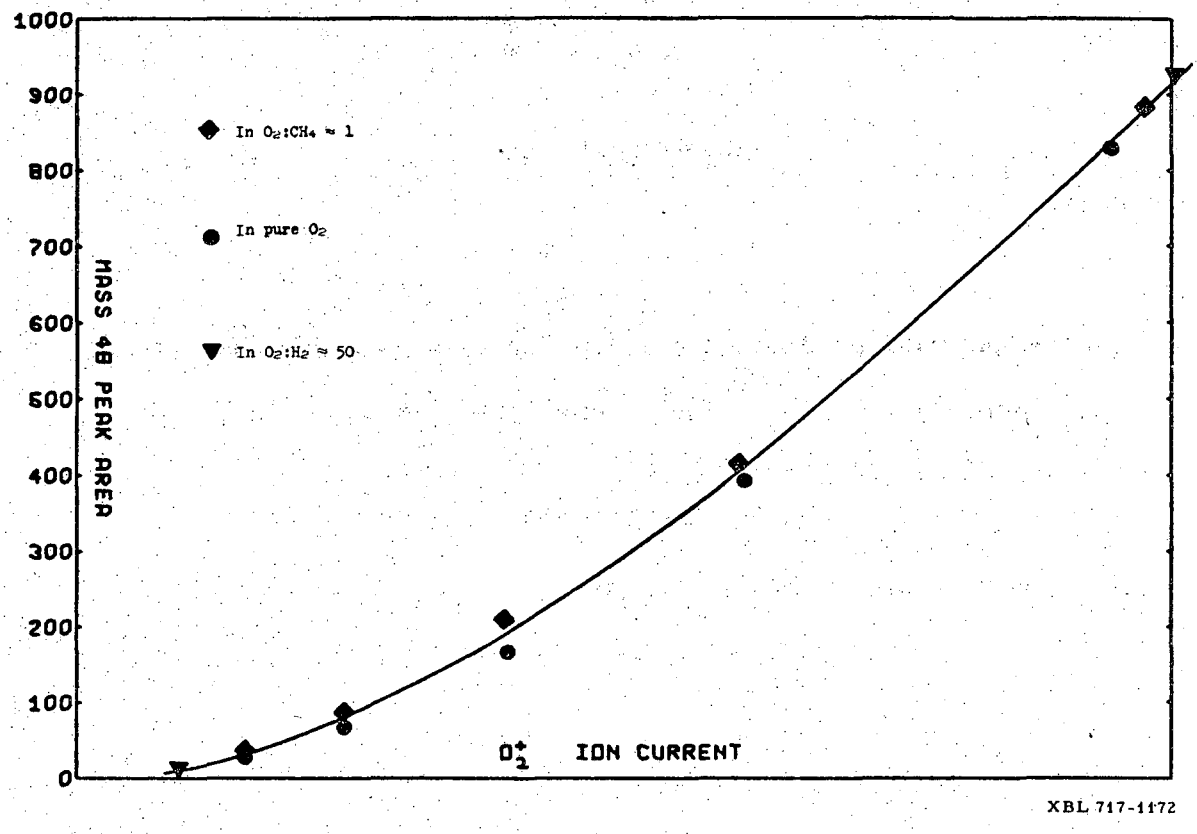

Fig. 1. Mass 48 peak area vs. O_2^+ ion current in pure oxygen (dot), O_2:CH_4 ≈ 1 (diamond) and O_2:H_2 ≈ 50 (triangle).

discussion is based largely on the data of Callear and Smith[26] who observed quenching of the $\tilde{A}$, $\tilde{C}$, and $\tilde{D}$ Rydberg states of NO by various other diatomic molecules. They express some alarm over the high rate of

12) $NO(\tilde{C}\ ^2\Pi) + N_2(\tilde{X}\ ^1\Sigma_g^+) \rightarrow NO(\tilde{X}\ ^2\Pi) + N_2(\tilde{A}\ ^3\Sigma_u^+)$,

which is on the order of 10^{-9} cm^3/molec-sec apparently in violation of the Franck-Condon principle, while

13) $CO(\tilde{a}\ ^3\Pi) + NO(\tilde{X}\ ^2\Pi) \rightarrow NO(\tilde{A}\ ^2\Sigma^+) + CO(X\ ^1\Sigma^+)$

appears not to occur. Burnett and North[25] and Callear and Smith[26] both prefer a two-step process

12) $NO(\tilde{C}\ ^2\Pi) + N_2(\tilde{X}\ ^1\Sigma_g^+) \rightarrow NO(\tilde{X}\ ^2\Pi) + N_2(\tilde{A}\ ^3\Sigma_u^+)$

14) $N_2(\tilde{A}\ ^3\Sigma_u^+) + NO(\tilde{X}\ ^2\Pi) \rightarrow N_2(\tilde{X}\ ^1\Sigma_g^+) + NO(\tilde{A}\ ^2\Sigma^+)$

over the equivalent one-step process

15) $NO(\tilde{C}\ ^2\Pi) + N_2(\tilde{X}\ ^1\Sigma_g^+) \rightarrow NO(\tilde{A}\ ^2\Sigma^+) + N_2(\tilde{X}\ ^1\Sigma_g^+)$

to explain the observed quenching of the δ-bands of NO nitrogen accompanied by an enhancement of the NO γ bands. They prefer 12 and 14 over 15 because the energy defects are much smaller, -2504 and -5678 cm^{-1}, respectively, for 12 and 14, but -8182 cm^{-1} for 15. However these energy defects are ΔT_e rather than $\Delta E(v'',v')$; taking this fact into account and using the more recent potential energy curves[20] one finds that 12, 14 and 15 are probably near resonant processes ($\Delta E \sim 500$ cm^{-1} or less) with large Franck-Condon factors. Indeed, the $\tilde{C}\ ^2\Pi$ and $\tilde{D}\ ^2\Sigma^+$ potential curves of NO are almost identical below about 1.18 Å, yet the $\tilde{C}$ state is quenched at a rate more than 20 times

0 0 0 0 3 6 0 3 3 8

greater than the $\tilde{D}$. Gilmore's potential energy curves,[20] however, show an avoided crossing of the $\tilde{C}\ ^2\Pi$ and the $\tilde{B}\ ^2\Pi$ at r_c = 1.18 Å which would greatly enhance the Franck-Condon factors for processes such as 15 over $\tilde{D}$ quenching:

16) $NO(\tilde{D}\ ^2\Sigma^+) + N_2(\tilde{X}\ ^1\Sigma_g^+) \rightarrow NO(A\ ^2\Sigma^+) + N_2(X\ ^1\Sigma_g^+) - \sim 8000\ cm^{-1}$.

Why 13 doesn't occur remains a mystery because 13a,

13a) $CO(\tilde{a}\ ^3\Pi,\ v=0) + NO(\tilde{X}\ ^2\Pi,\ v=0) \rightarrow NO(\tilde{A}\ ^2\Sigma^+,\ v=2) + CO(\tilde{X}\ ^1\Sigma^+, v=0)$,

has a large Franck-Condon factor and an energy defect of less than 100 cm^{-1}.

Collisional quenching of $O_2^+(\tilde{a}\ ^4\Pi_u)$ by O_2 can proceed by way of near resonance processes with large Franck-Condon factors. Reaction 5a,

5a) $O_2^+(\tilde{a}\ ^4\Pi_u, v=0) + O_2(\tilde{X}\ ^3\Sigma_g^-) \rightarrow O_2(\tilde{X}\ ^3\Sigma_g^-, v=4 \text{ to } 8) + O_2^+(\tilde{X}\ ^2\Pi_g, v=1 \text{ or } 2)$

is about 25,000 cm^{-1} exothermic and this large ΔE gives 5a a low rate, though it is spin-allowed and has large Franck-Condon factor. Quenching similar to 5a of the other vibrational levels of $O_2^+\ \tilde{a}\ ^4\Pi_u$ is also highly non-resonance ($\Delta E \sim 20000\ cm^{-1}$). Other quenching transitions are less exothermic, for example,

5b) $O_2^+(\tilde{a}\ ^4\Pi_u, v') + O_2(X\ ^3\Sigma_g^-, v=0) \rightarrow O_2(\tilde{b}\ ^1\Sigma_g^+, v=2 \text{ to } 4) + O_2^+(X\ ^2\Pi_g, v=1 \text{ or } 2)$,

but still have large energy defects and low rates: $\Delta E \sim 15000\ cm^{-1}$ for $v' = 0$ and $\sim 11000\ cm^{-1}$ for v' greater than 0. The final possibility is 5c,

enough information on the excited states of methane to guess whether 16s would be near-resonant. If CH_4^{+*} were formed in a predissociated state, then 16s could hardly escape being near-resonant since predissociated states tend to be quasi-continuums rather than discrete energy states. Charge exchange in polyatomic species such as in Reaction 16s may not be governed by the requirement of vertical transitions which leads to the Franck-Condon principle. However, that methane is a poor quenching agent for $O_2^+(\tilde{a}\ ^4\Pi_u)$ is an empirical fact which draws us to the conclusion that 16s is slow regardless of whether it seems not to have the usual constraints.

Summary

On the basis of their ΔH_f° one would expect O^+ and $O_2^+(\tilde{a}\ ^4\Pi_u)$ to be highly reactive species. Their interactions with O_2 however are reactive in only a few percent of the collisions. Charge exchange of O^+ with O_2 and quenching of $O_2^+(\tilde{a}\ ^4\Pi_u)$ by O_2 may both be slow because Franck-Condon factors for the interactions are small except where the processes have large energy defects.

0 0 0 0 3 6 0 3 8 4 0

References - Chapter V

1a. D. K. Bohme, P. P. Ong, J. B. Hasted, and L. R. Megill, Planetary Space Sci. 15, 1777 (1967).

b. M. M. Nakshbandi and J. B. Hasted, Planetary Space Science 15, 1781 (1967).

c. J. Sayers and D. Smith, Disc. Faraday Soc. 37, 167 (1964).

d. R. F. Stebbings, B. R. Turner, and J. A. Rutherford, J. Geophys. Res. 71, 771 (1966).

e. P. H. Batey, G. R. Court, and J. Sayers, Planetary Space Sci. 13, 911 (1965).

f. M. J. Copsey, D. Smith, and J. Sayers, Planetary Space Sci. 14, 1047 (1966).

g. D. B. Dunkin, F. C. Fehsenfeld, A. L. Schmeltekopf, and E. E. Ferguson, J. Chem. Phys. 49, 1365 (1968).

2. D. Rapp and W. E. Francis, J. Chem. Phys. 33, 1230 (1960).

3. J. B. Hasted, Physics of Atomic Collision, (London, 1964), p. 432.

4. D. W. Vance and T. L. Bailey, J. Chem. Phys. 44, 486 (1966).

5. D. Rapp and W. E. Francis, J. Chem. Phys. 37, 2631 (1962).

6. Ref. 3, p. 420.

7. Ref. 3, p. 434; concerning $Xe^+ + C_2H_4 \rightarrow Xe + C_2H_4^+$ of F. H. Field and J. L. Frankling, Electron Impact Phenomena (New York, 1957).

8a. P. D. Goldan, A. L. Schmeltekopf, F. C. Fehsenfeld, H. I. Schiff, and E. E. Ferguson, J. Chem. Phys. 44, 4095 (1966).

b. V. Aquilanti, and G. G. Volpi, Ric. Sci. 36, 359 (1966).

c. P. Warneck, Planetary Space Sci. 15, 1349 (1967).

9. R. K. Curran, J. Chem. Phys. 38, 2974 (1963).

10. J. L. Franklin, and M. S. B. Munson, Tenth Symposium on Combustion, 561 (1965).

11. J. J. Leventhal and L. Friedman, J. Chem. Phys. 46, 997 (1967).

12. M. Jeunehomme and A. B. F. Duncan, J. Chem. Phys. 40, 1692 (1964).

13. T. F. Moran and L. Friedman, J. Chem. Phys. 42, 2391 (1965).

14. B. R. Turner, J. A. Rutherford and D. M. J. Compton, J. Chem. Phys. 48, 1602 (1968).

15. J. W. Sidman, J. Chem. Phys. 29, 644 (1958).

16. W. T. Raynes, J. Chem. Phys. 44, 2755 (1966).

17. L. Wallace, Astrophys. J. Suppl. 7, 165 (1962).

18. L. Brewer, private communication, 1971.

19. W. L. Borst and E. C. Zipf, Phys. Rev. A3, 979 (1971).

20. F. R. Gilmore, J. Quant. Spectroscopy and Rad. Transfer, 5, 369 (1965).

21. H. Lefebure-Brion and F. Guerin, J. Chem. Phys. 49, 1446 (1968).

22. J. G. Calvert and J. N. Pitts, Photochemistry, 1966, p. 68.

23. R. C. Millikan, J. Chem. Phys. 38, 2855 (1963).

24. G. M. Burnett and A. M. North, Transfer and Storage of Energy by Molecules, (London, 1969), Volume 2, p. 153.

25. ibid., Volume 1, p. 21ff.

26. A. B. Callear and I. W. M. Smith, Trans. Faraday Soc., 61, 2383 (1965).

27. I. M. Campbell and B. A. Thrush, J. Quant. Spectroscopy and Rad. Transfer 8, 1571 (1968).

28. F. Stuhl and H. Niki, Chem. Phys. Letters 7, 473 (1970).

29. cf. the activation barrier to formation of $H_2O_2^+$ found by Mahan, et al., J. Chem. Phys. 50, 5418 (1969); ibid., 75, 1426(1971);

0 0 0 0 3 6 0 3 8 4 1

C. W. Tsao, University of California, Lawrence Radiation Laboratory, Report UCRL-19140 (1970).

30. D. R. Kearns, J. Am. Chem. Soc., 91, 6554 (1969).

VI. THE CROSS REACTIONS IN METHANE-OXYGEN MIXTURES

In Table III of Chapter IV the peaks observed in a typical mass spectrum of a methane-oxygen mixture were broken down into their component species. When the species produced from contaminants, discussed in Chapter IV, and from methane, discussed in Chapter III, are subtracted almost nothing remains in the typical mass spectrum except the O_2^+ peak. Further taking away the species produced from oxygen leaves that which will be discussed here - the species resulting from cross reactions of methane species with oxygen species.

Table I shows the rates of these cross interactions determined from the rate of loss of primary ions of each species. The rates shown are not the apparent loss rates but are instead the rates of loss after correction for the reactions discussed in Chapters III, IV, and V. Observe how the reaction of CH_n^+ with O_2 is fast for n=0 and 1, but drops an order of magnitude in going to n=2, and again to n=3. $CH_4^+ + O_2$ is not expected to fit the above pattern because it has two reaction channels - charge exchange and H atom transfer - which the $n<4$ interactions do not. The $O_2^+ + CH_4$ interaction likewise lacks these two channels of reaction and has a very small rate of reaction like $CH_3^+ + O_2$. $O^+ + CH_4$ on the other hand, shows the low rate of reaction even though charge exchange and H-atom transfer are exothermic.

Before we can begin to rationalize the pattern of observed rates of these cross reactions we must establish what are the product channels for each. Table II gives the enthalpy and spin change data for the channels of interest. The rate constants shown will be discussed later. A glance at the length of Table II and the possible complexity of reaction which it implies will convince one that even with a most powerful technique

0 0 0 0 3 6 0 3 3 4 2

Table I

Rate of Loss of Primary Ions due to Cross Reactions

Reaction Number	Primary Ion Species	Reactant Neutral	Loss Rate Constant ($\frac{x10^{-10}cm^3}{molec-sec}$)	Orbiting Reaction Rate Constant Rate ($x10^{-10}$)
20)	C^+	O_2	9.8 ±.8	9.93*
21)	CH^+	O_2	9.7 ±.7	9.65
	CD^+	O_2	9.2 ±.7	9.40
22)	CH_2^+	O_2	1.0 ±.04	9.40
	CD_2^+	O_2	0.9 ±.04	8.98
23)	CH_3^+	O_2	0.13±.01	9.18
	CD_3^+	O_2	0.13 ±.01	8.64
24)	CH_4^+	O_2	4.6 ±.2	8.98
	CD_4^+	O_2	4.2 ±.2	8.35
13)	O^+	CH_4	~0.50	13.24
	O^+	CD_4	0.47 ±.05	12.56
16)	O_2^+	CH_4	0.20 ±.004	11.47
	O_2^+	CD_4	0.12 ±.004	10.67

*Based on polarizability data from Chapter I, Ref. 12.

TABLE II

Cross Reaction Data*

	Reaction	ΔH (kcal/mole)	Δs**	k (x10^{-10}cm^3/molec-sec) $O_2 + CH_4$	k (x10^{-10}cm^3/molec-sec) $O_2 + CD_4$
20 a)	$C^+ + O_2 \rightarrow CO^+ + O$	-74	0	11.0	10.7
b)	$O_2^+ + C$	+18	0		
21 a)	$CH^+ + O_2 \rightarrow HCO^+ + O$	-145	0	9.7±.7	9.2±.7
b)	$OH^+ + CO$	-113	0	< .1	< .1
c)	$CO^+ + OH$	-93	0	< 1	< 1
d)	$O^+ + HCO$	-29	0	< .1	< .1
e)	$CO^+ + O + H$	+10	0	-	-
f)	$O_2^+ + CH$	+21	0	-	-
g)	$C^+ + HO_2$	+37	0	-	-
22 a)	$CH_2^+ + O_2 \rightarrow H_2O^+ + CO$	-126	0	< .1	< .1
b)	$CO_2^+ + H_2$	-110	0	< .05[a]	< .05[a]
c)	$HCO^+ + OH$	-130	0	< .01	< .01
d)	$CO^+ + H_2O$	-94	0	< .03	< .03
e)	$CO_2H^+ + H$	-92	0	< .01	< .01
f)	$H_2^+ + CO_2$	-71	0	< .001	< .001
g)	$H_2CO^+ + O$	-50	0	1.0±.04	0.9± .4
h)	$OH^+ + HCO$	-25	0	< .01	< .01
i)	$CO_2^+ + 2H$	-6	0	< .05[a]	< .05[a]
j)	$HCO^+ + O + H$	-18	0	< .01	< .01
k)	$O_2^+ + CH_2$	+39	0	-	-
l)	$CH^+ + HO_2$	+61	0	-	-
23 a)	$CH_3^+ + O_2 \rightarrow H_3O^+ + CO$	-130	-1	0	0
b)	$HCO^+ + H_2O$	-124	-1	0	0
c)	$CO_2H^+ + H_2$	-71	-1	0	0
d)	$H_3^+ + CO_2$	-58	-1	0	0
e)	$H_2O^+ + CHO$	-31	0	< .01[b]	< .01[b]

	f)	$CH_3O^+ + O$	-20	0	.13±.01	.13±.01
	g)	$H_2O^+ + CO + H$	-1	0	< .01[b]	< .01[b]
	h)	$O_2^+ + CH_3$	+51	0	-	-
	i)	$CH_2 + HO_2$	+78	0	-	-
24	a)	$CH_4^+ + O_2 \rightarrow H_3O^+ + HCO$	-122	0	< .005[c]	< .005[c]
	b)	$CO_2H_2^+ + H_2$	-110	0	< .001	< .001
	c)	$H_2CO^+ + H_2O$	-109	0	< .005	< .005
	d)	$CH_3O_2^+ + H$	-107	0	< .001	< .001
	e)	$H_3O^+ + CO + H$	-92	0	< .005[c]	< .005[c]
	f)	$CH_3O^+ + OH$	-89	0	< .01	< .01
	g)	$H_2O^+ + H_2CO$	-73	0	< .005[e]	< .005[e]
	h)	$H_2O^+ + H_2 + CO$	-71	0	< .005[e]	< .005[e]
	i)	$HCO^+ + H_2O + H$	-86	0	< .001[f]	< .001[f]
	j)	$CO_2^+ + 2H_2$	-51	0	< .001	< .001
	k)	$HCO^+ + OH + H_2$	-71	0	< .001[f]	< .001[f]
	l)	$CO^+ + H_2O + H_2$	-35	0	< .001	< .001
	m)	$HCO^+ + H_2 + H$	-60	0	< .001[f]	< .001[f]
	n)	$H_3^+ + CO_2H$	-17	0	< .001[d]	< .001[d]
	o)	$H_3^+ + CO_2 + H$	-14	0	< .001[d]	< .001[d]
	p)	$O_2^+ + CH_4$	-14	0	2.1±.2	1.9±.2
	q)	$CH_3OH^+ + O$	-12	0	< .001	< .001
	r)	$CH_3^+ + HO_2$	-9	0	2.5±.2	2.3±.2
13	a)	$O^+ + CH_4 \rightarrow H_2CO^+ + H_2$	-133	-1	0	0
	b)	$CH_3O^+ + H$	-124	-1	0	0
	c)	$CH_3^+ + OH$	-87	-1	0	0
	d)	$HCO^+ + H_2 + H$	-110	-1	0	0
	e)	$CH_2^+ + H_2O$	-81	-1	0	0
	f)	$H_3^+ + HCO$	-64	-1	0	0
	g)	$CO^+ + 2H_2$	-59	-1	0	0
	h)	$H_3O^+ + CH$	-58	-1	0	0
	i)	$H_3^+ + H + CO$	-34	-1	0	0
	j)	$H_2O^+ + CH_2$	-29	0	< .01	< .01
	k)	$H_2CO^+ + 2H$	-29	0	< .01	< .01
	l)	$H_2^+ + H_2CO$	-28	-1	< .01	< .01

m)		$CH_4^+ + O$	-22	0	.50±.05	.47±.05
n)		$OH^+ + CH_3$	-11	0		
16 a)	$O_2^+ + CH_4 \rightarrow$	$H_3O^+ + CHO$	-108	0	< .001[g]	< .001[g]
b)		$CO_2H_2^+ + H_2$	-96	0	< .001	< .001
c)		$H_2CO^+ + H_2O$	-95	0	< .01	< .01
d)		$CH_3O_2^+ + H$	-93	0	.07±.004	.04±.004
e)		$H_3O^+ + CO + H$	-78	0	< .001[g]	< .001[g]
f)		$CH_3O^+ + OH$	-75	0	.13±.004	.08± .04
g)		$H_2O^+ + H_2CO$	-59	0	< .001[h]	< .001[h]
h)		$H_2O^+ + H_2 + CO$	-57	0	< .001[h]	< .001[h]
i)		$HCO^+ + H_2O + H$	-72	0	< .001[i]	< .001[i]
j)		$CO_2^+ + 2H_2$	-37	0	< .001	< .001
k)		$HCO^+ + OH + H_2$	-57	0	< .001[i]	< .001[i]
l)		$CO^+ + H_2O + H_2$	-21	0	< .001	< .001
m)		$HCO^+ + H_2 + H$	-46	0	< .001[i]	< .001[i]
n)		$H_3^+ + CO_2H$	-3	0	< .001[j]	< .001[j]
o)		$H_3^+ + CO_2 + H$	0	0	< .001[j]	< .001[j]
p)		$CH_3OH^+ + O$	+2	0	< .001	< .001
q)		$CH_3^+ + HO_2$	+5	0	< .01	< .01
r)		$CH_4^+ + O_2$	+14	0	< .01	< .01

---

* This table is intended to comprise all exothermic channels of reaction and a few endothermic channels of interest.

** This quantity refers to the change in spin quantum number. The interaction of a doublet ion with a triplet neutral, for example, can produce a singlet product ion if the product neutral is a doublet or quartet, a doublet product ion if the product neutral is a singlet or triplet, a triplet product ion if the product neutral is a doublet, and a quartet product if the product neutral is a singlet; other possibilities arise if more than one product neutral is formed. This table will show $\Delta s = 0$ if any one of the possible combinations includes the spin change of the reaction being considered. Thus we show $\Delta s = 0$ for both 24a and 24q:

$$CH_4^+(\tilde{X}^2E) + O_2(\tilde{X}^3\Sigma_g^-) \rightarrow H_3O^+(\tilde{X}^1A_1) + HCO(\tilde{X}^2A')$$

0 0 0 0 3 6 0 - 0 4 4

$$CH_4^+(\tilde{X}^2E) + O_2(\tilde{X}^3\Sigma_g^-) \rightarrow CH_3OH^+(\tilde{X}^2E) + O(\tilde{X}^3P).$$

Consequently, few reactions listed show $\Delta s \neq 0$.

[a] The total rate of Reactions 22b and 22i combined is less than .05 x 10^{-10}cm^3/molec-sec.

[b] The total rate of Reactions 23e and 23g combined is less than .01 x 10^{-10}cm^3/molec-sec.

[c] The total rate of Reactions 24a and 24e combined is less than .005 x 10^{-10}cm^3/molec-sec.

[d] The total rate of Reactions 24m and 24o combined is less than .001 x 10^{-10}cm^3/molec-sec.

[e] The total rate of Reactions 24g and 24h combined is less than .005 x 10^{-10}cm^3/molec-sec.

[f] The total rate of Reactions 24i, 24m and 24k combined is less than .001 x 10^{-10}cm^3/molec-sec.

[g] The total rate of Reactions 16a and 16e combined is less than .001 x 10^{-10}cm^3/molec-sec.

[h] The total rate of Reactions 16g and 16h combined is less than .001 x 10^{-10}cm^3/molec-sec.

[i] The total rate of Reactions 16i, 16k and 16m combined is less than .001 x 10^{-10}cm^3/molec-sec.

[j] The total rate of Reactions 16n and 16o combined is less than .001 x 10^{-10}cm^3/molec-sec.

like cyclotron double resonance the going will be difficult. Indeed, a weak technique like appearance potential measurements has proven to be of little value. Ion ejection double resonance in the low mass range (12-14) has proven too noisy for definitive results in the methane-oxygen system. Ion ejection double resonance has been able to establish some of the ions for which CH_4^+ (or CD_4^+) and O_2^+ are precursors. Tables III and IV show results of ejecting CH_4^+ and CD_4^+, respectively, in mixtures of equal amounts of oxygen and, respectively, methane and methane-d_4. The only significant effects observable in Table IV are probably due to Reactions 10 and 11:

		double resonance
10)	$CD_3^+ + CD_4 \rightarrow C_2D_5^+ + D_2$	18→34
11)	$CD_4^+ + CD_4 \rightarrow CD_5^+ + CD_3$	20→22.

The effects at masses 23 and 35 are due to ^{13}C analogues of Reactions 10 and 11. The significant effects seen in Table III are due to Reactions 10 and 11, above, and 14, 33, and 34, below:

14)	$H_2O^+ + CH_4 \rightarrow H_3O^+ + CH_3$	18→19
33)	$CH_4^+ + H_2O \rightarrow H_2O^+ + CH_4$	16→18
34)	$CH_4^+ + H_2O \rightarrow H_3O^+ + CH_3$	16→19

There is a large effect in both Tables III and IV at mass 48; we know that this ion is entirely O_3^+ in both mixtures (we can assume $CD_2O_2^+$ is absent from CD_4-O_2 mixtures since $CH_2O_2^+$ is not formed in CH_4-O_2 mixtures; and $CH_4O_2^+$ is absent from CH_4-O_2 mixtures since $CD_4O_2^+$ is not formed in CD_4-O_2 mixtures). There can be no chemical connection between the methane reactant ions and O_3^+ product ions; therefore, these effects at the higher masses probably are due to random errors and to systematic errors in calculating the effects of direct ejection (the numbers shown

Table III. Expt 184 $CH_4:O_2 \cong 1$ CW Ion Ejection at Mass 16

Ion Detected	Peak Area w/o Ejection	Peak Area with Ejection	Calculated	Difference	Ratio (%)
2	31	30	31	-1	-3.3
12	719	715	716	-1	-.2
13	2465	2456	2447	9	.4
14	7205	7072	7073	-0	-.0
15	36970	34800	34540	268	.8
16	47530	37230	36510	712	1.9
17	15430	12850	14130	-1286	-10.0
18	489	438	473	-34	-8.0
19	381	336	374	-37	-11.4
26	1184	1170	1180	-9	-.8
27	4739	4707	4723	-15	-.3
28	3898	3794	3886	-91	-2.4
29	39190	36460	39070	-2608	-7.2
30	1741	1591	1736	-144	-9.1
31	1781	1772	1776	-3	-.2
32	181300	178800	180900	-2084	-1.2
33	719	729	717	12	1.7
34	799	777	797	-20	-2.6
44	1573	1563	1570	-6	-.4
45	1865	1851	1861	-9	-.5
47	1352	1325	1349	-24	-1.9
48	960	926	958	-31	-3.5

VI-III

Table IV. Expt 197 $CD_4:O_2 \cong 1$ CW Ion Ejection at Mass 20

Ion Detected	Peak Area w/o Ejection	Peak Area with Ejection	Calculated	Difference	Ratio (%)
2	27	27	27	0	.0
12	661	653	660	-6	-1.1
14	2902	2980	2892	88	2.9
15	100	100	99	1	.1
16	19940	19450	19740	-296	-1.5
17	778	761	763	-1	-.3
18	44370	41570	42470	-901	-2.2
19	1472	1291	1289	2	.2
20	42940	30640	30950	-309	-1.0
21	876	743	747	-3	-.5
22	24430	19790	22840	-3050	-15.4
23	284	239	274	-34	-14.7
28	3082	3048	3053	-4	-.2
29	130	127	129	-1	-1.6
30	9788	9505	9717	-211	-2.2
31	186	181	185	-3	-2.3
32	176000	172200	175000	-2752	-1.6
33	1145	1143	1139	4	.3
34	47560	45030	47310	-2275	-5.1
35	1013	928	1008	-79	-8.7
44	834	830	831	-1	-.1
46	956	980	953	27	2.8
48	710	681	708	-26	-4.0
50	914	878	911	-32	-3.8

in the column labelled "Calculated"). Ion ejection of O_2^+ (Tables V and VI) on the other hand, gives a substantial effect at the highest two masses. The 32→48 effect, of course, is Reaction 29:

29) $O_2^{+*} + O_2 \rightarrow O_3^+ + O$ 32→48

The 32→47 in CH_4:O_2 ~ 1 and the 32→50 in CD_4:O_2 ~ 1 are both due to 16d:

16d) $O_2^+ + CH_4 \rightarrow CH_3O_2^+ + H$ 32→47 for CH_4; 32→50 for CD_4

Based on the rate of 29 observed in pure oxygen and in methane-oxygen mixtures, the rate coefficient for the effect due to 16d can be determined as $7.0\pm.4 \times 10^{-12}$ cm^3/molec-sec from the magnitude of the ion ejection effect in CH_4-O_2 mixtures. In CD_4-O_2 mixtures the effect shows the rate of 16d as $3.8\pm.4 \times 10^{-12}$. From this same sort of calculation, we can determine that the rate of 24d,

24d) $CH_4^+ + O_2 \rightarrow CH_3O_2^+ + H$ 16→47 for CH_4; 20→50 for CD_4

is less than 4×10^{-13} cm^3/molec-sec. These figures agree well with the quantitative results of the final data fitting procedure, which give the rate of 16d as $7.0\pm.1$ and $4.0\pm.1 \times 10^{-12}$ cm^3/molec-sec in CH_4-O_2 and CD_4-O_2 mixtures, respectively, and of 24d as less than 10^{-13}. The remaining effects in Tables V and VI are probably not significant relative to random error.

In discussing the reactions of C^+ with methane in Chapter III, we mentioned that adding small amounts of CO or CO_2 enhanced the C^+ concentration and gave us additional information about the $C^+ + CH_4$ reactions. The opportunity to gain this additional insight was dependent on the fact that no interferences arose; by that, we mean, for example, that the

Table V. Expt 184 $CH_4:O_2 \cong 1$ CW Ion Ejection at Mass 32

Ion Detected	Peak Area w/o Ejection	Peak Area with Ejection	Calculated	Difference	Ratio (%)
2	31	31	31	0	.0
12	719	719	719	0	.0
13	2465	2463	2463	0	.0
14	7205	7198	7198	0	.0
15	36970	36920	36920	1	.0
16	47530	47460	47460	2	.0
17	15400	15400	15400	0	.0
18	489	487	488	0	.0
19	381	380	380	0	.0
26	1184	1162	1151	10	.9
27	4739	4613	4540	73	1.6
28	3898	3710	3639	70	1.9
29	39190	36520	34840	1683	4.6
30	1741	1532	1404	128	8.4
31	1781	1211	1207	4	.3
32	181300	109800	108500	1322	1.2
33	719	509	480	29	5.7
34	799	620	619	1	.2
44	1573	1537	1534	3	.2
45	1865	1818	1823	-4	-.3
47	1352	911	1326	-415	-45.7
48	960	705	943	-237	-33.8

Table VI. Expt 197 $CD_4:O_2 = 1$ CW Ion Ejection at Mass 32

Ion Detected	Peak Area w/o Ejection	Peak Area with Ejection	Calculated	Difference	Ratio (%)
2	27	27	27	0	.0
12	661	655	661	-5	-.9
14	2902	2917	2899	18	.6
15	100	99	100	-0	.0
16	19940	19630	19900	-273	-1.4
17	778	770	776	-6	-.9
18	44370	43930	44260	-330	-.8
19	1472	1490	1467	23	1.5
20	42950	42070	42760	-692	-1.6
21	876	859	871	-11	-1.4
22	24430	24450	24250	202	.8
23	284	276	281	-5	-2.0
28	3082	2948	2878	71	2.4
29	130	118	116	3	2.2
30	9788	8475	7895	580	6.8
31	186	144	126	18	12.5
32	176050	106400	105300	1065	1.0
33	1145	867	764	102	11.8
34	47560	40180	36850	3329	8.3
35	1013	925	862	62	6.7
44	834	823	813	10	1.2
46	956	965	936	29	3.0
48	710	537	697	-159	-29.9
50	914	591	900	-307	-52.2

VI-VI

0 0 0 0 3 6 0 0 8 4 7

reactions of C^+ with methane gave products known to be of different masses from the products of reactions of CH_4^+ with CO, CO^+ with CH_4, etc. We have the opportunity to rely upon an analogous set of circumstances in the mixtures of oxygen and chloromethanes (CH_3Cl, CH_2Cl_2, and $CHCl_3$) which were studied in Experiments 201-203. These mixtures must be predominantly oxygen so that the effects of even the fast reactions of chloromethane ions with chloromethanes will be negligible. There is necessarily some concern over the reactions of O_2^+ with chloromethanes; however, it appears that these interactions lead predominantly to charge exchange. It seems at least that no product ion of mass less than 50 is produced from reactions of O_2^+ with chloromethanes (peaks of mass 50 and greater were not examined). This means that except for charge exchange the reactions of O_2^+ with chloromethanes are, in keeping with the reactions of O_2^+ with methane, very slow (at most, they produce ions of mass 50 or greater). Somewhat more HO_2^+ was observed than expected; however, since none of the reactions

$$CH_n^+ + O_2 \rightarrow HO_2^+ + CH_{n-1} \qquad n=1 \text{ to } 4$$

is exothermic, we ignored the extra HO_2^+. Perhaps it is produced from O_2^+* + CH_3Cl, for example, or from Reaction 19, $H_2^+ + O_2 \rightarrow HO_2^+ + H$, if there were more H_2^+ in these experiments; unfortunately H_2^+ was not measured.

In each of these experiments, mixture composition was estimated from the pressure measurements gotten on the gas mixing manifold when the mixture was prepared, instead of the usual procedure of determining mixture composition mass spectrometrically. We need an accurate measurement of the oxygen partial pressure in the mass spectrometer during experiments, but only a very approximate estimate of the chloromethane partial pressure. We can calculate the O_2 partial pressure in the

0 0 0 0 3 6 0 3 8 4 8

following three ways:

1. From the TIC using the value of σ_t for electron impact on O_2 from Table II of Chapter II and assuming that $\sigma_t(CH_4) \approx \sigma_t$(any chloromethane).

2. From the O_2^+ peak area assuming O_2^+ charge exchanges with a chloromethane at a rate of 2×10^{-10} cm^3/molec-sec.

3. From the O^+ peak area assuming O^+ charge exchanges with a chloromethane at a rate of 5×10^{-11}.

Each of these calculations is obviously crude for moderate chloromethane relative concentrations but fairly good when chloromethanes made up only 5% of the sample or less. All three calculations agreed to within 6% generally and the average calculated oxygen partial pressure was used for rate calculations. In each each experiment a low pressure spectrum was observed for masses in the 12 to 34 and 40 to 48 ranges to determine any H_2O, CO, or CO_2 contamination. The circumstances, then, are ideal for examining the products of the reactions of $CH_n^+ + O_2$ where n=1, 2, or 3, without the interferences due to those of $CH_4^+ + O_2$ or $O_2^+ + CH_4$.

In the O_2:$CHCl_3 \approx 25$ mixture (Expt 203) secondary contributions were found for masses 28 and 29. The CH_n^+ primary ions comprised only modest peaks at masses 12 (C^+), 13 (CH^+, $^{13}C^+$) and 14 ($^{13}CH^+$). It was determined in a low pressure spectrum that H_2O, CO, and CO_2 contaminants were present; at high pressure the small secondary component of mass 28 could be accounted for fully by Reaction 20a,

20a) $C^+ + O_2 \rightarrow CO^+ + O$,

which has a rate of 1.10×10^{-9} cm^3/molec-sec.[1,2,3] On the basis of the fact that all the secondary CO^+ was accounted for by Reaction 20a, we determined an upper limit on 21c,

21c) $CH^+ + O_2 \rightarrow CO^+ + OH$

of 10^{-10} cm^3/molec-sec. Because masses 16 and 17 were entirely primary

(primary ions from O_2 and H_2O) we determined an upper limit on 21b and d,

21b) $CH^+ + O_2 \rightarrow OH^+ + CO$

21d) $CH^+ + O_2 \rightarrow O^+ + HCO$

of 10^{-12} cm^3/molec-sec. 21a was determined to have a rate of $10 \pm 1 \times 10^{-10}$ cm^3/molec-sec,

21a) $CH^+ + O_2 \rightarrow HCO^+ + O$

in good agreement with Franklin's[3] measurement of 10^{-9} and with the least squares data fitting for the results in methane-oxygen mixtures which gave a rate for 21a of $9.7 \pm .7 \times 10^{-10}$ cm^3/molec-sec in CH_4-O_2 mixtures and $9.2 \pm .7 \times 10^{-10}$ in CD_4-O_2 mixtures.

Experiment 202 was a study of an O_2:$CH_2Cl_2 \approx 16$ mixture. In this mixture at low pressure, primary ions C^+, CH^+, CH_2^+ ($^{13}CH_2^+$ as well), O^+, H_2O^+, CO^+ and CO_2^+ were seen in the mass range below 50. At high pressure the only secondary species not accounted for by reactions of C^+ with O_2 and CH^+ with O_2 was the mass 30 peak. This peak is produced from 22g,

22g) $CH_2^+ + O_2 \rightarrow CH_2O^+ + O$

which has a rate of $1.0 \pm .08 \times 10^{-10}$ cm^3/molec-sec. This reaction accounts for all the CH_2O^+ observed in mixtures of methane and oxygen; analysis of the data for these mixtures gives the rate of 22g as $1.0 \pm .04 \times 10^{-10}$ cm^3/molec-sec in CH_4-O_2 mixtures and $0.9 \pm .2 \times 10^{-10}$ in CD_4-O_2 mixtures. On the basis of experiment 202 and the analysis of the methane-oxygen data we can determine upper limits on the rates of the other exothermic channels of $CH_2^+ + O_2$; these upper limits are given in Table II.

0 0 0 0 3 6 0 3 8 4 9

In Experiment 201 a mixture of O_2:$CH_3Cl \approx 50$ only one additional reaction was observed than in Experiment 202 and it was 23f,

23f) $\quad CH_3^+ + O_2 \rightarrow CH_3O^+ + O$

which showed a rate of $1.3 \pm .4 \times 10^{-11}$ cm^3/molec-sec, in agreement with the subsequent data analysis for CH_4-O_2 mixtures which gave a rate for 23f as $1.3 \pm .1 \times 10^{-11}$ cm^3/molec-sec (for CD_4-O_2 mixtures 23f gave a rate of 1.3×10^{-11} as well). Again, the upper limits on the rates of the other exothermic reaction channels were determined from Experiment 201 and from data analysis of the reactions in methane- and methane-d_4-oxygen mixtures. These estimates are shown in Table II.

The final method for determining precursors for the product ions in methane-oxygen mixtures is ion cyclotron double resonance. Tables VII and VIII give the results of our double resonance experiments in which the average reactant ion center-of-mass kinetic energy was around 20 kcal/mole. The first column in Table VII gives all the signals observed and qualitative estimates of their intensities. The second column lists some of the non-chemical signals one might expect; we shall discuss these in more detail below. The third column lists the signals seen in pure methane; and the fourth, what remains from the first column which cannot be accounted for by entries in the second and third columns. Figures 1 and 2 make clear what we have attemped in Table VII. Compare the 0.4 VPTP double resonance spectrum observed in CH_4:$O_2 \approx 1$ (Fig. 1) with that observed in pure CH_4 (Fig. 2). They are qualitatively the same, although the signals in pure methane are somewhat more intense. That they are qualitatively the same would indicate that no new path for forming mass 15 ions occurs in methane-oxygen mixtures besides those that occur in pure methane. Unfortunately we have good evidence, which

TABLE VII

Cyclotron Double Resonance (CDR) Observed in $CH_4:O_2 \approx 1$
Compared with CDR in Pure CH_4

CDR $CH_4:O_2 \approx 1$	non chemical Signals ?	Pure CH_4	Remainder
16 → 48 vw-*	16 → 48 vw-		
32 → 48 vw-	32 → 48 vw-		
15 → 47 vw-	15 → 47 vw-		
16 → 47 vw-	16 → 47 vw-		
32 → 47 vw+	32 → 47 vw-		32 → 47 vw+
15 → 45 vw-	15 → 45 vw-		
16 → 45 vw-	16 → 45 vw-		
32 → 45 vw-	32 → 45 vw-		
16 → 44 vw-	16 → 44 vw-		
32 → 44 vw-	32 → 44 vw-		
15 → 34 vw-	15 → 34 vw-		
16 → 34 vw-	16 → 34 vw-		
32 → 34 vw-	32 → 34 vw-		
15 → 33 vw+	15 → 33 vw-		
16 → 33 m+	16 → 33 vw-		16 → 33 m+
32 → 33 vw+	32 → 33 vw-		
15 → 32 m-	15 → 32 m-		
16 → 32 m-	16 → 32 m-		
17 → 32 m-	17 → 32 m-		
15 → 31 vw-	15 → 31 vw-		
16 → 31 vw-	16 → 31 vw-		
17 → 31 vw-	17 → 31 vw-		
32 → 31 s+	32 → 31 vw-		32 → 31 s+

0 0 0 0 5 6 0 3 8 5 0

CDR $CH_4:O_2 \approx 1$	non chemical Signals ?	Pure CH_4	Remainder
14 →30 m+			14 →30 m+
15 →30 ?	15 →30 vw-?	15 →30 w+?	
16 →30 w+	16 →30 vw-	16 →30 w+	
32 →30 m+	32 →30 vw-		32 →30 m+
15 →29 s+	15 →29 vw-	15 →29 s+	
16 →29 w-	16 →29 vw-	16 →29 w-	
17 →29 vw-	17 →29 vw-	17 →29 vw-	
32 →29 vw-	32 →29 vw-		
14 →28 vs+		14 →28 vs+	
15 →28 vw-	15 →28 vw-	15 →28 vw-	
16 →28 vw-	16 →28 vw-	16 →28 vw-	
32 →28 vw-	32 →28 vw-		
12 →27 s+		12 →27 s+	
13 →27 s+		13 →27 s+	
14 →27 m+		14 →27 m+	
15 →27 vw-	15 →27 vw-		
16 →27 vw-	16 →27 vw-		
32 →27 vw-	32 →27 vw-		
13 →26 ?		13 →26 ?	
14 →26 w+		14 →26 w+	
15 →26 vw+	15 →26 vw-	15 →26 vw+	
16 →26 vw+	16 →26 vw-	16 →26 vw+	
32 →26 vw-	32 →26 vw-		
16 →19 vw+	16 →19 vw-		16 →19 vw+
16 →18 vw+	16 →18 vw-		16 →18 vw+
32 →18 vw-	32 →18 vw-		

CDR $CH_4:O_2 \approx 1$	non chemical Signals ?	Pure CH_4	Remainder
15 →17 w+	15 →17 vw-	15 →17 w+	
16 →17 m+	16 →17 vw-	16 →17 m+	
32 →17 vw-	32 →17 vw-		
15 →16 w-	15 →16 vw-	15 →16 w-	
17 →16 vw+	17 →16 vw-	17 →16 vw+	
14 →15 m-		14 →15 m-	
16 →15 s+	16 →15 vw-	16 →15 s+	16 → 15 w±?
17 →15 vw+	17 →15 vw-	17 →15 vw+	
32 →15 vw+	32 →15 vw-		32 →15 vw+
15 →14 w+	15 →14 vw-	15 →14 w+	
16 →14 vw+	16 →14 vw-	16 →14 vw+	
32 →14 vw-	32 →14 vw-		

*The notation 16 →48 vw- indicates that in a cyclotron double resonance experiment a very weak signal was seen while detecting mass 48 ions with the marginal oscillator while heating the mass 16 ions to a center-of-mass kinetic energy of about 20 kcal/mole. The - sign indicates that in a continuous wave double resonance (CWDR) experiment the mass 48 signal would diminish slightly when heating mass 16 ions. As discussed in the text, this sign may also give the sign of dk/dE for the reaction connecting the two masses. A question mark is shown after the two masses whenever ambiguity arises due to the electronic artifacts which arise when the ratio of the frequencies of the marginal and irradiating oscillators is integral.

0 0 0 0 3 6 0 3 5 1

TABLE VIII

Cyclotron Double Resonance (CDR) Observed in $CD_4:O_2 \approx 1$
Compared with CDR in Pure CH_4

CDR $CD_4:O_2 \approx 1$	non chemical Signals ?	Pure CD_4	Remainder
18 → 50 vw-[x]	18 → 50 vw-		
20 → 50 vw-	20 → 50 vw-		
32 → 50 vw+	32 → 50 vw -		32 → 50 vw+
20 → 48 vw-	20 → 48 vw-		
32 → 48 vw-	32 → 48 vw-		
20 → 46 vw-	20 → 46 vw-		
32 → 44 vw-	32 → 44 vw-		
18 → 34 s+	18 → 34 vw-	18 → 34 s+	
20 → 34 m+	20 → 34 vw-	20 → 34 w-	20 → 34 m+
32 → 34 s+	32 → 34 vw-		32 → 34 s+
16 → 32 s+		16 → 32 vs+	
18 → 32 m-	18 → 32 m-		
20 → 32 m-	20 → 32 m-		
22 → 32 m-	22 → 32 m-		
12 → 30 s+		12 → 30 s+	
14 → 30 s+		14 → 30 s+	
16 → 30 m+		16 → 30 m+	
18 → 30 vw-	18 → 30 vw-		
20 → 30 vw-	20 → 30 vw-		
32 → 30 vw-	32 → 30 vw-		

CDR $CH_4:O_2 \approx 1$	non chemical Signals ?	Pure CD_4	Remainder
14 → 28 ?		14 → 28 ?	
16 → 28 w+		16 → 28 w+	
18 → 28 vw+	18 → 28 vw-	18 → 28 vw+	
20 → 28 w+	20 → 28 vw-	20 → 28 vw+	
32 → 28 w-	32 → 28 vw-		
18 → 22 w+	18 → 22 vw-	18 → 22 w+	
20 → 22 m+	20 → 22 vw-	20 → 22 m+	
16 → 20 w-			16 → 20 w-
18 → 20 w-	18 → 20 vw-	18 → 20 w-	
32 → 20 vw-	32 → 20 vw-		
16 → 18 w-		16 → 18 w-	
20 → 18 m+	20 → 18 vw-	20 → 18 w+	20 → 18 m+
32 → 18 w-	32 → 18 vw-		32 → 18 w-
18 → 16 vw+	18 → 16 vw-	18 → 16 vw+	
20 → 16 vw+	20 → 16 vw-	20 → 16 vw+	
32 → 16 ?	32 → 16 vw-		

*The same notation is used as was in Table VII.

0 0 0 0 3 6 0 3 8 5 2

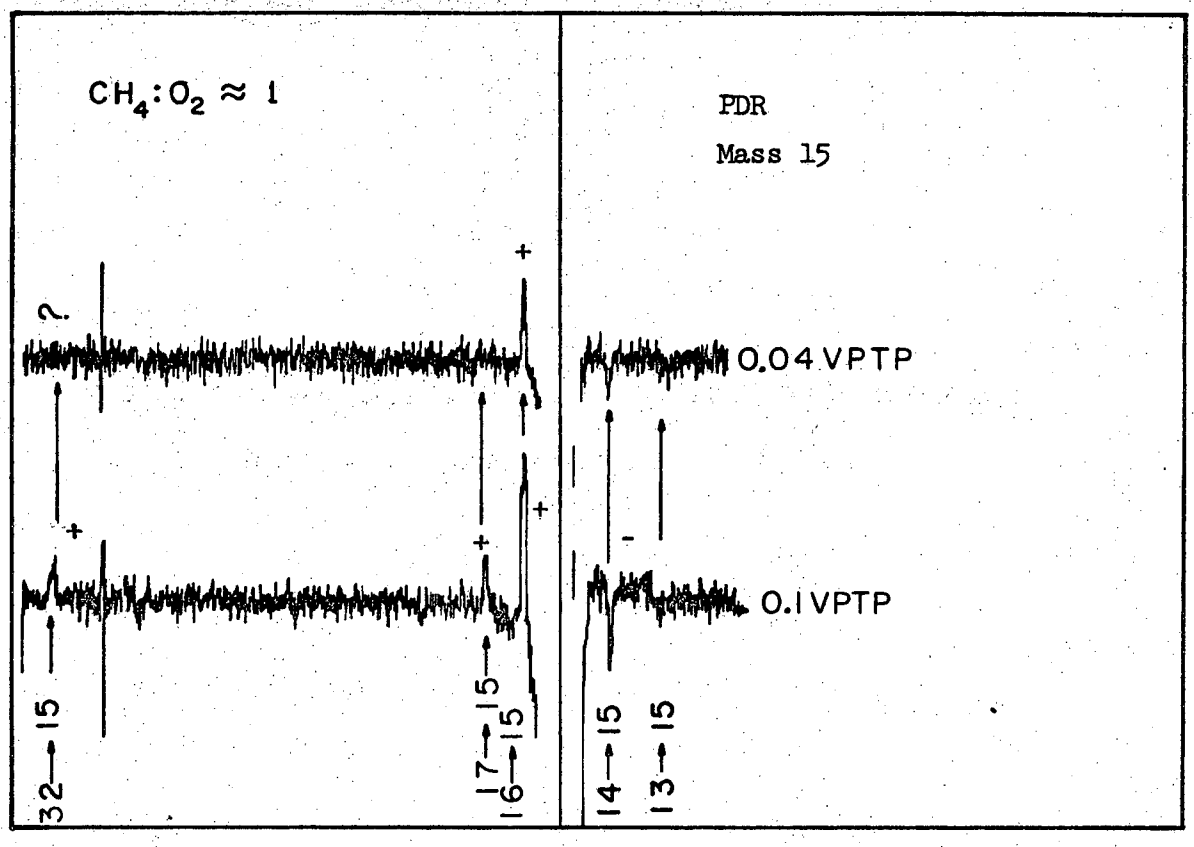

XBL717-3869

Fig. 1. Pulsed cyclotron double resonance experiment in $CH_4:O_2 \approx 1$. Mass 15 is being detected.

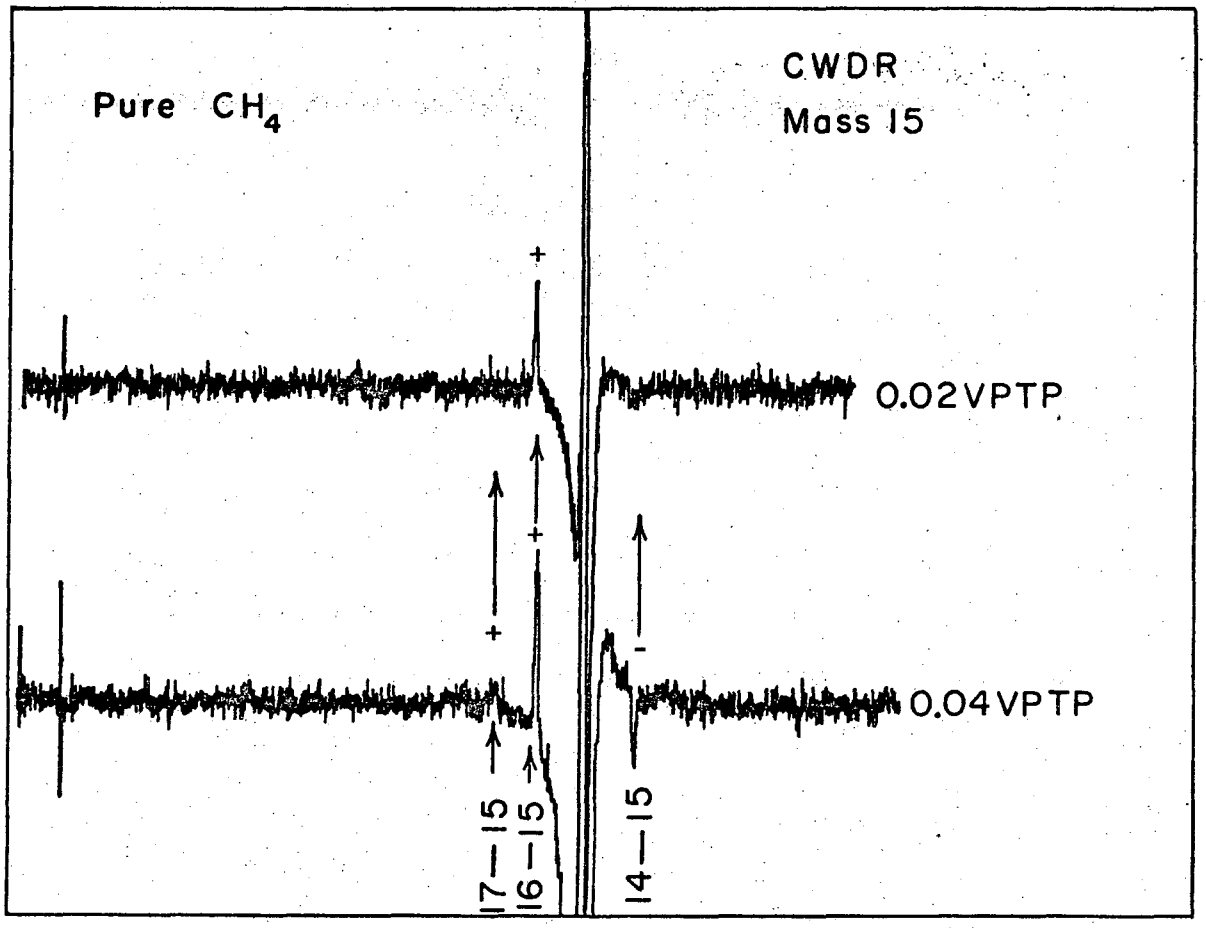

XBL716-3725

Fig. 2. CW cyclotron double resonance experiment in pure methane. This figure is a reproduction of Fig. II-9. Notice how the lower spectrum (0.04 volts peak to peak irradiating oscillator amplitude) resembles the upper spectrum of Fig. VI-1.

0 0 0 0 3 6 0 3 8 5 3

we will present later, that 24r occurs with a rate of 2.5 ±.2 x 10^{-10} cm^3/molec-sec:

24r) $CH_4^+ + O_2 \rightarrow CH_3^+ + HO_2$.

The failure of the comparison of Figs. 1 and 2 clearly to reveal the occurrence of 24r is probably due to dk/dE being small and is a weakness in the comparisons presented in Tables VII and VIII which we shall have to keep in mind.

Another feature which Figures 1 and 2 point out is the dependence of the signals on ion energy. At irradiating oscillator amplitude of 0.04 VPTP the ions in the methane-oxygen mixture are heated less than in pure methane. In these experiments it is ion-neutral collision which limits, for the most part, the length of time during which resonant ions absorb energy. Equation 11 of Chapter II gives

II-11 $$E = \frac{3}{2} kT + \frac{q^2 \mathcal{E}_o^2 \tau^2}{4m}$$

as the energy an irradiated ion reaches during the time τ since the last thermalizing elastic collision. From II-11 we estimate that the average center-of-mass ion energy for the experiments compared in Tables VII and VIII is about 20 kcal/mole. While the partial pressure of methane is the same for the experiments shown in Figs. 1 and 2, the additional oxygen partial pressure in the experiment shown in Fig. 1 makes τ about half that in Fig. 2. Therefore it is more proper to compare the 0.1 VPTP spectrum in Fig. 1 with the 0.04 VPTP spectrum in Fig. 2. The resemblance of the two figures is striking. The one signal which the 0.1 VPTP spectrum in Fig. 1 has which the 0.04 VPTP spectrum in Fig. 2 lacks is the weak 32→15 signal, which has positive dk/dE. The reaction,

16q) $O_2^+ + CH_4 \rightarrow CH_3^+ + HO_2$ $\Delta H = +5$ kcal/mole

has a thermal rate of less than 10^{-12} cm^3/molec-sec although it may be thermoneutral or exothermic for the O_2^+ ion of average energy. That dk/dE for this reaction is positive does not show that the reaction is endothermic, but only that it may be. The proof that 16q has a very low rate, however, comes from the least squares data analysis and from Tables V and VI in which O_2^+ ejection shows little or no effect on CH_3^+ (or CD_3^+).

We are now ready to begin examining all the double resonance signals we see in mixtures of methane and oxygen. The large number of signals (nearly sixty) contradicts the assertion that this system is unreactive, made by Franklin[3] and made here when we pointed out that in a typical experiment given in Table III of Chapter IV, little remains when we take away from the mass spectrum what is due to primary and secondary ions from pure methane, pure oxygen, and known contaminants. The number of signals seen is reduced by 40% when we subtract those due to reactions of methane ions with methane. Another 40% of the signals share the common features that they are very weak, generally result from heating one of the more important ion species, and show the product ion signal diminishes when the reactant ion is heated.* It seems likely that these signals are so remarkably similar because they all stem from the same non-chemical phenomenon. While it is not clear what the phenomenon is, we cannot escape the conclusion that it is non-chemical. It was noted

* For brevity, we shall use the notation k' = vw- to refer to a cyclotron double resonance signal in which the "product" ion signal diminishes very slightly when the "reactant" ion is heated. We cannot refer to dk/dE for a CDR signal which is of non-chemical origin because there is by definition no chemical reaction involved, hence no rate coefficient k. However when the signal is of chemical origin we can identify k' as dk/dE.

0 0 0 0 3 6 0 . 3 3 4

in Chapter II that when dk/dE is negative, a thermoneutral or exothermic reaction must be involved for only such can occur at thermal energy and only those reactions which occur at thermal energy can diminish in rate with increasing ion energy. But how can 16→48 vw- or 17→32 m- be explained? Only by means of non-chemical phenomena.*

In order to examine how these non-chemical signals might arise, consider equation II-10:

$$\text{II-10} \qquad A_s(\omega_1) = \frac{n_s^+ q^2 \mathcal{E}_1^2 \tau}{4m_s} \frac{1}{1 + \tau^2(\omega_1 - \omega_{cs})^2}$$

where $A_s(\omega_1)$ is the power absorption by n_s^+ secondary ions of mass m_s, charge q, and cyclotron frequency ω_{cs} from the r.f. electric field of amplitude $\mathcal{E}_1$ and frequency ω_1. We first tune either ω_1 or ω_{cs} (by altering one of the parameters which determine ω_{cs}) until $\omega_1 = \omega_{cs}$. Then we sweep the irradiating oscillator of amplitude $\mathcal{E}_2$ from frequency ω_2 to $\omega_2 + d\omega_2$; if some other ion P is being heated at ω_2 and/or $\omega_2 + d\omega_2$ then a double resonance signal change $dD(\omega_2)$ may result such that

$$1) \qquad dD(\omega_2) = d\omega_2 \frac{dD(\omega_2)}{d\omega_2} = \frac{dA_s(\omega_2)}{d\omega_2} d\omega_2$$

---

*The rates for $O^+ + O_2 + M \rightarrow O_3^+ + M$ or
$CH_4^+ + O_2 + M \rightarrow CH_4O_2^+ + M$
in order to explain 16→48vw- would have to be an incredible 10^{-24} cm^6/molec^2-sec, three or four orders of magnitude greater than most three body ion-molecule reactions.

$CH_5^+ + O_2 \rightarrow O_2^+ + CH_4 + H$
is 91 kcal/mole endothermic and hence calls for dk/dE positive. The two exothermic reactions

$OH^+ + CH_4 \rightarrow CH_3OH^+ + H$ or
$OH^+ + O_2 \rightarrow O_2^+ + HO$
would have to have rates on the order of an incredible 10^{-7} cm^3/molec-sec in order to explain 17→32m-, based on reasonable $n^+(OH^+)$ estimates.

The change in $D(\omega_2)$ will be non-zero so long as $dA_s(\omega_1)/d\omega_2$ is non-zero:

$$\frac{1}{A_s(\omega_1)}\frac{dA_s(\omega_1)}{d\omega_2} = \frac{1}{n_s^+}\frac{dn_s^+}{d\omega_2} + \frac{2}{\mathcal{E}_1}\frac{d\mathcal{E}_1}{d\omega_2} + \left[\frac{1}{\tau} - \frac{2\tau(\omega_1-\omega_{cs})^2}{1+\tau^2(\omega_1-\omega_{cs})^2}\right]\frac{d\tau}{d\omega_2}$$

2)

$$+ \left[\frac{2\tau^2(\omega_1-\omega_{cs})^2}{1+\tau^2(\omega_1-\omega_{cs})^2}\right]\frac{d\omega_{cs}}{d\omega_2} .$$

If we ignore all but the first term on the right hand side of 2, we can get the result of Beauchamp (see Chapter II, ref. 15) by writing

3) $$\frac{1}{A_s(\omega_1)}\frac{dA_s(\omega_1)}{d\omega_2} = \frac{1}{n_s^+}\frac{dn_s^+}{dk}\frac{dk}{dE_p}\frac{dE_p}{d\omega_2} .$$

The rate of change of n_s^+ with the value of the rate coefficient k can be derived from Equation 13 of Chapter II:

$$n_s^+ = \frac{j_p(t=0)}{nk}\left[nk(t_s'-t_s) + \exp(-nkt_s') - \exp(-nkt_s)\right] ,$$

whence

4) $$\frac{dn_s^+}{dk} = \frac{j_p(t=0)}{nk^2}\left[(nkt_s+1)\exp(-nkt_s) - (nkt_s'+1)\exp(-nkt_s')\right]$$

5) $$\text{or } \frac{dn_s^+}{dk} \approx \tfrac{1}{2}\, n\, j_p(t=0)\,(t_s'^2 - t_s^2) \approx \frac{n_s^+}{k} , \text{ when } nkt_s' \ll 1.$$

In these equations t_s and t_s' are the times when secondary ions enter and leave, respectively, the analyzer region of the cell; they are not to be confused with τ, which is the mean free time during which an ion suffers no thermalizing collisions. For simplicity we assume that primary and secondary ions have approximately equal mean free time, τ. This means, as is observed, that cyclotron resonance peaks for various species will have about the same width. To get $dE_p/d\omega_2$ we re-write II-11 for the primary ion:

0 0 0 0 3 6 0 . 8 5 5

$$6) \qquad E_p = 3/2\ KT + \frac{q^2 \mathcal{E}_2^2 \tau^2}{4m_p} L(\omega_2, \omega_{cp}, \tau) ,$$

from which we get

$$7) \qquad \frac{dE_p}{d\omega_2} = A_p(\omega_2) \frac{2\tau^3(\omega_2 - \omega_{cp})}{1+\tau^2(\omega_2-\omega_{cp})^2} .$$

Combining 4 and 7 with 3 reveals that the final factor in 3 is the only ω_2-dependent factor. We can therefore integrate 3 over $d\omega_2$ to get

$$8) \qquad D(\omega_2) = \int dD(\omega_2) = \frac{A_s(\omega_1)}{n_s^+} \frac{dn_s^+}{dk} \frac{dk}{dE_p} \int \frac{dE_p}{d\omega_2} d\omega_2$$

Substituting the value of dn_s^+/dk from 4 and of $dE_p/d\omega_2$ from 7 gives the result of Beauchamp.

We can write each term in 2 as the sum of two terms, as for example,

$$9) \qquad \frac{dn_s^+}{d\omega_2} = \frac{\partial n_s^+}{\partial k} \frac{\partial k}{\partial E_p} \frac{dE_p}{d\omega_2} + k'(n_s^+),$$

where k' is given by

$$10) \qquad k' = \frac{dn_s^+}{d\omega_2} - \frac{\partial n_s^+}{\partial k} \frac{dk}{d\omega_2}$$

and represents all those parameters which may depend on ω_2 and on which n_s^+ depends. We know from 5 that n_s^+ depends on n, $j_p(t=0)$, t_s', and t_s; but none of these depends in turn on ω_2. However, for the other terms in 2 this may not be the case:

$$\frac{1}{A_s(\omega_1)} \frac{dA_s(\omega_1)}{d\omega_2} = \left[\frac{1}{n_s^+} \frac{dn_s^+}{dk} + \frac{2}{\mathcal{E}_1} \frac{\partial \mathcal{E}_1}{\partial k} + \frac{1}{\tau} \frac{\partial \tau}{\partial k} \right] \frac{dk}{dE_p} \frac{dE_p}{d\omega_2}$$

$$+ \left[\frac{2}{\mathcal{E}_1} k'(\mathcal{E}_1) + \frac{1}{\tau} k'(\tau) + 2\tau^2(\omega_1 - \omega_{cs})\, k'(\omega_{cs}) \right] \qquad (11$$

in which we have noted that $\frac{\partial \omega_{cs}}{\partial k} = 0$,

$$\frac{1}{\tau} - \frac{2\tau(\omega_1-\omega_{cs})^2}{1+\tau^2(\omega_1-\omega_{cs})^2} \approx \frac{1}{\tau}, \text{ and } \frac{2\tau^2(\omega_1-\omega_{cs})}{1+\tau^2(\omega_1-\omega_{cs})^2} \approx 2\tau^2(\omega_1-\omega_{cs}) .$$

From (5) we know that

$$\frac{1}{n_s^+}\frac{dn_s^+}{dk} \approx k^{-1}.$$

When k approaches the elastic collision rate, the mean free time τ is approximately $(nk)^{-1}$; hence,

$$\frac{1}{\tau}\frac{d\tau}{dk} \approx k^{-1}.$$

One might think that so long as the amplitude of the marginal oscillator is fixed, then $\frac{d\mathcal{E}_1}{d\omega_2}$ would be zero. This is untrue, however, as can be seen from Figure 3. The amplitude of the signal which an ion produces is proportional to the average of $\mathcal{E}_1^2$ which it experiences. For the most part ions stay within the narrow rectangle near the horizontal center line of the cell. Ions near the center of this rectangle experience nearly the ideal $\mathcal{E}_1^o$ which would fill the cell if the upper and lower plates were infinite planes. Because all ions execute harmonic motion in the direction parallel to the magnetic field $\vec{B}$, all ions spend some time near the center of the cell; however, the average $\mathcal{E}_1^2$ experienced by ions which spend any time near the sides of the cell is certain to be less than $\mathcal{E}_1^{o2}$. $\frac{\partial \mathcal{E}_1}{\partial \omega_2}$ will be non-zero as a result of any effect which alters the average of $\mathcal{E}_1^2$ which product ions experience. Obviously, if the rate constant is a function of E_p, then changing ω_c can through its effect on k alter the distribution of points at which secondary ions are formed and their distribution of kinetic energies (hence cyclotron orbit radii). Therefore

0 0 0 0 3 6 0 0 8 5 6

CONTOURS OF EQUAL OSCILLATOR INTENSITY

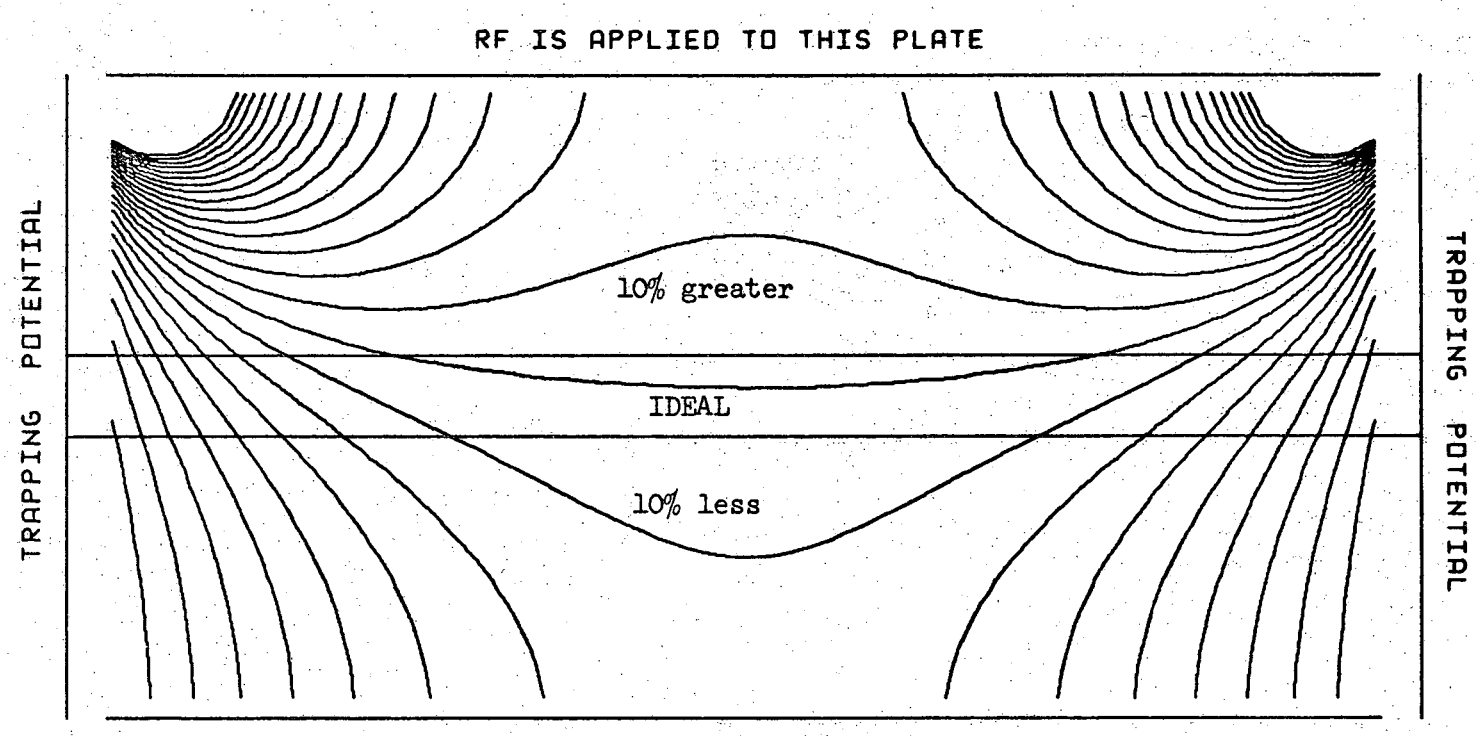

XBL 708-6411

Fig. 3. Contour of equal oscillator intensity within the ICR cell when rf is applied to the upper plate. These contours are derived in the same way as were Figs. II-11 - II-13. If changing ω_2 causes a change in the positions of ions being detected, then $d\mathcal{E}_1/d\omega_2$ will be non-zero.

$\frac{2}{\mathcal{E}_1}\frac{\partial \mathcal{E}_1}{\partial k}$ could indeed be non-zero. Unfortunately we cannot intuit its order of magnitude or for that matter, its sign, without expensive calculation.

The $\frac{d\mathcal{E}_1}{d\omega_2}$ term can clearly have $k'(\mathcal{E}_1)$ components as well. One of these is due to the effect of the ions' space-charge. If the ion current due to one species is large enough, then irradiating that species at ω_2 could move the ion beam or deplete the space-charge due to the irradiated species. These effects would be reflected in changes in the average $\mathcal{E}_1^2$ which all other ions experience, including that which is being detected. As with $\frac{2}{\mathcal{E}_1}\frac{\partial \mathcal{E}_1}{\partial k}$, we can intuit neither the sign nor size of $k'(\mathcal{E}_1)$.

If $k'(\tau)$ and $k'(\omega_{cs})$ are due to ions' space-charge we can at least guess the sign of the effect. We know that the electron beam's space-charge can shift and broaden the ion cyclotron resonance signals (see Chapter II, refs. 9-11). If irradiating a major ion species p at ω_2 alters the space charge due to that ion then for any other species S a non-zero value of $\frac{\partial \tau}{\partial \omega_2}$ will arise from the broadening or narrowing of the detected signal $A_s(\omega_1)$ and a non-zero value of $\frac{\partial \omega_{cs}}{\partial \omega_2}$ will come from the shift in ω_{cs}. Observe that in ll $k'(\omega_{cs})$ has the factor $(\omega_1-\omega_{cs})$ which was set initially equal to zero; however, if $\frac{\partial \omega_{cs}}{\partial \omega_2}$ is non-zero then $(\omega_1-\omega_{cs})$ will be non-zero also.

We can estimate $k'(\tau)$ due to ion space charge fairly well. At a typical pressure and electron beam current, the concentration of neutrals will be on the order of 10^{11} cm^{-3} and of ions, 10^4 cm^{-3}. Assuming the ion-ion collision cross section ($\sim 10^{-10}$ cm^2) is almost 10^4 times* as great as the ion-neutral elastic collision cross-section

* The Rutherford formula, ctn $\theta/2 = 4\pi \epsilon_o$ Kb/Ze^2, predicts that the center-of-mass scattering angle will be 90° for two thermal ions

0 0 0 0 3 6 0 . 0 5 7

($\sim 10^{-14}$ cm^2), then the ion-ion collision frequency will be .1% that of the ion-neutral collision frequency. Obviously, this effect will be negligible relative to the effect of a chemical reaction which occurs at virtually every ion-neutral collision, but will not be small in comparison with reactions, with rates of 10^{-12} cm^3/molec-sec, as we have attempted to measure. From the Rutherford formula, we expect the ion-ion collision mean free time to increase in proportion to the relative velocity of collision. Thus as irradiation increases the velocity of ions, any double resonance signal produced by ion-ion collisions will die off quickly and will show an apparent dk/dE which is positive because elimination of ion-ion collisions will sharpen the peaks, $A_s(\omega_1=\omega_{cs})$. Unfortunately this effect seems to be of the same order of magnitude as the effects we are attempting to explain, but is of the opposite sign.

A shift in cyclotron frequency, ω_{cs}, will always give an effect of the right sign because ω_1 is set equal to ω_{cs} initially by determining the maximum of $A_s(\omega_1)$. If ω_{cs} changes subsequently, $A_s(\omega_1 \neq \omega_{cs})$ is always less than $A_s(\omega_1=\omega_{cs})$.

The effect of the space charge of the ions in the cell has been evaluated by solving Poisson's Equation,

$$\nabla^2 \phi + \rho = 0$$

as was discussed in Chapter II except here ρ is not zero. The density of charge ρ was estimated by assuming the ion density for a typical experiment is uniformly distributed over a volume contained by a right

interacting with impact parameter b of about 600 Å. This is two orders of magnitude greater than typical ion-neutral orbiting impact parameters.

parallelepiped which has dimensions 8.89 cm by 2.54 cm by d where d is the thickness of the ion beam. If the ions' orbits were infinitesimal then d would be about the width of the electron beam, 0.16 cm $\equiv d_o$. For typical thermal ions the cyclotron orbital radii are about .06 cm; thus for thermal ions the beam width is estimated as .22 cm. For ions of about 1 eV energy the beam thickness is estimated as about .52 cm. Thus when ions are thermal, a typical charge density will be about 3×10^{-4} statcoulombs/cm^3 and when cyclotron double resonance irradiation raises the energy of most of the ions to about 1 eV, the charge density drops to about 1×10^{-4} statcoulombs/cm^3. The potential $\phi_\rho(x,y)$ within the cell which is due to the ion space charge is a maximum in the center of the cell. This potential, ϕ_ρ, and the gradient, $\mathcal{E}_{\rho,x}$, perpendicular to the magnetic field and to the direction of ion drift through the cell are shown in Figure 4.

Figure 4 shows the effect of the ion beam's space charge for the case in which ions have been heated to a kinetic energy of about 1 eV. The force on the ions in the x-direction, $e\mathcal{E}_{\rho,x}$, is approximately proportional to x, the distance of the ion from the center of the cell. This approximation holds rather accurately within the ion beam. Outside the ion beam $e\mathcal{E}_{\rho,x}$ becomes approximately constnat. The force $e\mathcal{E}_{\rho,y}$, in the direction parallel to the magnetic field is also approximately proportional to the distance from the center of the cell. The ion motion which results from these forces can be determined in a treatment quite analogous to that made by Beachamp and Armstrong[4] in determining the ion motion under the influence of the quadrupole trapping potentials. The effect of the force due to the ions' space charge parallel to the magnetic field is to slightly reduce the

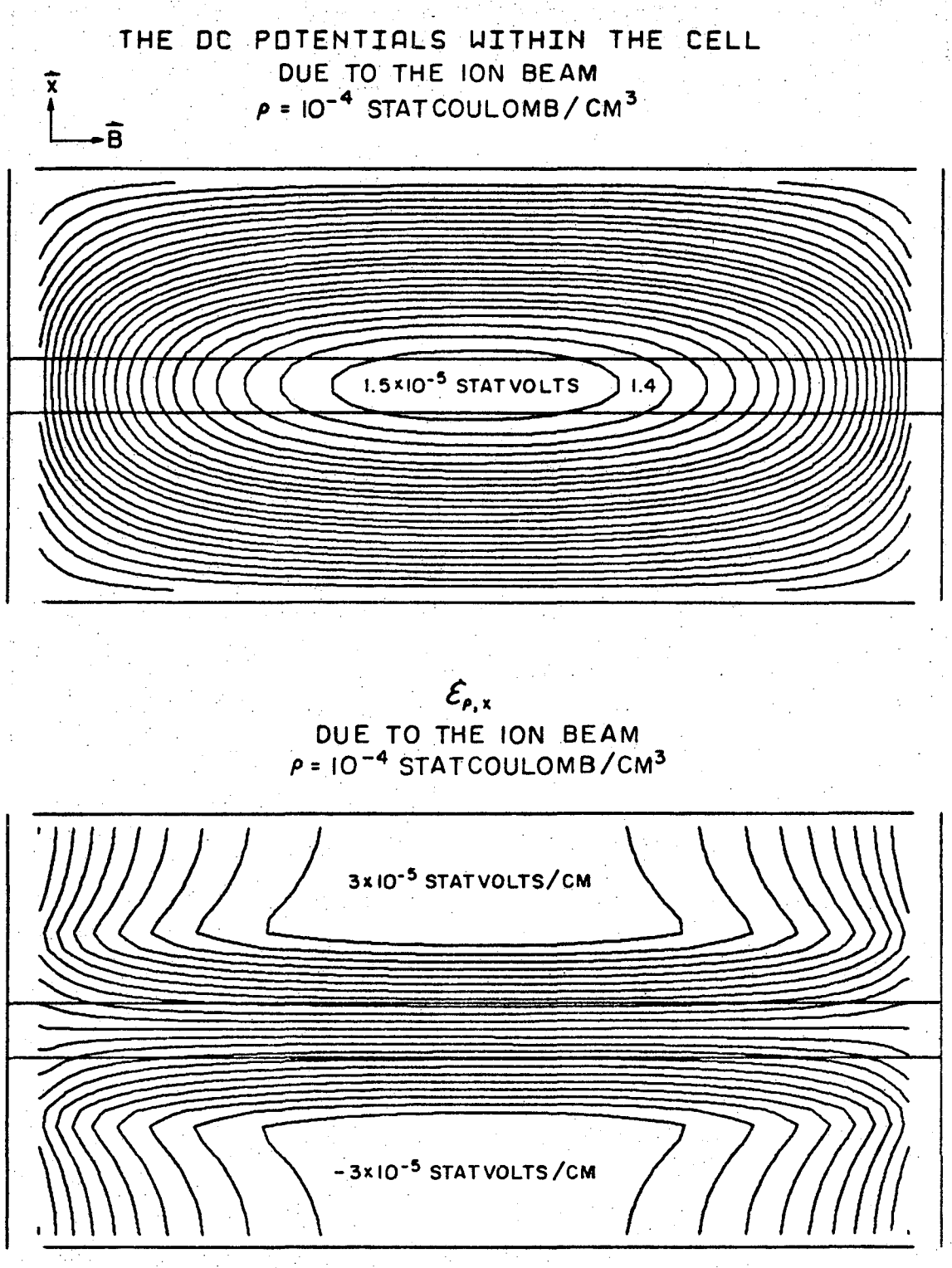

Fig. 4. The potential and electric field in the cell due to ion space charge.

effective trapping potential. The effect of the force in the x-direction is to shift the cyclotron frequency on the order of 100 Hz:

$$\frac{\omega_\rho}{2\pi} = \left[\frac{e}{m}\frac{d\mathcal{E}_{\rho,x}}{dx}\right]^{\frac{1}{2}} = \frac{453 \text{ Hz}}{\sqrt{m}} \quad .$$

The potentials and electric fields due to the ion beam's space charge when the ions are thermal are similar to those shown for translationally hot ions in Figure 4. The region over which $\mathcal{E}_{\rho,x}$ is equal to $\pm 3 \times 10^{-5}$ statvolts/cm is larger in both the x-direction and the direction parallel to $\vec{B}$. The region over which $\mathcal{E}_{\rho,x}$ is approximately linear is narrower; hence $\frac{d\mathcal{E}_{\rho,x}}{dx}$ is larger by a factor of about $2\frac{1}{2}$. Heating an ion species which makes up an appreciable fraction of the total ion current will reduce the space charge that all other ion species experience. The reduction in space charge will increase the cyclotron frequency by about 100 Hz. Thus the term in (11) due to this shift,

$$2\tau^2 (\omega_1 - \omega_{cs}) \frac{\partial \omega_{cs}}{\partial \omega_2}$$

will be on the order of 2% of the $\frac{1}{n_s^+}\frac{dn_s^+}{dk}\frac{dk}{dE_p}\frac{dE_p}{d\omega_2}$ term for a typical fast reaction, exactly the size of the effect we are seeking to explain. If, for any one of a number of reasons, this $\frac{1}{n_s^+}\frac{dn_s^+}{dk}$ ... term is two orders of magnitude smaller than for a typical fast reaction, the effect of this term can be masked by the term due to the cyclotron frequency shift because of a change in ion space charge.

The consideration of Tables VII and VIII can now be resumed, since we now have an adequate explanation of the non-chemical signals we have postulated and tabulated in the second column of Tables VII and VIII. We focus our attention on the column labelled "Remainder."

0 0 0 0 3 6 0 3 8 5 9

Observe that the non-chemical effect apparently masks the signal for Reaction 29 in both CH_4-O_2 and CD_4-O_2 mixtures.

29) $O_2^+(\tilde{a}^4\Pi_u) + O_2 \rightarrow O_3^+ + O$

has a rate of about 1% that of typical fast reactions; it would seem that dk/dE for 29 is also quite small.

The double resonance signal for Reaction 16d,

16d) $O_2^+ + CH_4 \rightarrow CH_3O_2^+ + H$,

fortunately is not masked because its dk/dE is positive, although the size of dk/dE is probably quite small. 16d gives the 32 → 47 vw+ signal in CH_4-O_2 mixtures and the 32 → 50 vw+ signal in CD_4-O_2 mixtures.

Masses 44 and 45 are fully accounted for by the known CO_2 contamination and the reactions involving CO_2 contaminant discussed in Chapter IV. We have already discussed the upper limits placed on the rates of reactions such as 22b,e, and 23c:

22b) $CH_2^+ + O_2 \rightarrow CO_2^+ + H_2$ $\quad k < 5 \times 10^{-12}$ cm^3/molec-sec

22c) $CH_2^+ + O_2 \rightarrow CO_2H^+ + H$ $\quad k < 1 \times 10^{-12}$

23c) $CH_3^+ + O_2 \rightarrow CO_2H^+ + H_2$ $\quad k \approx 0$ (spin forbidden).

We can now also place upper limits on the rates of 24j and 16j:

24j) $CH_4^+ + O_2 \rightarrow CO_2^+ + 2H_2$ $\quad k < 10^{-13}$ cm^3/molec-sec

16j) $O_2^+ + CH_4 \rightarrow CO_2^+ + 2H_2$ $\quad k < 10^{-13}$,

and 24m and 16m:

24m) $CH_4^+ + O_2 \rightarrow CHO_2^+ + H_2 + H$ $\quad k < 10^{-13}$ cm^3/molec-sec

16m) $O_2^+ + CH_4 \rightarrow CHO_2^+ + H_2 + H$ $\quad k < 10^{-13}$.

It is known that mass 34 is a primary ion in CH_4-O_2 mixtures and its signal area can be accurately accounted for by measuring the mass 32 peak area and calculating the mass 34 signal area by assuming that ^{18}O is present in its naturally occurring abundance. Since no CD_3OD^+ (mass 36) is observed in CD_4-O_2 mixtures and since we can explain as non-chemical the double resonance signals in CH_4-O_2 mixtures for "product" ion mass 34, we can set an upper limit on 24q at 10^{-13} cm^3/molec-sec:

24q) $\quad CH_4^+ + O_2 \rightarrow CH_3OH^+ + O,$

and state with confidence that mass 34 in CH_4-O_2 mixtures is entirely $^{18}O^{16}O^+$.

It has been discussed in Chapter IV that that part of mass 33 in methane-oxygen mixtures is HO_2^+ produced from the reaction of H_2^+ with oxygen or of O_2^{+*} with H_2; the remainder is due to $^{17}O^{16}O^+$ and there is little or nothing else contributing to it. However, Table VII shows three cyclotron double resonance signals. Two of these, 15 → 33 vw+ and 32 → 33 vw+, are probably non-chemical. They show a positive $k'(\omega_{cs})$ rather than the expected negative $k'(\omega_{cs})$ probably because the very intense neighboring mass 32 peak is shifted (through the space charge change) to higher frequency and thus the net overlap of the mass 32 peak with the relatively small mass 33 peak increases. The 16 → 33m+ is probably too intense a signal to explain by that means; instead it probably represents the opening-up of the endothermic reaction channel 24s:

24s) $\quad CH_4^+ + O_2 \rightarrow HO_2^+ + CH_3 \qquad \Delta H = +36$ kcal/mole

0 0 0 0 3 6 3 3 6 0

The 20 → 34 m+ signal seen in methane-d_4 - oxygen mixtures corroborates this deduction. Part of the energy requirement is probably supplied by internal excitation of the CH_4^+ but most would have to come from the ~25 kcal/mole relative kinetic energy to which the CH_4^+ ions are heated upon irradiation. This would indicate that kinetic energy is relatively effectively invested toward driving the reaction. Therefore it seems quite likely that in the conventional mass spectrometry experiments on this system by Franklin and Munson[3] this reaction was in fact occurring at an appreciable rate, since the average ion kinetic energy was always greater than about 70 to 100 kcal/mole. If the CH_4^+ ions are at thermal kinetic energy, however, the rate of 24s cannot be more than about 10^{-13} cm^3/molec-sec. This would indicate that CH_4^+ is on the average not highly excited internally.

Three moderate sized signals for mass 32 "product" ion are probably non-chemical. Their intensities are approximately the same relative size as the relative ion currents of CH_3^+, CH_4^+, and CH_5^+. That we are very hard put to present reasonable chemical explanations for 15 → 32 m- and 17 → 32 m- is adequate reason to believe they are not of chemical origin. The 16 → 32m- is probably also largely not of chemical origin, although two reactions may contribute:

26) $O^+ + O_2 \rightarrow O_2^+ + O$ $\quad k = 1.69 \times 10^{-11}$ cm^3/molec-sec

24p) $CH_4^+ + O_2 \rightarrow O_2^+ + CH_4$ $\quad k = 2.1 \pm .2 \times 10^{-10}$.

While these reactions seem to have relatively small dk/dE, the values shown for their rates are fairly well established. The rate for Reaction 26 is taken from the literature as discussed in Chapter V; and the rate for 24p has been determined from the present experimental

data. A slightly smaller rate was measured for 24p in the perdeutero- system. The 18 → 32m-, 20 → 32m-, and 22 → 32m- double resonance signals seen in that system are analogous to those seen in the perhydro- system and are likewise non-chemical. The 16 → 32s+ signal seen in CD_4-O_2 mixtures is probably due to Reaction 7:

7) $CH_2^+ + CH_4 \rightarrow C_2H_4^+ + H_2$

which is seen in pure methane and methane-d_4 with rates of 2.75 and 2.50×10^{-10} cm^3/molec-sec respectively.

The cyclotron double resonance signals for "product" ion mass 31 in methane-oxygen mixtures are all of non-chemical origin except for 32 → 31s+. Reaction 16f is responsible for it:

16f) $O_2^+ + CH_4 \rightarrow CH_3O^+ + OH \qquad k = 13 \pm .4 \times 10^{-12}$ cm^3/molec-sec

In the perdeutero- system 16f causes the 32 → 34s+ double resonance signal and has a rate constant of $8 \pm 4 \times 10^{-12}$ cm^3/molec-sec. Significant ion ejection double resonance responses for reaction 16f are not seen in Tables V and VI because its rate is relatively small and the error is relatively great in correcting the ion ejection results to account for direct ejection for the masses near that mass on which the ejection is centered.

Since 16f is an open reaction channel we might expect the slightly more exothermic 24f also to be open:

24f) $CH_4^+ + O_2 \rightarrow CH_3O^+ + OH.$

However since no ion ejection or cyclotron double resonance responses are seen which are attributable to 24f, we conclude that it does not occur. Furthermore, the observed amount of CH_3O^+ can be well accounted for by Reactions 16f (above) and 23f:

0 0 0 0 3 6 0 3 8 6 1

23f) $CH_3^+ + O_2 \rightarrow CH_3O^+ + O \quad k = 1.3\pm.1\times10^{-11} cm^3/molec\text{-}sec,$

whose rate was established in the experiments with the CH_3Cl-O_2 mixture.

The significant cross-reaction cyclotron double resonance signals for product ion mass 30 in methane-oxygen mixtures are 14 → 30m+ and 32 → 30m+. The former simply corroborates the conclusion reached from the data of the CH_2Cl_2-O_2 mixture that 22g has an appreciable rate:

22g) $CH_2^+ + O_2 \rightarrow CH_2O^+ + O \quad k = 1.0\pm.04\times10^{-10} cm^3/molec\text{-}sec.$

This reaction fully accounts for the CH_2O^+ seen in methane-oxygen mixtures. On this basis that no CH_2O^+ appears to be formed from 16c, 13k, or 24c, we can establish upper limits on the rates,

16c) $O_2^+ + CH_4 \rightarrow CH_2O^+ + H_2O \quad k < 10^{-12}\ cm^3/molec\text{-}sec$

24c) $CH_4^+ + O_2 \rightarrow CH_2O^+ + H_2O \quad < 10^{-12}$

13k) $O^+ + CH_4 \rightarrow CH_2O^+ + 2H \quad < 10^{-12}$

at $10^{-12} cm^3/molec\text{-}sec$. The 32-30m+ signal would indicate that while 16c is very slow at thermal energy, its rate increases rapidly with O_2^+ ion kinetic energy in the range up to about 20 kcal/mole (center-of mass). One concludes that 16c probably was occurring in the experiments of Franklin and Munson.[3]

The cyclotron double resonance signals for "product" ion masses 26 to 29 can be accounted for by non-chemical means and by the signals which are seen in pure methane. Mass 29 is predominantly $C_2H_5^+$. Because the very small additional amount of mass 29 is due to HCO^+ produced from Reactions 21a, 15, 30, and 31, which have already been discussed here and in Chapter IV,

21a) $CH^+ + O_2 \rightarrow HCO^+ + O$ $k = 0.7 \times 10^{-10} cm^3/molec\text{-}sec$

15) $CO^+ + CH_4 \rightarrow HCO^+ + CH_3$ 11.7

30) $CH_4^+ + CO \rightarrow HCO^+ + CH_3$ 8.7

31) $CH_5^+ + CO \rightarrow HCO^+ + CH_4$ 5.54,

we can conclude that the rates for 16i and k and 24i are all very small:

16i) $O_2^+ + CH_4 \rightarrow HCO^+ + H_2O + H \leftarrow CH_4^+ + O_2$ (24i

16k) $\rightarrow HCO^+ + OH + H_2 \leftarrow$ (24k

Likewise, since mass 28 is due to $C_2H_4^+$ and CO^+ from known contamination due to CO and CO_2, we can conclude that CO^+ is not produced by Reactions 16ℓ and 24ℓ:

16ℓ) $O_2^+ + CH_4 \rightarrow CO^+ + H_2O + H_2 \leftarrow CH_4^+ + O_2$. (24ℓ

The contamination due to water has been discussed in Chapter IV and shown to be responsible for the mass 18 and 19 peaks in the mass spectrum of methane-oxygen mixtures. The 16 → 19vw+ and 16 → 18vw+ signals seen in these mixtures probably represent Reactions 33 and 34:

33) $CH_4^+ + H_2O \rightarrow H_2O^+ + CH_4$ $k \sim 2 \times 10^{-9} cm^3/molec\text{-}sec$

34) $CH_4^+ + H_2O \rightarrow H_3O^+ + CH_3$ $k \sim 3 \times 10^{-9}$,

rather than 13j or 24a,e,g, or h:

13j) $O^+ + CH_4 \rightarrow H_2O^+ + CH_2$

24a or e) $CH_4^+ + O_2 \rightarrow H_3O^+ + (HCO \text{ or } H + CO)$

24g or h) $CH_4^+ + O_2 \rightarrow H_2O^+ + (H_2CO \text{ or } H_2 + CO)$.

Even if the H_2O^+ and H_3O^+ were due to, say 24g and 24a, respectively, the rate coefficients could be no more than about 5×10^{-12} $cm^3/molec\text{-}sec$. However, the measured rates of 33 and 34 are sufficiently

0 0 0 0 3 6 0 3 8 6 2

accurate that an upper limit on 24a, e, g, and h can be placed another order of magnitude lower, at 5×10^{-13}. Similar limits apply to 16a, e,g and h:

16a or e) $O_2^+ + CH_4 \rightarrow H_3O^+ + (HCO \text{ or } H + CO)$

16g or h) $O_2^+ + CH_4 \rightarrow H_2O^+ + (H_2CO \text{ or } H_2 + CO)$.

The rate of 13j is probably less than $10^{-12} cm^3/molec\text{-}sec$.

The 32 → 15vw+ cyclotron double resonance signal has already been discussed above in connection with Figures 1 and 2, and has been assigned to Reaction 16q. It has a very small rate at thermal kinetic energy but probably the rate increases rapidly in the range up to about 20 kcal/mole, center of mass kinetic energy. The corresponding reaction leading to this product in the $CH_4^+ + O_2$ interaction is Reaction 24r: $CH_4^+ + O_2 \rightarrow CH_3^+ + HO_2$. The rates of $2.5 \pm .2 \times 10^{-10}$ $cm^3/molec\text{-}sec$ in CH_4-O_2 mixtures and of $2.3 \pm .2 \times 10^{-10}$

in CD_4-O_2 mixtures have been determined for 24r. Figure 5 shows the dependence of the mass 15 peak area in CH_4-O_2 mixtures upon TIC. The solid straight line would be the peak area dependence if there were no reaction. The lower curve in Fig. 5 represents the expected peak area due to CH_3^+ calculated from the loss of CH_3^+ due to reaction with methane, Reaction 10:

10) $CH_3^+ + CH_4 \rightarrow C_2H_5^+ + H_2$ $\quad k = 9.92 \times 10^{-10} cm^3/molec\text{-}sec$,

and a very much smaller loss of CH_3^+ due to reaction with O_2:

23f) $CH_3^+ + O_2 \rightarrow CH_3O^+ + O$ $\quad k = .13 \pm .01 \times 10^{-10} cm^3/molec\text{-}sec$.

The difference between this curve in Fig. 5 and the curve fit to the data represents the gain of CH_3^+ due to 24r.

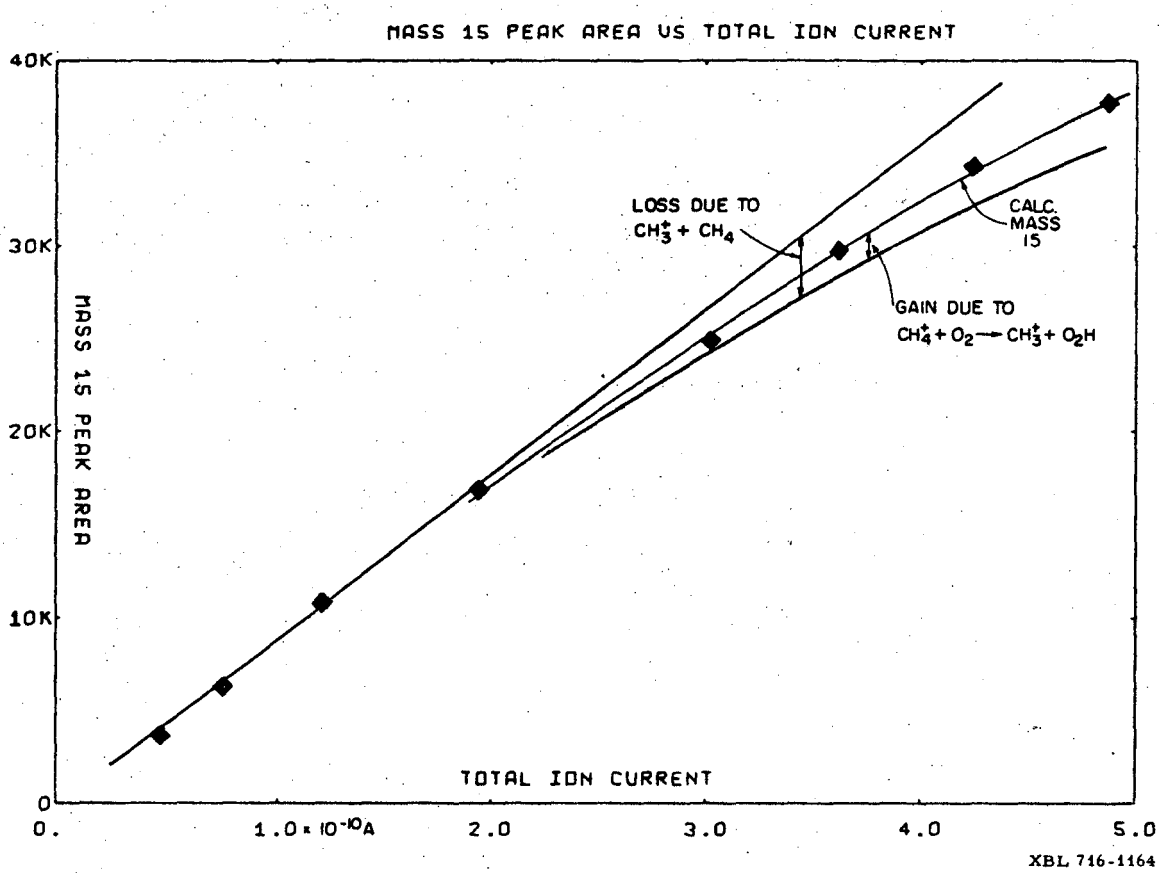

Fig. 5. Mass 15 peak area in methane:oxygen ≈ 1.

0 0 0 0 3 6 0 3 8 6 3

Reaction 24r represents only about half the loss of CH_4^+ due to reaction with O_2. The plot of mass 16 peak area versis TIC in methane: oxygen ≈ 1 is shown in Figure 6. The curve shown in Fig. 6 for the contribution due to O^+ is calculated assuming the rate of 13m is $.50 \times 10^{-10} cm^3/molec\text{-}sec$; this reaction will be discussed below. The solid straight line would be the peak area due to primary ion O^+ and CH_4^+ if there were no reaction. The curve just below the straight line is the peak area assuming the only reactions occurring are 11a:

11a) $CH_4^+ + CH_4 \rightarrow CH_5^+ + CH_3 \quad k = 12.0 \times 10^{-10} cm^3/molec\text{-}sec$

and 13m, the minor O^+ loss mentioned. The difference between this curve and the curve fit to the data represents the loss of CH_4^+ due to reactions 24a through 24r, of which the only reactions with even moderately large rates are 24p and 24r:

24p) $CH_4^+ + O_2 \rightarrow O_2^+ + CH_4$

24r) $CH_4^+ + O_2 \rightarrow CH_3^+ + HO_2$

24p apparently has a fairly small dk/dE, so that the cyclotron double resonance signal, if any, due to 24p is masked by the non-chemical effects. The double resonance signal seen in pure methane masks the occurrence of 24r in the perhydro-methane-oxygen mixtures but in perdeutero-methane the 20 → 18 signal due to 24r is not overwhelmed by the 20 → 18w+ signal seen in pure CD_4.

The only double resonance signal remaining to be explained is the 16 → 20w- signal seen in CH_4-O_2 mixtures. It probably represents charge exchange between oxygen atom and methane:

13m) $O^+ + CD_4 \rightarrow CD_4^+ + O.$

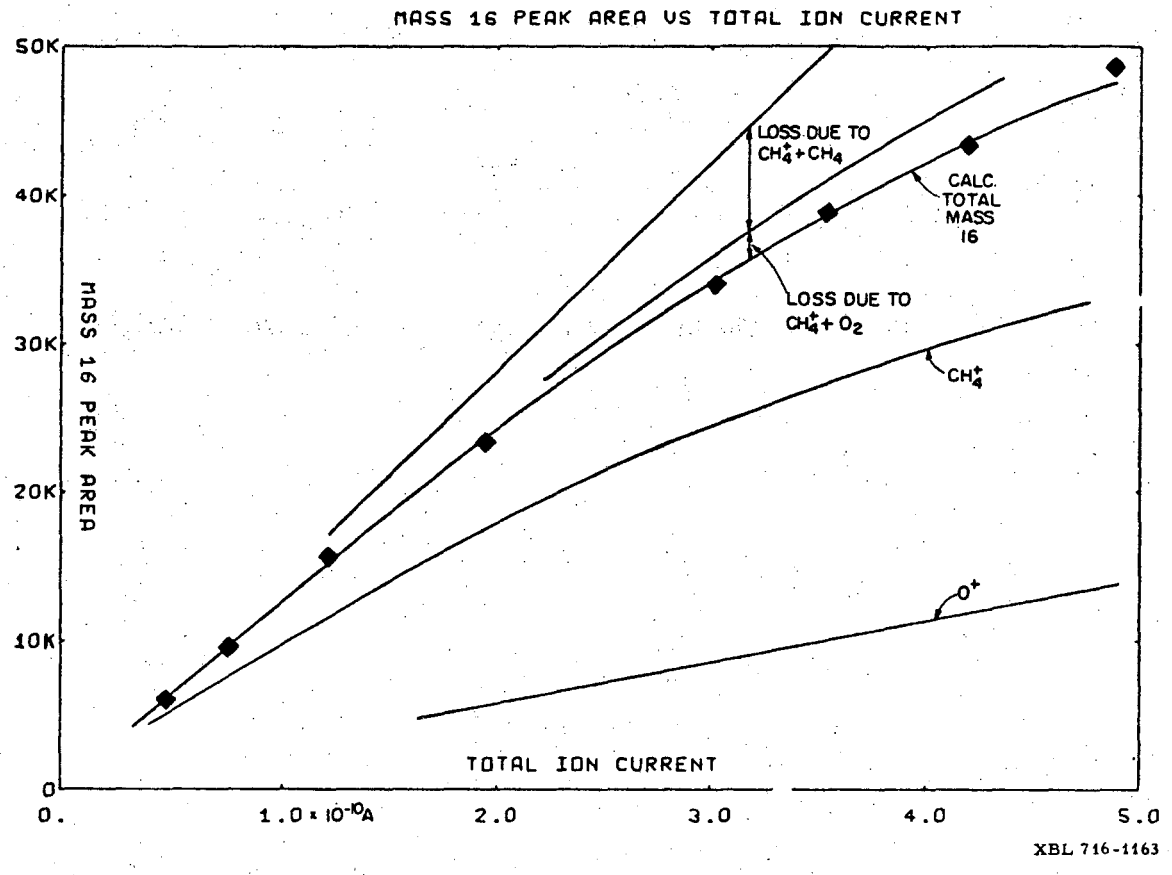

Fig. 6. Mass 16 peak area in methane:oxygen ≈ 1.

0 0 0 0 3 6 0 0 8 6 4

The rate of loss of O^+ due to reaction with CD_4 is $4.7\pm.5\times10^{-11}cm^3$/molec-sec, determined to within about 10% because the rate of loss of CD_2^+ is well-known; and the rate of loss of mass 16 in CD_4-O_2 mixtures is due to this known CD_2^+ loss and to O^+ loss through reactions 13m and 13n:

13n) $$O^+ + CD_4 \rightarrow OD^+ + CD_3 .$$

Unfortunately, there is no unambiguous way in which 13n can be proven to occur or not. The double resonance signals are masked in both the perdeutero- and perhydro- systems. The contribution of 13n to mass 17 in CH_4-O_2 mixtures and to 18 in CD_4-O_2 mixtures cannot be measured even if the rate of 13n were the full 5×10^{-11}. The rate of $O^+ + CD_4$ reaction is only a small fraction of the orbiting reaction rate prediction; if the $O^+ + CH_4$ rate is the same fraction of the orbiting reaction rate then the rate will be $5.0\times10^{-11}cm^3$/molec-sec. Table II shows these rates for the sum of 13m and n.

Summary

At this point all the reactions in Table II and the rates ascribed to each has been discussed. In agreement with Franklin and Munson[3] very little reaction is observed. The comparison of their results with the present results and the implications drawn from the comparison and from the results themselves will be deferred until Chapter VII.

References - Chapter VI

1. E. Gustaffson and E. Lindholm, Arkiv. Fysik 18, 219 (1960).

2. F. C. Fehsenfeld, A. L. Schmeltekopf and E. F. Ferguson, J. Chem. Phys. 45, 23 (1966).

3. J. L. Franklin and M. S. B. Munson, Tenth Symposium on Combusion, 561 (1965).

4. J. L. Beauchamp and J. T. Armstrong, Rev. Sci. Instr. 40, 123 (1969).

5. C. A. Coulson and H. L. Strauss, Proc. Roy. Soc. (London) A269, 443 (1962).

6. J. J. Kaufman and W. S. Koski, presented at the 155th American Chemical Society National Meeting before the Division of Nuclear Chemistry and Technology, San Francisco, California, April 1968, Abstract 166.

7a. D. B. Dunkin, F. C. Fehsenfeld, A. L. Schmeltekopf, E. E. Ferguson, J. Chem. Phys. 49, 1365 (1968).

b. A. L. Schmeltekopf, F. C. Fehsenfeld, G. I. Gilman, and E. E. Ferguson, Plan. Space. Sci. 15, 401 (1967).

c. A. L. Schmeltekopf, E. E. Ferguson, and F. C. Fehsenfeld, J. Chem. Phys. 48, 2966 (1968).

8. H. S. Johnston, Gas Phase Reaction Rate Theory, Ronald Press, New York (1966).

0 0 0 0 3 6 0 3 8 6 5

VII. CONCLUSION

The thermal ion molecule reactions occurring in gaseous mixtures of methane and oxygen have been discussed in Chapters III, IV, V, and VI, and are compliled in Table I. The reaction numbers given in Table I are in harmony with the numbers given each reaction in previous chapters. One can see in Table I that with the exception of the methane-oxygen cross reactions, the rates of ion-molecule reactions are generally high, very often approaching the elastic collision rate. The only reactions in Table I which have not been thoroughly discussed in the literature are the methane-oxygen cross reactions; therefore, the prime emphasis of this chapter will be on those reactions.

In agreement with Franklin and Munson[10] very few and relatively slow cross-reactions have been observed. In several cases reactions were pointed out which probably occurred in their experiments although the reactions did not occur in the present experiments. In two cases the two experiments differ. The appearance potential measurement of CDO^+ is quoted as being near that of CD_4^+ and CDO^+ is first order in both methane and oxygen partial pressures; hence the reaction

$$CD_4^+ + O_2 \rightarrow CDO^+ + (D_2O + D \text{ or } D_2 + OD) \qquad (24i \text{ or } k)$$

is ascribed a rate of $6.6 \pm 2 \times 10^{-11}$ cm^3/molec-sec at ionizing electron energy of 50 eV and 1.5×10^{-11} at about 14.5 eV. "Thus CDO^+ is also formed from an ion of a higher appearance potential than CD_4^+."[1] However the appearance potential measurement and dependency

Table I. The Thermal Ion-Molecule Reactions in Methane-oxygen Mixtures

Reaction Number	Reaction	ΔH kcal/mole	k^{*} $\times 10^{-10}$ cm^3/molec-sec	k^{**} $\times 10^{-10}$ cm^3/molec-sec
1	$C^+ + CH_4 \rightarrow C_2H_2^+ + H_2$	-96	5.2 ±.2***	5.2 ±.2
2	$\rightarrow C_2H_3^+ + H$	-92	4.0 ±.2	3.8 ±.2
3	$\rightarrow CH_3^+ + CH$	-11	∿5.0	∿4.5
4a	$CH^+ + CH_4 \rightarrow C_2H_3^+ + H_2$	-112	3.1 ±.1	2.9 ±.1
5	$\rightarrow CH_2^+ + CH_3$	-15	∿6	∿6
6	$\rightarrow C_2H_2^+ + H_2 + H$	-12	4.0 ±.1	3.8 ±.1
7a	$CH_2^+ + CH_4 \rightarrow C_2H_4^+ + H_2$	-62	2.75 ±.008	2.50 ±.008
8a	$\rightarrow CH_3^+ + CH_3$	-22	5.8 ±.05	5.3 ±.05
9	$\rightarrow C_2H_3^+ + H_2 + H$	+6	6.1 ±.05	5.6 ±.05
10	$CH_3^+ + CH_4 \rightarrow C_2H_5^+ + H_2$	-23	9.92 ±.01	8.97 ±.01
11a	$CH_4^+ + CH_4 \rightarrow CH_5^+ + CH_3$	-2	12.0 ±.01	10.7 ±.01
12	$CH_5^+ + \rightarrow C_2H_5^+ + 2H_2$	+18	?	?
13m	$O^+ + CH_4 \rightarrow CH_4^+ + O$	-22	≈0.50	0.47 ±.05
13n	$\rightarrow OH^+ + CH_3$	-11		
14	$H_2O^+ + CH_4 \rightarrow H_3O^+ + CH_3$	-16	∿12[a]	
15	$CO^+ + CH_4 \rightarrow HCO^+ + CH_3$	-53	12[a]	

Reaction Number	Reaction	ΔH kcal/mole	k^{*} $\times 10^{-10}$ cm^3/molec-sec	k^{**} $\times 10^{-10}$ cm^3/molec-sec
16d	$O_2^+ + CH_4 \rightarrow CH_3O_2^+ + H$	-93	0.07 ±.004	0.04 ±.004
16f	$\rightarrow CH_3O^+ + OH$	-75	0.13 ±.004	0.08 ±.004
18	$CO_2^+ + CH_4 \rightarrow CO_2H^+ + CH_3$	+17	10[a]	
19	$H_2^+ + O_2 \rightarrow HO_2^+ + H$	-33	80[a]	
20a	$C^+ + O_2 \rightarrow CO^+ + O$	-74	11.0 ±.8	10.7 ±.8
21a	$CH^+ + O_2 \rightarrow HCO^+ + O$	-145	9.7 ±.7	9.2 ±.7
22g	$CH_2^+ + O_2 \rightarrow H_2CO^+ + O$	-50	1.0 ±.04	0.9 ±.04
23f	$CH_3^+ + O_2 \rightarrow CH_3O^+ + O$	-20	0.13 ±.01	0.13 ±.01
24p	$CH_4^+ + O_2 \rightarrow O_2^+ + CH_4$	-14	2.1 ±.2	1.9 ±.2
24r	$\rightarrow CH_3^+ + HO_2$	-9	2.5 ±.2	2.3 ±.2
26	$O^+ + O_2 \rightarrow O_2^+ + O$	-36	0.169[b]	0.169[b]
27	$H_2O^+ + O_2 \rightarrow O_2^+ + H_2O$	-13	∿2 [a]	
28	$CO^+ + O_2 \rightarrow O_2^+ + CO$	-45	2.0[a]	
29	$O_2^{+*} + O_2 \rightarrow O_3^+ + O$	∿0	.07[b]	.07[b]
30	$CH_4^+ + CO \rightarrow HCO^+ + CH_3$	-2	8.7 [a]	
31	$CH_5^+ + CO \rightarrow HCO^+ + CH_4$	-19	5.54 [a]	
32	$H_2^+ + H_2O \rightarrow H_3O^+ + H$	-90	20[a]	

Reaction Number	Reaction	ΔH kcal/mole	k^{*} $\times 10^{-10}$ cm^3/molec-sec	k^{**} $\times 10^{-10}$ cm^3/molec-sec
33	$CH_4^+ + H_2O \rightarrow H_2O^+ + CH_4$	-1	~ 20 [a]	
34	$\rightarrow H_3O^+ + CH_3$	-27	~ 30 [a]	
35	$CH_5^+ + H_2O \rightarrow H_3O^+ + CH_4$	-23	50 [a]	
36	$H_2O^+ + H_2O \rightarrow H_3O^+ + OH$	-10	25 [a]	
37	$HCO^+ + H_2O \rightarrow H_3O^+ + CO$	-33	25 [a]	

*Rate coefficients for the perhydro-system.

**Rate coefficients for the perdeutero-system. Thus the rate constant for the perdeutero-reaction 8a, $CD_2^+ + CD_4 \rightarrow CD_3^+ + CD_3$ is 5.3×10^{-10} cm^3/molec-sec.

***Limits show the accuracy of the data fitting. Because the fitting may for a particular mass involve several adjustable parameters, the rate constants, the actual uncertainty in the rate constants is probably a factor or two more than the accuracy of the fitting.

[a]References and discussion given in Chapter IV.

[b]References and discussion given in Chapter V.

0 0 0 0 3 6 0 3 8 6 7

on methane and oxygen partial pressures can equally well be interpreted as was done here as:

$$CD_4^+ + CO \rightarrow CDO^+ + CD_3 \qquad k = 8.7 \times 10^{-10} \text{ cm}^3/\text{molec-sec}, \qquad (30)$$

by assuming that the oxygen has CO contamination. We agree that CDO^+ is formed from an ion of a higher appearance potential than CD_4^+:

$$CD^+ + O_2 \rightarrow CDO^+ + O \qquad k = 9.2 \pm .7 \times 10^{-10} \ . \qquad (21a)$$

The other discrepancy between the two experiments is understandable in terms of the weakness of the appearance potential method as a means of establishing precursors. Franklin and Munson[1] measured an appearance potential of 12.9 eV for CH_3O^+; our data would predict it to be about 12.2 eV. Thus they conclude that CH_3O^+ is formed from

$$CH_4^+ + O_2 \rightarrow CH_3O^+ + OH \qquad (24f)$$

We determined the rate for 24f is less than 10^{-12}, while CH_3O^+ is actually formed by 16f and 23f:

$$O_2^+ + CH_4 \rightarrow CH_3O^+ + OH \qquad k = 7 \pm .4 \times 10^{-12} \text{ cm}^3/\text{molec-sec} \qquad (16f)$$

$$CH_3^+ + O_2 \rightarrow CH_3O^+ + O \qquad k = 1.3 \pm .1 \times 10^{-11} \ . \qquad (23f)$$

The one most important question which the experiments of Franklin and Munson answered is whether or not electronicly excited

O_2^+ is responsible for the cross-reaction products. Could there be an energy barrier which prevents reactants from reaching at room temperature the intermediate configuration which must be achieved before one of the highly exothermic product channels can be entered? If there were an activation barrier, a reactant ion such as $O_2^+(\tilde{a}\ ^4\Pi_u)$ with 100 kcal/mole more internal energy than ground state O_2^+ would more likely be able to react. However, Franklin and Munson have shown that all these cross-reaction products have appearance potentials lower than that of $O_2^+(\tilde{a}\ ^4\Pi_u)$ or $O_2^+(\tilde{A}\ ^2\Pi_u)$. The conclusion is that there is no marked difference in the rate of reaction of methane with excited oxygen ions compared to that with ground state oxygen ions. Two further deductions can be made. First, the fact that a few percent of the $O_2^+(\tilde{X}\ ^2\Pi_g)$ collisions with methane are reactive indicates that for some collisions there is little or no energy barrier. Second, the same fraction of collisions of $O_2^+(\tilde{a}\ ^4\Pi_u)$ are also probably reactive, but not a significantly greater fraction. Therefore, except for a few percent of the collisions there must be a barrier to reaction greater than 100 kcal/mole.

An energy barrier seems responsible[2] for the three orders of magnitude difference in the rates of thermal reactions 20a and 38:

$$C^+ + O_2 \rightarrow CO^+ + O \qquad k = 1.10 \times 10^{-9}\ cm^3/molec\text{-}sec \qquad (20a)$$

$$O^+ + N_2 \rightarrow NO^+ + N \qquad k = 1.2 \times 10^{-12}\ (ref.\ 7), \qquad (38)$$

even though the reaction intermediates (COO^+ and NNO^+) are isoelectronic linear molecules and the reactions are both exothermic

0 0 0 0 3 6 0 3 6 8

(ΔH = -74 kcal/mole for 20a and -26 kcal/mole for 38). Spin and electron orbital symmetry conservation forbids either reaction's reaching the electronic ground state ($^2\Pi$) of the intermediate.[2] However, 20a is "down-hill all the way." That is, the reaction proceeds by way of a high-lying state of COO^+ but this excited state is nevertheless still lower in energy than the reactants. In Reaction 38 the high-lying quartet intermediate state is of slightly greater energy than the reactants at 300°K (internally exciting the N_2 reactant in 38 by several vibrational quanta increases the rate of 38 an order of magnitude or more[3b]). The activation barrier therefore inhibits reaction.

In Table I a pattern can be seen for the series of reactions $H_nC^+ + O_2$ in which

$$H_nC^+ + O_2 \rightarrow H_nCO^+ + O, \qquad n = 0, 1, 2, \text{ or } 3,$$

is the predominant reactive process. The n = 0 case has been examined thoroughly and may lend valuable insight into the mechanism of the others. This pattern probably warrants additional theoretical consideration so as to reveal the basis of its origin. The understanding gained would ideally explain why this channel of reaction, in which the ion is substituted for an oxygen atom, predominates over other channels of reactions, and why the rate of the reactions diminishes with increasing n. If this series of reactions can to any extent be thought of as

$$H_nC^+ + O_2 \rightarrow H_{n-1}COH^+ + O, \qquad n = 1,2,3$$

then the pattern may be extrapolated to the n=4 case to give valuable insight into the mechanism of reactions involving $CH_4^+ + O_2$.

The essential difference between the $CH_4^+ + O_2$ interaction and the $CH_n^+ + O_2$ interactions for $n \neq 4$ is that charge exchange and H-atom transfer are exothermic for n=4 and endothermic otherwise. The transfer of relatively light particles such as the electron or hydrogen atom can occur over greater distances and less energy is required to accomplish the transfers in times on the order of the duration of a single collision. In pure methane the reaction of CH_n^+ with methane involves H-atom transfer:

$$CH_n^+ + CH_4 \rightarrow CH_{n+1}^+ + CH_3$$

$$\text{or } CH_3^+ + CH_{n+1} \qquad n = 0,1,2,3$$

with substantial rate in every case where energy and spin conservation allow it. H-atom transfer is clearly facile. Therefore in the reaction of CH_4^+ with oxygen it is not surprising that highly exothermic channels of reaction which may involve energy barriers and/or configurational bottlenecks are slighted in favor of simple particle exchanges:

$$CH_4^+ + O_2 \rightarrow O_2^+ + CH_4 \qquad (24p)$$

$$\rightarrow CH_3^+ + HO_2 \,. \qquad (24r)$$

Configurational bottlenecks will be discussed further below.

The same difference which distinguishes $CH_4^+ + O_2$ from the other $CH_n^+ + O_2$, $n \neq 4$, cases also distinguishes $CH_4^+ + O_2$ from

$O_2^+ + CH_4$. The total rate of reaction from the former entrance channel, $CH_4^+ + O_2$, is 40% of the ion-neutral collision rate, while the total rate from the latter is only 2%. This difference only further underscores the facility of those simple reactions 24p and r.

The concern Franklin and Munson[1] expressed over the great difference which stems simply from the placement of a single electron probably is best understood from classical theories of chemical kinetics,[4] which hypothesize that the course of reaction is determined by the intermediate which is formed as reactants evolve into products. Since the intermediates formed from $O_2^+ + CH_4$ and $CH_4^+ + O_2$ should be quite similar, the subsequent reactions should also be similar. The most stable intermediate configuration is $H_2C(OH)_2^{+*}$, which has a ground state heat of formation of about 120 kcal/mole (see the Appendix). The ground state of $H_2C(OH)_2^+$ is bound with respect to its lowest decomposition channel by about 50 kcal/mole and is about 140 kcal/mole lower in energy than the $O_2^+ + CH_4$ reactants. However, in order to form this intermediate it would seem that insertion of the oxygen atoms into the two C-H bonds would have to be concerted with the O-O bond scission. This concerted reaction would be more difficult in $O_2^+ + CH_4$ than in $CH_4^+ + O_2$ since all bonds are stronger and shorter in the former pair of reactants. However, either pair of reactants would have to be able to pass a configurational bottleneck in order to reach the $H_2C(OH)_2^{+*}$ intermediate. That is, each atom would have to be properly placed so that the concerted reaction could take place. Only a small fraction of the collisions bring the reactant atoms into sufficient proximity to the proper geometry to permit reaction by way of the $H_2C(OH)_2^{+*}$ complex. For $CH_4^+ + O_2$ however

a relatively large range of configurations bring the reactants to a point at which electron or H-atom transfer can take place. This large range of configurations represents a gaping "probability window" which the reaction can pass through in a large fraction of the collisions of CH_4^+ with O_2 while the $O_2^+ + CH_4$ collisions will remain non-reactive unless the orientations of the atoms is nearly ideal.

Objections can be raised to our choice of the intermediate, for a plausible alternative intermediate of structure CH_3OOH^{+*} does not require that the O-O bond be broken in order to form the complex and only a single insertion into a C-H bond is required. However thermodynamic arguments given in the Appendix show that while CH_3OOH^{+*} can be formed from $O_2^+ + CH_4$ or $CH_4^+ + O_2$, the intermediate will be unstable with respect to several paths of decomposition, including $CH_3O^+ + OH$ and $HC(OH)_2^+ + H$. These two pairs of products, of course, are those formed by reaction of O_2^+ with CH_4. It is most unlikely that half as much $HC(OH)_2^+ + H$ as $CH_3O^+ + OH$ could be formed from CH_3OOH^{+*} decomposition since the former product requires extensive rearrangement to be formed. If we estimate the lifetime of the CH_3OOH^{+*} complex to be on the order of 10^{-14} sec then the OH group must be accelerated to a kinetic energy on the order of 10 eV in order that it move the several Ångstrom distance to form the rearrangement product $H + HC(OH)_2^+$. It is unlikely that the energy requirements could be met for thermal reactants. It is furthermore unlikely that the CH_3OOH^{+*} complex could rearrange to form the $H_2C(OH)_2^{+*}$ complex. The occurrence of Reaction 16d,

$$O_2^+ + CH_4 \rightarrow HC(OH)_2^+ + H \qquad k = 7 \pm .4 \times 10^{-12} \text{ cm}^3/\text{molec-sec}, \quad (16d)$$

0 0 0 0 3 6 0 0 8 7 0

in which two C-O bonds have been formed, is sound evidence that the CH_3OOH^{+*} reaction intermediate is not formed.

The $HC(OH)_2^+ + H$ product seems to be "the image of its progenitor," $H_2C(OH)_2^+$ in that the O-O bond is broken and two C-O bonds have been formed. However we still don't have proof that the reaction does not proceed by some more impulsive mechanism, for example, in which the reaction of O_2^+ with CH_4 leads to an unstable product $H + CH_3OO^+$ by knocking off a hydrogen atom as the C-OO linkage is formed. The CH_3OO^+ is unstable but it might persist long enough in a fraction of the cases to rearrange to $HC(OH)_2^+$ before decomposition led to $CH_3O^+ + O$. Unfortunately the first step

$$O_2^+ + CH_4 \rightarrow CH_3\text{-}OO^+ + H$$

is probably 70 kcal/mole endothermic. Thus this particular example will probably not suffice as an alternative reaction mechanism. Nevertheless there may be mechanisms of reaction not considered so far which do not require assuming the $H_2C(OH)_2^{+*}$ intermediate.

Further experiments can be devised to test the reaction mechanism. $H_2C(OH)_2^+$ is stable and has many vibrational modes to participate in sharing any vibrational excitation. Therefore we can expect the $H_2C(OH)_2^{+*}$ to be a long-lived complex, probably capable of surviving for times long compared with the rotational period of the molecule, so that the products of the decomposition of the complex will be ejected at random center-of-mass angles. If the reaction were studied in a tandem mass spectrometer capable of measuring the angles at which products come from the ion-neutral

collision site, then the scattering would be isotropic in center-of-mass angle if the long-lived complex mechanism were involved. Unfortunately the reactions have very small rates and the expected cross-sections for reactive scattering in the tandem mass spec experiment may be too low clearly to prove scattering isotropy.

The reactants CH_2^+ + HOOH can probably reach the $H_2C(OH)_2^{+*}$ complex much more easily than can O_2^+ + CH_4. If the complex formed in similarly excited internal states from CH_2^+ + HOOH as from O_2^+ + CH_4, then the pattern of products formed will be similar. Unfortunately CH_2^+ + HOOH is more nearly like CH_4^+ + O_2 in respect to the H-atom and charge transfer processes, but complex-formation may still be seen in a fraction of the collisions since no very severe geometrical restrictions are expected here. By selectively labelling the hydrogen atoms in the reactants we can get a good idea of the extent of rearrangement within the complex, an estimate of its lifetime, and an idea of its structure (especially as to whether it is CH_3OOH^{+*} or $H_2C(OH_2)^{+*}$). Since the heat of formation of CH_2^+ + HOOH is similar to that of CH_4^+ + O_2 and O_2^+ + CH_4, the complex would probably be of comparable lifetime when formed from any of these three channels.

There are, of course, several other convenient reactant pairs which should theoretically lead to the same complex (with different extents of internal excitation). A study of O^+ + CH_3OH would probably not be very informative since the very stable OH and OH^+ can be formed by simple H-atom transfer. Thus H-atom transfer is expected to be very facile and might take place to the exclusion of most other reaction channels. $HC(=O)OH^+$ + H_2 has a very high probability of involving a

long-lived complex. There are few exothermic channels of reaction available:

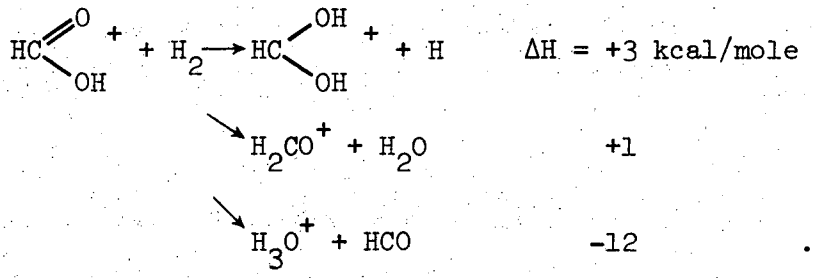

Thus the rate of reaction into a given exothermic channel should be relatively large. Isotopic labelling and tandem mass spec experiments would be easy and would tell a great deal about the structure of the complex. It is unlikely, however, that the structural parameters (such as normal mode frequencies) determined for the complex formed from $HCOOH^+ + H_2$ could be extrapolated to give the structural parameters for the same complex with an an additional 100 kcal/mole internal energy. Thus the results would probably clearly establish the mechanism for the reaction of $HCOOH^+$ with H_2 but would tell us nothing of the mechanism for $O_2^+ + CH_4$ reaction. The same statement would be true to a somewhat lesser degree of a study of $H_2O^+ + CH_2O$. Perhaps if both $HCOOH^+ + H_2$ and $H_2O^+ + CH_2O$ were studied some valuable inferences could be made from the pooled results.

Probably the largest gap in our knowledge of the ion-molecule reactions in the methane-oxygen system concerns the $O^+ + CH_4$ cross-reaction. Franklin and Munson[3] found nothing they could attribute to this interaction. The present study has measured the rate of disappearance of O^+ in CD_4-O_2 mixtures and found it to be small. There the results end and speculation begins. Chemical intuition suggests that O^+ should be very highly reactive; therefore, the

relative unreactivity observed here indicates further study of this system should be undertaken in order to advance the state of present chemical intuition.

A theoretical basis for understanding the relatively low reactivity of the methane-oxygen cross-reactions probably already exists in the theory of electron orbital symmetry conservation. What is needed in order to apply this theory is an accurate quantum mechanical calculation of the energies of the molecular orbitals. A firmer knowledge of the mechanism of the reactions is needed to provide a better focus for the quantum mechanical investigation and more experimental data on the internal and kinetic energy dependence of the reactions is needed for testing the results of the theory. Thus the investigation of the ion-molecule reactions in methane-oxygen mixtures has only just begun.

0 0 0 0 3 6 0 3 8 7 1

REFERENCES

1. J. L. Franklin and M. S. B. Munson, Tenth Symposium on Combustion, 561 (1965).

2. J. J. Kaufman and W. S. Koski, Chapt. VI, Ref. 6

3a. D. B. Dunkin, et.al., Chapter VI, Ref. 7a.

3b. A. L. Schmeltekopf, et.al., Chapter VI, Ref. 7b.

4. H. S. Johnston, Gas Phase Reaction Rate Theory, Ronald Press, New York (1966).

VIII. Acknowledgements

I thank Professor Bruce Mahan for his guidance of this work. His wisdom has made this great challenge surmountable. I take this opportunity to acknowledge publicly my gratitude for the emotional and financial support provided by my wife Ann. I owe much to the Berkeley scientific community, especially to Professors Ron Herm and Leo Brewer. This research was conducted under the auspices of the U. S. Atomic Energy Commission.

APPENDIX

Table I. Selected Thermodynamic Data[1]
Heats of Formation of Ions

Ion	Term*	Symmetry	ΔH_f°(kcal/mole)
H^+	^1S	K_h	366
H_2^+	$^2\Sigma_g^+$	$D_{\infty h}$	356
H_3^+	$^1A_1'$	D_{3h}	296
C^+	^2P	K_h	431
CH^+	$^1\Sigma^+$	$C_{\infty v}$	399
CH_2^+	$^2A_1$	C_{2v}	333
CH_3^+	$^1A_1'$	D_{3h}	260
CH_4^+	^2E	C_{3v}	274
CH_5^+	$^1A'$	C_S	221
$C_2H_2^+$			317
$C_2H_3^+$			269
$C_2H_4^+$			253
$C_2H_5^+$			219
O^+	$\tilde{X}^4S$	K_h	374
	$\tilde{a}^2D$		450
OH^+	$\tilde{X}^3\Sigma^-$	$C_{\infty v}$	312
	$\tilde{a}^1\Delta$		~360
OH_2^+	$^2B_1$	C_{2v}	233
OH_3^+	$^1A_1$	C_{3v}	156
O_2^+	$\tilde{X}^2\Pi_g$	$D_{\infty h}$	278
	$\tilde{a}^4\Pi_u$		371
O_2H^+	$^1A'$	C_S	271
$O_2H_2^+$			223

Ion	Term*	Symmetry	ΔH_f°(kcal/mole)
O_3^+	$^2A_2$	C_{2v}	318
CO^+	$^2\Sigma^+$	$C_{\infty v}$	297
COH^+	$^1\Sigma^+$	$C_{\infty v}$	196[2]
COH_2^+	$^2B_2$	C_{2v}	223
COH_3^+	$^1A_1$	C_{3v}	180
COH_4^+	^2E	C_{3v}	202
CO_2^+	$^2\Pi_g$	$D_{\infty h}$	223
CO_2H^+	$^1A'$	C_S	189
$HCOOH^+$	$^2A''$	C_S	164
$HC(OH)_2^+$	$^1A_1$	C_{2v}	115
$H_2C(OH)_2^+$			~120

*Ground state unless noted. $\tilde{X}$ means ground state $\tilde{A}$ means first excited state of the same spin multiplicity as ground state, and $\tilde{a}$ means first excited state of different spin.

[1]J. L. Franklin, et al., NSRDS NBS 26, June 1969.

[2]Mathews and Warneck, J. Chem. Phys., 854 (1969).

0 0 0 0 3 6 0 3 8 7 3

Table IL Selected Thermodynamic Data[1]
Heats of Formation of Neutrals

Neutral	Term*	Symmetry	ΔH_f°(kcal/mole)
H	^2S	K_h	52
H_2	$^1\Sigma_g^+$	$D_{\infty h}$	0
C	^3P	K_h	171
CH	$^2\Pi$	$C_{\infty v}$	142
CH_2	$^3\Sigma_g^-$	$D_{\infty h}$	94
CH_3	$^2A_2''$	D_{3h}	33
CH_4	$^1A_1$	T_d	-18
O	$\tilde{X}^3P$	K_h	60
	$\tilde{a}'D$		105
OH	$^2\Pi$	$C_{\infty v}$	9
OH_2	$^1A_1$	C_{2v}	-58
O_2	$^3\Sigma_g^-$	$D_{\infty h}$	0
O_2H	$^2A''$	C_S	5
O_2H_2			-33
O_3	$^1A_1$	C_{2v}	34
CO	$^1\Sigma^+$	$C_{\infty v}$	-26
COH	$^2A'$	C_S	-4
COH_2	$^1A_1$	C_{2v}	-28
COH_3	^2E	C_{3v}	$-\frac{1}{2}$
COH_4	$^1A'$	C_S	-48
CO_2	$^1\Sigma_g^+$	$D_{\infty h}$	-94
CO_2H	$^2A_1$	C_{2v}	-39
CO_2H_2	$^1A'$	C_S	-90

Estimation of ΔH_f° for Species of Stoichiometry CH_4O_2, CH_3O_2, $CH_4O_2^+$, and $CH_3O_2^+$.

An ion of mass 47 in mixtures of methane and oxygen has the stoichiometry $CH_3O_2^+$ but it has two possible structures, $CH_3\text{-}OO^+$ or $HC(OH)(OH)^+$. Franklin[2] dismissed the fiest structure since it is not observed in the mass spectrum of dimethyl peroxide; this fact gives a lower bound on the ΔH_f° of $CH_3\text{-}OO^+$ of 240 kcal/mole from the requirement that

$$CH_3\text{-}OO^+ \rightarrow CH_3O^+ + O \qquad \Delta H = 240 \text{ kcal/mole} - \Delta H_f^\circ(CH_3\text{-}OO^+) \tag{1}$$

be exothermic or thermoneutral. There can be little doubt that $CH_3\text{-}OO^+$ is formed from 15 to 20 eV and greater electron impact upon $CH_3\text{-}OO\text{-}CH_3$; especially considering that HOO^+ is a major ion from HOOH. Failure to see CH_3OO^+ in CH_3OOCH_3 must be interpreted as proof that Reaction 1 is spontaneous (hence exothermic).

We can get good estimates for the heats of formation of the species CH_3OO, $HC(OH)_2$, CH_3OOH, $H_2C(OH)_2$, and their ions by using the data compilation and methods of Benson[3] to augment the data of Tables I and II. Thermodynamic data from pyrolysis gives the following three bond dissociation energies:

$$\begin{aligned} D(HO\text{-}OH) &= +50.0 \text{ kcal/mole} \\ D(CH_3O\text{-}OH) &= +42 \\ D(CH_3O\text{-}OCH_3) &= +33 \end{aligned} \tag{2}$$

0 0 0 0 5 6 0 5 3 7 4

Using ΔH_f° (OH) = +9 kcal/mole and ΔH_f° (CH_3O) = + $\frac{1}{2}$ kcal/mole from Table II and the above data one gets

$$\Delta H_f^\circ(HOOH) = -32.5 \text{ kcal/mole (in agreement with } -33 \text{ from Table II)}$$
$$\Delta H_f^\circ(CH_3OOH) = -32 \qquad (3)$$
$$\Delta H_f^\circ(CH_3OOCH_3) = -32$$

Benson[3] estimates $\Delta H_f^\circ(CH_3OO) = +5$ kcal/mole by assuming $D(HOO-H) = D(CH_3OO-H) = 89.5$ kcal/mole. This $\Delta H_f^\circ(CH_3OO)$ is also in accord with assuming that $D(CH_3-OOH) = D(CH_3-OOCH_3) = +6$ kcal/mole. These D's seem unreasonably small, but where the problem lies is not known. ΔH_f° (formic acid) is -90 kcal/mole while Benson's method predicts -87. This agreement is in keeping with the generally good agreement between predictions of Benson's method and measured values for several thousands of different compounds. This method predicts $\Delta H_f^\circ(H_2C(OH)_2) = -94$ kcal/mole. That compounds such as $H_2C(OH)_2$ have not as yet been observed is generally ascribed to the fact that they spontaneously decompose as follows

$$H_2C(OH)_2 \qquad H_2C{=}O + H_2O \qquad \Delta H = \Delta H_f^\circ(H_2C(OH)_2) + 86 \text{ kcal/mole}$$

an indication that $\Delta H_f^\circ(H_2C(OH)_2) \lesssim -86$ kcal/mole. Since the -94 kcal/mole estimate is determined from data for $H_2C(OR)_2$ where R is CH_3, CH_3CH_2, etc., it is not expected to be very accurate. Thus the ΔH_f° for this species is probably within ten kcal/mole of -86. We can estimate the H-C bonding energy in $H_2C(OH)_2$ from

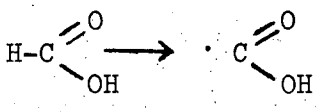

ΔH = +103 kcal/mole (4)

to get

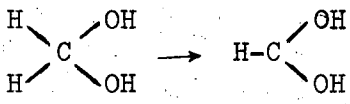

$\Delta H \approx +103$ kcal/mole (5)

which implies that ΔH_f° (H-C(OH)(OH)) ≈ -35 kcal/mole.

Estimating the heats of formation of the ions of these compounds will have to be equally uncertain or more so, except for ΔH_f° (H-C(OH)$^+$(OH)) which is known to be +115 kcal/mole from Table I, ref. 1. Equation (4) gave an estimate for the strength of a two-electron C-H bond; another estimate comes from

$$HCOOH^+ \longrightarrow H + COOH^+ \qquad \Delta H = 89 \text{ kcal/mole} \qquad (6)$$

In order to estimate ΔH_f° (H_2C(OH)$^+$(OH)) we observe that

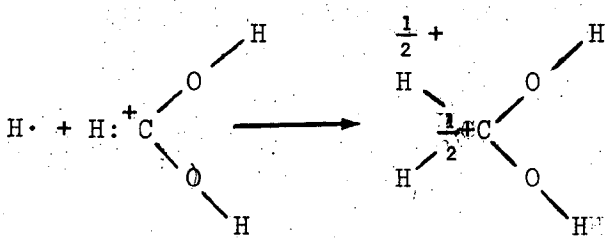

(7)

involves formation of a one electron C-H bond. If we estimate ΔH for (7) to be about half that of (4) or (6) we get ΔH_f°(H_2C(OH)(OH)+) $\approx$ +120 kcal/mole.

There are several ways in which to estimate ΔH_f°(CH_3-OOH$^+$). The first is to assume the proton affinity of HOO and CH_3OO are the

0 0 0 0 3 6 0 0 0 7 5

same:

$$\begin{aligned} HOO + H^+ &\longrightarrow HOOH^+ \qquad \Delta H = -148 \text{ kcal/mole} \\ CH_3OO + H^+ &\longrightarrow CH_3OOH^+ \qquad \Delta H \approx -148 \text{ kcal/mole;} \end{aligned} \tag{8}$$

this implies $\Delta H_f^{\circ}(CH_3OOH^+) \approx 223$ kcal/mole. (9)

Another estimate comes from comparing the following system of relationships:

$$\begin{array}{ccccccccc} HOO + H & \xrightarrow{\Delta H_1 = +64} & HO + O + H & \xrightarrow{+314} & HO + O^+ + H & \xrightarrow{\Delta H_3 = -112} & HOO^+ + H \\ \downarrow -89 & & \downarrow -103 & & \downarrow -134 & & \downarrow -100 \\ HOOH & \xrightarrow[\Delta H_2 = +50]{} & HO + OH & \xrightarrow{+303} & HO + OH^+ & \xrightarrow[\Delta H_4 = -98]{} & HOOH^+ \end{array} \tag{10}$$

with the similar system:

$$\begin{array}{ccccccccc} CH_3OO + H & \xrightarrow{\Delta H_1^1 = +56} & CH_3O + O + H & \xrightarrow{+314} & CH_3O + O^+ + H & \xrightarrow{\Delta H_3^1} & CH_3OO^+ + H \\ \downarrow -89 & & \downarrow -103 & & \downarrow -134 & & \downarrow \\ CH_3OOH & \xrightarrow[\Delta H_2^1 = +42]{} & CH_3O + OH & \xrightarrow{+303} & CH_3O + OH^+ & \xrightarrow[\Delta H_4^1]{} & CH_3OOH \end{array} \tag{11}$$

Observe that $\Delta H_1 = \Delta H_1^1 + 8$

and $\Delta H_2 = \Delta H_2^1 + 8$. (12)

If we now postutate that

$$\begin{aligned} \Delta H_3 &\approx \Delta H_3^1 + 8 \\ \text{and } \Delta H_4 &\approx \Delta H_4^1 + 8 , \end{aligned} \tag{13}$$

one finds that

$$\Delta H_f^\circ(CH_3OOH^+) \approx +223 \text{ kcal/mole} \qquad (14)$$

in agreement with (9).

The postulates (13) furthermore establish that the hydrogen atom affinity of HOO^+ and CH_3OO^+ are equal (-100 kcal/mole) and give $\Delta H_f^\circ(CH_3OO^+)$ as about +270 kcal/mole in agreement with our earlier observation that $\Delta H_f^\circ(CH_3OO^+) \gtrsim 240$ kcal/mole. On the basis of this earlier observation, we must reject a third method of estimating $\Delta H_f^\circ(CH_3OOH^+)$. This estimate derives from equating the ionization potential difference between HOH and HOOH to that between CH_3OH and CH_3OOH:

$$\begin{aligned} IP(H_2O) - IP(HOOH) &\approx IP(CH_3OH) - IP(CH_3OOH) \\ = 291 - 256 \qquad &= 250 - 215(?) \end{aligned} \qquad (15)$$

implies that $IP(CH_3OOH) \approx 215$ kcal/mole,

whence $\Delta H_f^\circ(CH_3OOH^+) \approx 183$ kcal/mole and
$\Delta H_f^\circ(CH_3OO^+) \approx 231$ kcal/mole (16)

Summary

The following estimates have been made for the species of stoichiometry CH_3O_2, CH_4O_2, and their ions:

Approximate ΔH_f°(kcal/mole)	Neutral	Ion
Structure		
CH_3OOH	-32	~+223
$H_2C(OH)(OH)$	$\lesssim$-86	~+120
CH_3OO	+5	~+270
$HC(OH)(OH)$	~-35	+115

This table predicts that CH_3OO^+ will be unstable, as observed by Franklin, and will decompose as follows:

$$CH_3OO^+ \longrightarrow CH_3O^+ + O \qquad \Delta H \approx -30 \text{ kcal/mole;}$$

furthermore CH_3OOH^+ will also be unstable:

$$CH_3OOH^+ \longrightarrow CH_3O^+ + OH \qquad \Delta H \approx -34 \text{ kcal/mole.}$$

Table III. Slope of Log-Log Plots of Peak Area Vs. Reciprocal Drift Voltage

Expt.	Mass	Slope	Std. Deviation	No. of Pts.
158	12	.808	.0172	29
	13	.805	.0119	
	14	.818	.0168	
	15	.891	.0122	
	16	.835	.0124	
	17	1.839	.0141	
	18	1.877	.0150	
	26	1.794	.0210	
	27	1.824	.0197	
	28	1.365	.0165	
	29	1.920	.0148	
158	30	1.891	.0184	29

0 0 0 0 3 6 0 3 8 7 7

Table IV. Slope of Log-Log Plots of Peak Area Vs. TIC

Expt.	Mass	Slope	Std. Dev.	No. of Pts.	
158-163	12	.88	.024	6	
	13	.88	.020	6	
	14	.87	.021	6	
	15	.94	.022	6	
	16	.90	.026	6	
	17	1.81	.014	6	
	18	1.81	.015	6	CH_4
	26	1.85	.031	6	
	27	1.88	.026	6	
	28	1.28	.022	6	
	29	1.93	.011	6	
158-163	30	1.90	.024	6	
164-169	12	.90	.032	6	
	14	.89	.011	6	
	16	.86	.028	6	
	18	.89	.021	6	
	20	.86	.031	6	
	22	1.90	.018	6	CD_4
	28	1.03	.012	6	
	30	1.90	.013	6	
	32	1.85	.028	6	
164-169	34	1.95	.020	6	

Expt.	Mass	Slope	Std. Dev.	No. of Pts.	
170-175	16	1.01	.012	6	
	28	.99	.009	6	
	32	1.02	.016	6	
	33	1.19	.023	5	"pure O_2"
	34	1.01	.017	6	
	44	1.01	.014	6	
170-175	48	1.83	.026	6	
184-189	12	.80	.027	6	
	13	.80	.027	6	
	14	.88	.022	6	
	15	.99	.025	6	
	16	.90	.022	6	
	17	1.76	.020	6	
	18	1.56	.019	6	
	19	2.02	.016	4	
	26	1.79	.019	6	
	27	1.86	.026	6	
	28	1.14	0.17	6	CH_4: O_2 = 1
	29	1.95	.014	6	
	30	1.89	.021	6	
	31	1.98	.028	6	
	32	.98	.017	6	
	33	1.31	.032	6	
	34	1.00	.014	6	
	44	.89	.034	6	
	45	1.86	.016	6	
	47	2.02	.011	6	
	48	1.70	.026	5	

LEGAL NOTICE

This report was prepared as an account of work sponsored by the United States Government. Neither the United States nor the United States Atomic Energy Commission, nor any of their employees, nor any of their contractors, subcontractors, or their employees, makes any warranty, express or implied, or assumes any legal liability or responsibility for the accuracy, completeness or usefulness of any information, apparatus, product or process disclosed, or represents that its use would not infringe privately owned rights.

TECHNICAL INFORMATION DIVISION
LAWRENCE RADIATION LABORATORY
UNIVERSITY OF CALIFORNIA
BERKELEY, CALIFORNIA 94720